19

Fibre breakage and fatigue

19.1 Fibre-fracture morphology

Data on the tensile strength of fibres were included in Chapter 13 with its time dependence in Chapter 16. Loop and knot strength and breaking twist were covered in Chapter 17. This chapter is concerned with the forms of fracture and with fatigue failures due to repeated deformation. As a result of scanning electron microscope (SEM) studies since the 1970s, the appearances of fibre ends resulting from breakage by high loads, fatigue or other causes have been classified into the 18 types shown in Fig. 19.1, and a comprehensive collection of pictures of the fractography has been published by Hearle *et al.* [1].

The following forms are included in Fig. 19.1 for completeness and will not be discussed further: (14) the rounding of fibre ends, which develops after prolonged wear on fibres that have broken in use in a textile material; (17) melting of thermoplastic fibres; (18) the natural ends formed during the growth of fibres such as cotton.

19.2 Monotonic breaks

19.2.1 Tensile failures of manufactured fibres

Depending on the nature of the fibre, different forms of tensile fracture are found. In elastic fibres, whether inextensible (glass and ceramic) fibres or highly extensible (spandex)[1], the break follows the classical mode of brittle failure described by Griffiths, as illustrated in Fig. 19.2. When the load reaches a certain level, the break initiates from a flaw and propagates rapidly as a smooth crack running across the fibre under the influence of stress concentration at the tip of the crack. Usually, when the stress on the unbroken part becomes sufficiently large, multiple-fracture initiation will start and give a rougher portion to complete the break. In some cases, the crack runs at an angle on the line of maximum shear stress for all or a part of the fracture.

The mechanism in ductile fibres, such as nylon and polyester fibres, is not dissimilar, except that the crack propagates in a controlled manner under a gradually increasing

[1]Note that although elastomeric fibres have a low initial modulus, they have a high modulus in the final stage before break.

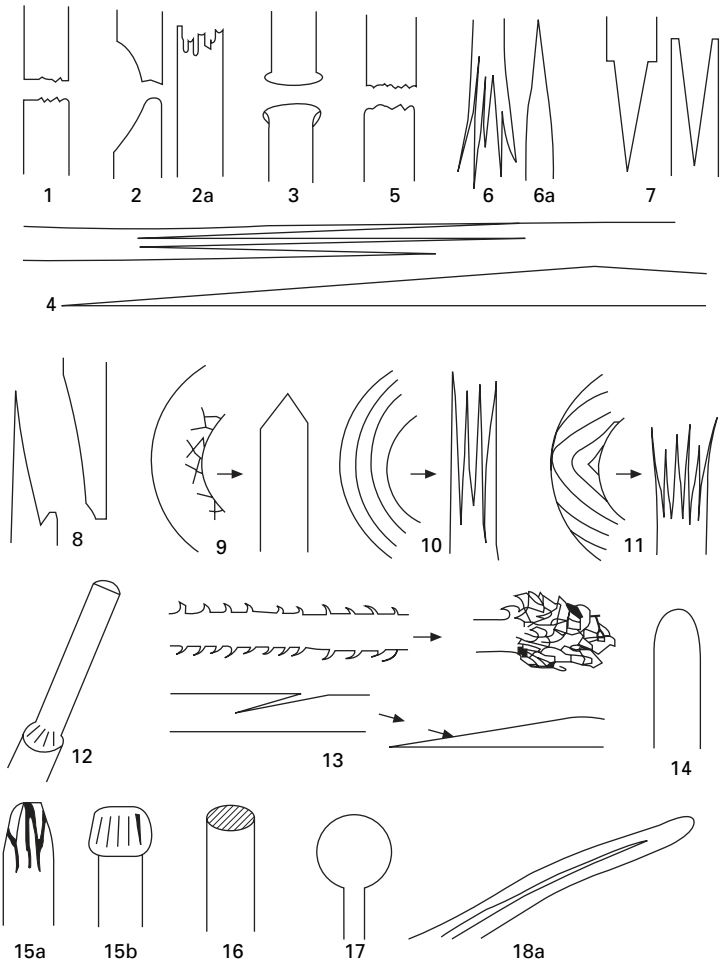

19.1 Classification of fibre ends. *Tensile failures*: (1) brittle fracture; (2) ductile fracture, (2a) modified form (light-degraded nylon); (3) high-speed break in melt-spun fibre; (4) axial split; (5) granular failure; (6) independent fibrillar failure; (6a) fibrillar break intr fibrils collapsed onto free end; (7) stake-and-socket break. *Fatigue failures*: (8) tensile fatigue; (9) flex fatigue kink-band; (10) flex fatigue-split; (11) multiple split-bend and twist fatigue; (12) surface wear; (13) peeling and splitting; (14) rounding. *Other forms*: (15a,b) transverse pressure, (a) mangled, (b) localised; (16) sharp cut; (17) melt; (18) natural fibre ends, e.g., (18a) cotton tip.

total load and opens into a V-notch owing to the drawing (high plastic extension) of the remainder of the fibre, until a final multiple crack initiation zone completes the failure. The fracture morphology was described by Hearle and Cross [2] and is shown in Fig. 19.3 with break starting at a point. The other end of the break is a mirror image of the one shown. There are variant forms [1]. Many breaks start from an extended defect perpendicular to the fibre axis. Occasionally the defect is angled, which distorts the form of failure and may lead to multiple final stages. Rarely, cracks start from

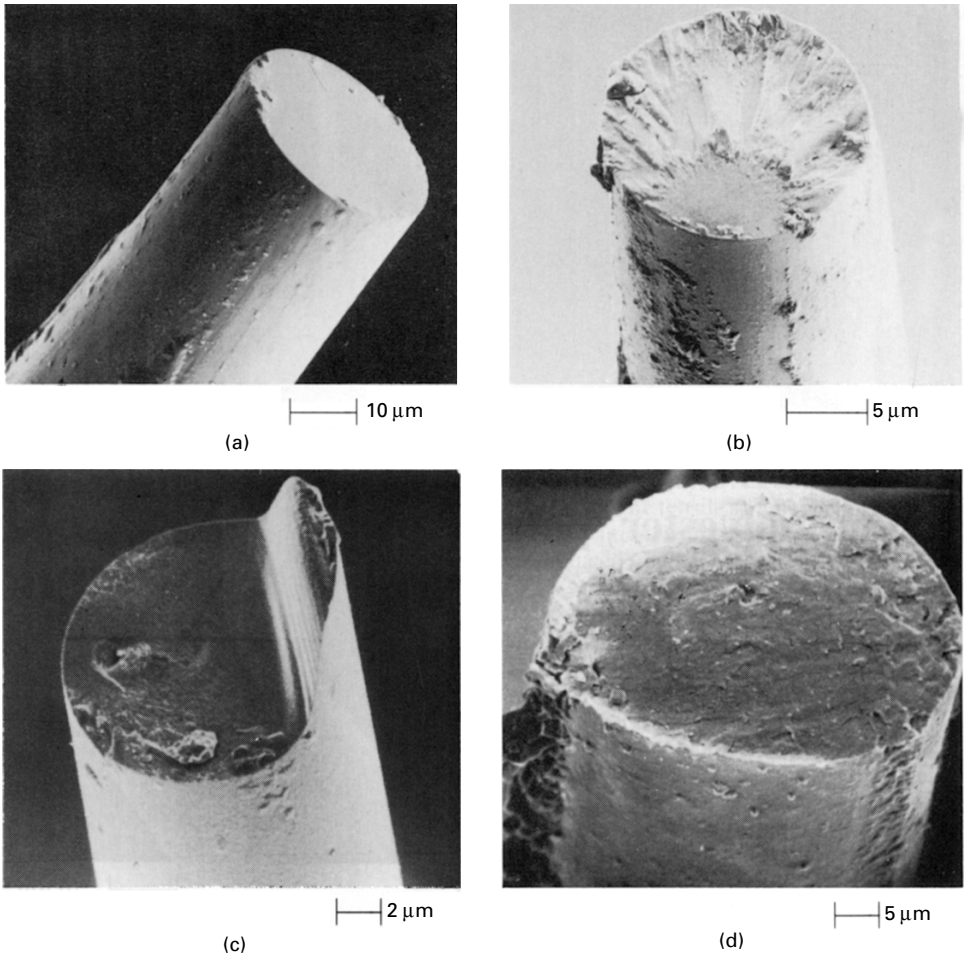

19.2 Tensile fracture of brittle fibres: (a) glass fibre with single cleavage plane; (b) glass fibre showing mirror and hackled zones; (c) ceramic fibre, Nextel *312* (silicon carbide), showing diversion at end of crack; (d) spandex, Lycra.

more than one place, joining for the final stage, or start at an internal defect to give a double cone leading to the final stage. In a heat-set nylon 6 fibre, there were small multiple V-notches along the fibre, one of which had propagated to form the break.

A break in progress in a coarse nylon bristle is shown in Fig. 19.4. Such a break can be detected long before the final failure. In these breaks of coarse bristles, put into the Instron Tensile Tester in the undrawn form, Hearle and Cross were able to identify five zones as shown in Fig. 19.5. These were A initiation, B controlled ductile tearing, C 'slip-stick' crack growth, D fast crack growth and, E final overall failure. In light-degraded nylon, the fracture, as shown in Fig. 19.6, appears to be very different, but, in fact, it is probably due to similar failure mechanisms of ductile crack growth, starting from many internal voids [1].

As the rate of loading increases, the size of the V-notch reduces. The final stage becomes larger and may become smooth and rounded. After ballistic impact, by

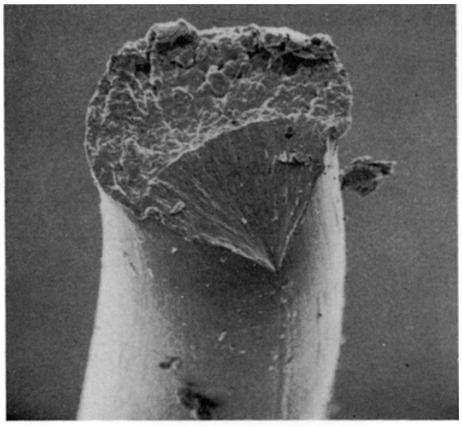

19.3 Tensile break of nylon fibre: experimental nylon 66 filament, with initiation of break at point.

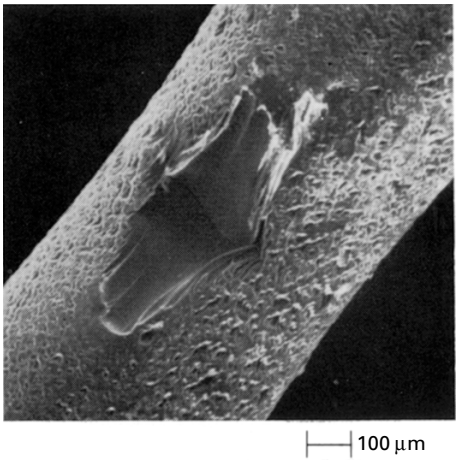

19.4 Rupture of a coarse undrawn nylon 66 bristle, 1 mm diameter, extended at a strain rate of $8 \times 10^{-4}\ s^{-1}$.

release of a pendulum or a relaxation catapult, the form of break changes completely to a mushroom end, as shown in Fig. 19.7. This is due to a change from isothermal to adiabatic conditions. The rapid plastic extension, following the start of break, generates heat and softens or melts the region of the break. Snap-back after break causes a collapse to the mushroom form.

Chemical degradation attacks outer layers first and, under tension, a crack may form around the fibre. A variant of the tensile break then occurs with a circular 'V-notch' leading to a circular catastrophic failure in the centre of the fibre [1]. In other circumstances the shear stress at the tip of the circular crack may lead to an axial split penetrating into the fibre, as shown in Fig. 19.8. The final failure is a stake-and-socket break (Fig. 19.9).

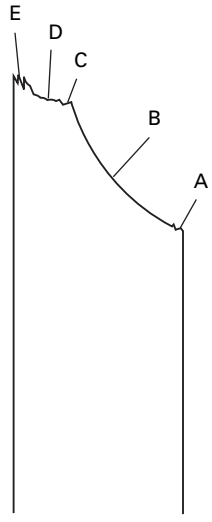

19.5 Breakage zones in nylon bristle.

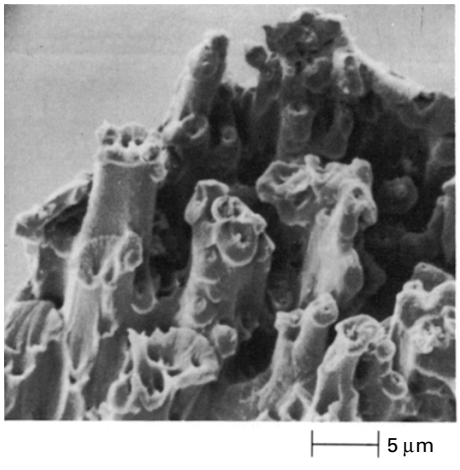

19.6 Tensile breaks of light-degraded nylon 66, 16 dtex, exposed in summer in Manchester, facing WSW: 24 weeks' exposure.

Tensile breaks of acrylic fibres are quite different [1] as shown in Fig. 19.10. The granular appearance is probably due to the independent fracture of many fibrillar sub-units. Sometimes, the final granular break is preceded by a V-notch and sometimes separate granular cracks are joined by an axial split. Granular breaks are also found in regenerated cellulose fibres, polyvinyl alcohol (PVA) and polybenzimidazole (PBI) fibres, ceramic fibres some carbon fibres, and thermally degraded nylon and polyester fibres [1].

In acetate fibres, Simmens and Howlett [3] found, by optical microscopy, that many surface cracks developed in highly stressed filaments, as shown in Fig. 19.11. This can lead to multiple fracture, with the fibre finally shattering into many fragments.

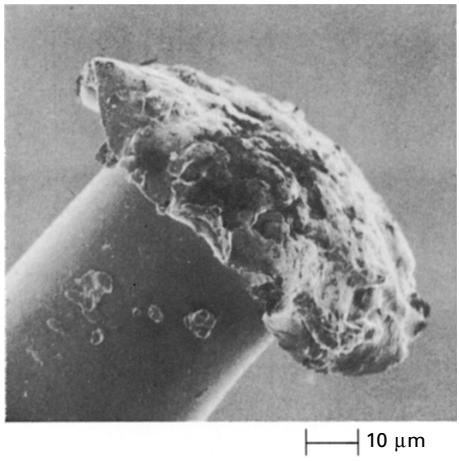

19.7 High-speed tensile break of nylon 66.

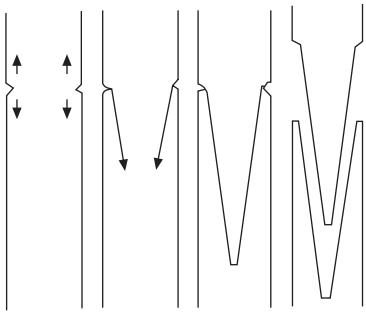

19.8 Shear cracking, following degradation round surface of fibre.

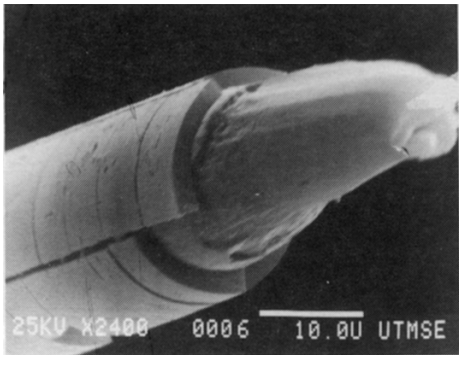

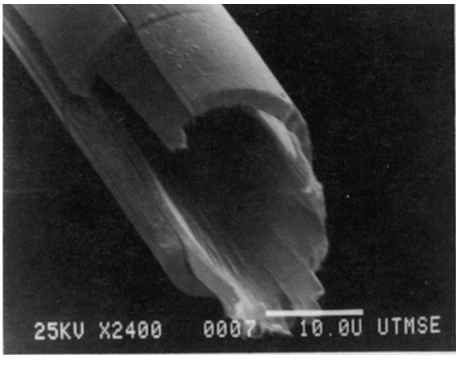

19.9 Stake-and-socket break of polyester fibre after exposure to *n*-butylamine vapour.

The occurrence of fissures during extension, but before fracture, has been observed in many fibres by Cumberbirch *et al.* [4].

In the highly oriented linear-polymer fibres, para-aramid and HMPE, tensile fracture occurs by long axial splits [5]. This is because the forces holding the molecules

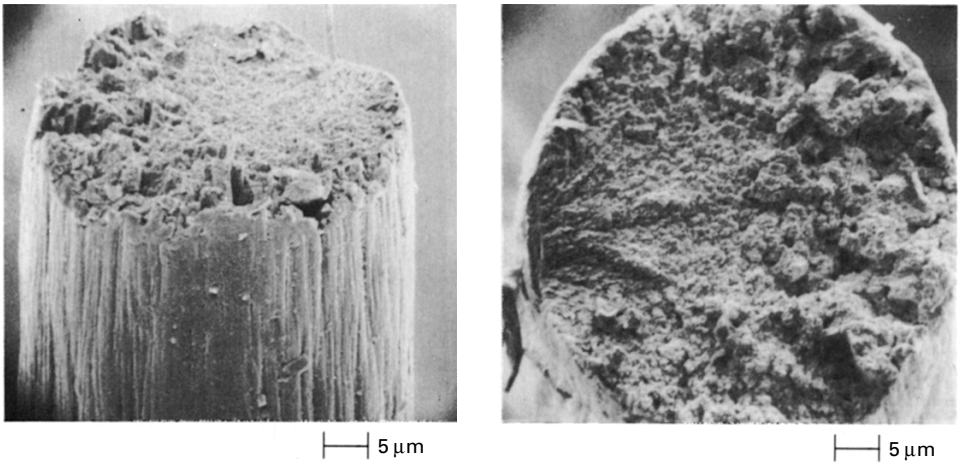

19.10 Granular fractures of acrylic fibres.

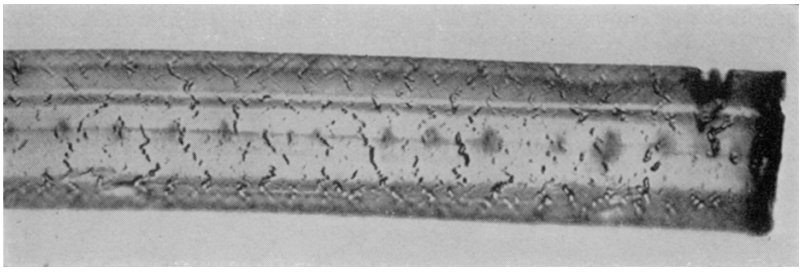

19.11 cracks in stressed acetate filaments as observed by Simmens and Howlett [3].

together across the fibre are much weaker than the forces acting along the molecules in the axial direction. If there are any defects or discontinuities in the structure, the resultant shear stress causes rupture by an axial split in preference to the imposed tensile stress causing a transverse crack. If the splits are slightly off-axis, they will eventually cross the fibre and so separate it into pieces, with the break extending over a length equal to many fibre diameters. An SEM picture of a break is shown in Fig. 19.12. Frequently, one end has a single split and the other end has a multiple split, as illustrated in Fig. 19.13. This is a geometrical consequence of an axial crack starting at the surface of the fibre and branching as it propagates along and across the fibre. The extensive axial splitting means that, in fibre assemblies and composites, more energy is absorbed during breakage than when fibres break sharply.

19.2.2 Tensile failures of natural fibres

Tensile breaks of natural fibres are strongly influenced by their particular internal morphologies. In cotton, the form varies according to test conditions. At 65% r.h., Hearle and Sparrow [6] showed that tensile failure is started by splitting between

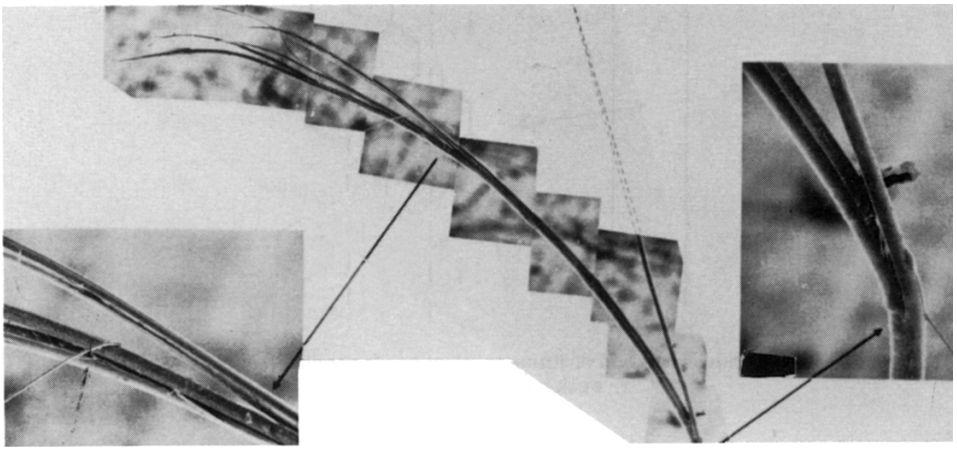

19.12 Tensile break of aramid fibre, Kevlar 29.

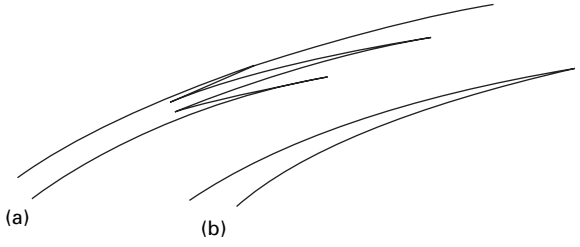

19.13 Fractures of Kevlar: (a) multiple split; (b) single split end.

fibrils (Fig. 19.14). The break occurs adjacent to a reversal, and the split, which follows the helical path of the fibrils around the fibre, is due to the untwisting forces. Eventually a tear develops along the edge of the concave region of the cross-section to join up the two ends of the helical split, as illustrated in Fig. 19.15.

The form changes as the strength of bonding between fibrils varies. When it is weak, in wet cotton, the break is fibrillar. The cause is illustrated in Fig. 19.16. Fibrils can be regarded as independent entities, which break at different weak places. Eventually all fibrils have broken over a short fibre length and the two ends separate. In the SEM, the separate fibrils may be seen (Fig. 19.17), but often the broken fibrils coalesce into a tapered end. Where the bonding is stronger, in dry cotton, the fracture runs across the fibre as a granular break with little splitting. If the fibre is clamped at a nominally zero gauge length without a reversal between the jaws, there is again usually little splitting, with the break running straight across the fibre.

In resin crosslinked cotton, the increased bonding causes the break to be straight across the fibre at 65% r.h. and has a split form, similar to Fig. 19.14, when broken in water.

In wool and hair fibres, tensile failures occur by cracks running across the fibre in a granular break, which may be coarse enough to reflect separate breaks of cells. It is fairly common for cracks at different positions along the fibre to be linked by an

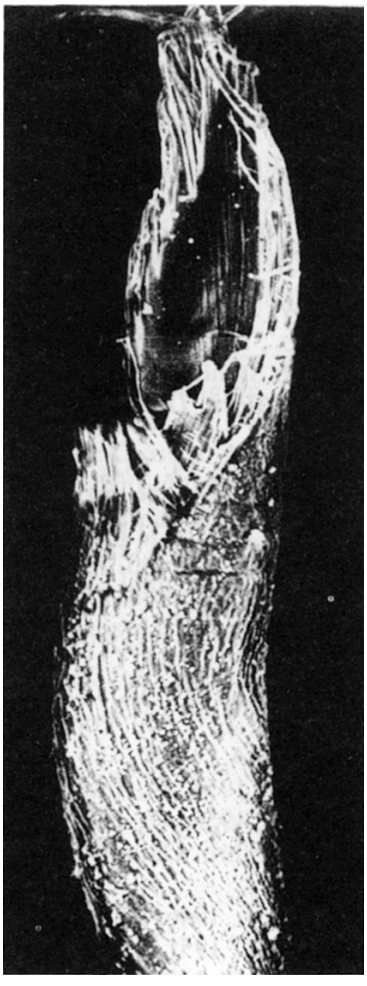

19.14 Tensile fracture of cotton fibre under standard conditions.

axial crack. Cracks in the cuticular layer of wool have been examined by Makinson [7].

Haly [8] noted that transverse striations developed in wool between 2 and 30% extension. However, these are probably regions of high local deformation and not cracks. Crazing in synthetic polymers is another phenomenon, in which there is some continuity of material across an apparent crack.

19.2.3 Twist, lateral cohesion and compression

As stated in Section 17.3.1, the major deformation at high twist levels is extension of the outer layers due to the longer helical path. This results in twist breaks being essentially tensile breaks, which are distorted by the twisting and may include axial splits [1].

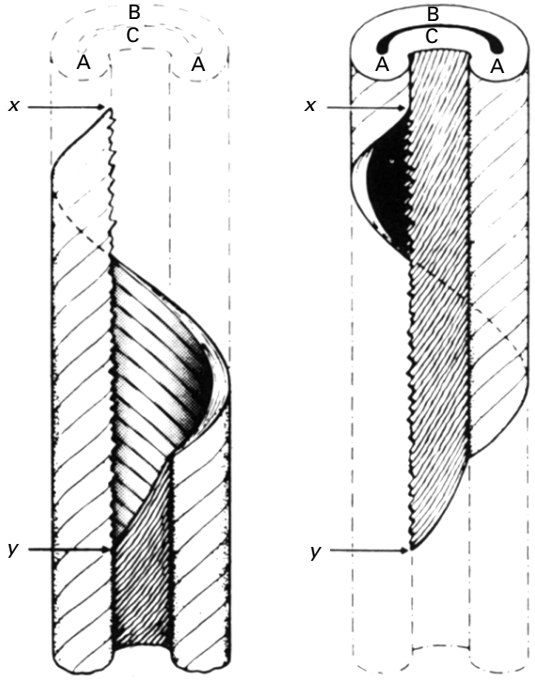

19.15 Idealised picture of break of cotton fibre at 65% r.h. A, B and C are the separate zones shown in Fig. 1.37. The split runs from x to y.

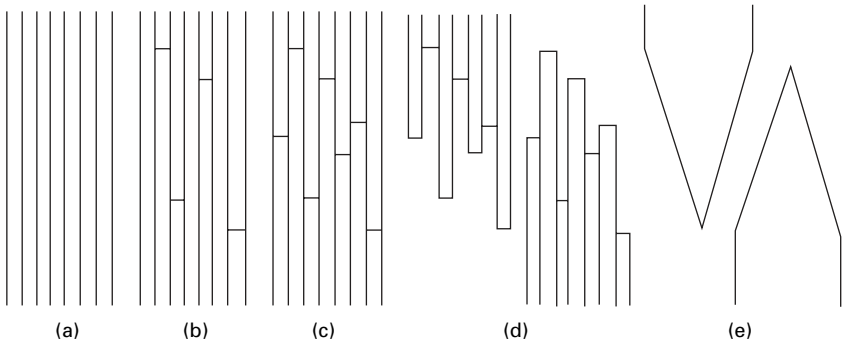

19.16 Schematic of fibrillar break. (a) Unbroken fibrils; (b) isolated breaks; (c) all fibrils broken; (d) separated ends; (e) collapse of ends.

Law and Mukhopadhyay [9] describe in detail a method of measuring the lateral cohesion of fibres. Briefly stated, a fibre is mounted between tabs and a micromanipulator is used to open a split in the centre (Fig. 19.18(a)). Pieces of copper ribbon are then stuck to the fibre in the positions shown in Fig. 19.18(b) and the split is cut on one side The test specimen is then cut away (Fig. 19.18(c)) and mounted between jaws (Fig. 19.18(d)) of a tensile tester, which incorporates a micro-balance and a micro-drive unit. The tearing force required to pull the two ends apart can then be measured.

19.17 Fibrillar break of wet mercerised cotton.

The force is divided by the width of the tear, assumed to be the fibre diameter for a central tear, and expressed in N/m (= J/m^2). Figure 19.19(a) shows the tearing force for an aramid filament, which has three regions as indicated in Fig. 19.19(b). SEM examination shows that the tear is in regions 1 and 2. There may be a precursor crack from the initial split formation, which reduces the tear force in region 1, or the occurrence of a hemispherical skin tear may increase the force in region 2. Although not mentioned by the authors, the energy loss in the bend at the splitting point must also contribute to the tear force. The change to region 3 is due to the onset of multiple splitting, which would increase the surface energy and hence require more force. It is estimated that the lateral cohesion or energy for crack propagation is the value in region 2, namely 160 J/m^2. Other tests were carried out on acrylic fibres, but it was not possible to test dry fibres. Never-dried fibres impregnated with glycerol were used.

The failure properties in transverse compression have been studied by Settle and Anderson [10] by pressing metal cutting wires against fibres. The loads needed for cutting increase with the fibre and wire diameters: typical values are given in Table 19.1. With wires finer than 100 μm, the cutting load decreases rapidly. Subsidiary experiments led to an estimate of the principal strains at failure, which were much larger laterally than axially. The fibre was observed to be squeezed out sideways, and

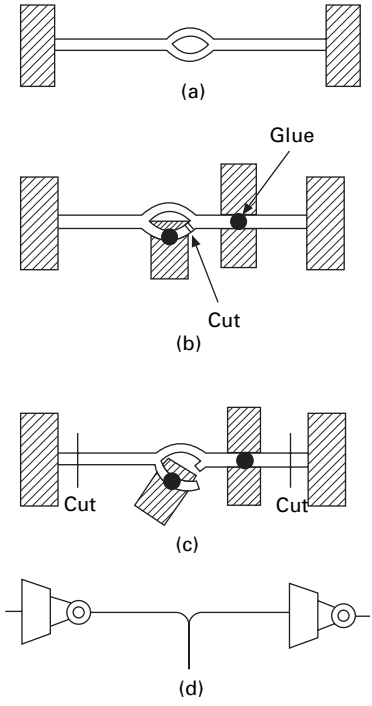

19.18 Stages in measuring lateral cohesion of fibres. From Law and Mukhopadhyay [9].

then, after a certain degree of penetration, a V-shaped cleft appeared and penetrated through the fibre. The elastic recovery was poor (about 50%) even when the applied load was only a quarter of the load needed for cutting.

Shin *et al*. [11] investigated the cut resistance of HM–HT yarns using the apparatus in Fig. 19.20. Neighbouring yarns were removed from a piece of fabric clamped on a base plate, in order to leave isolated yarns subject to the cut. The force–displacement plot is shown in Fig. 19.21(a) for aramid *Kevlar*, HMPE *Spectra* and PBO *Zylon*. The massive reduction in cut resistance when the slice angle is reduced from 90 to 80° is shown in Fig. 19.21(b). Blade sharpness has a major effect, with a 2.5-fold increase in resistance for a blade radiu change form 2 to 20 μm. Some end beaks were fairly straight across the fibres, but others showed considerable squashing.

19.2.4 Fracture mechanics

Theoretical analysis of fibre strength and detailed understanding of how and why strengths fall below maximum possible values are not easy. The basic theory of the tensile strength of a perfect crystal is illustrated in Fig. 19.22. The internal energy U is a minimum at the equilibrium spacing x_0 between the atoms; but as the crystal is extended, so that x increases, U reaches a maximum and then falls asymptotically to zero. Differentiation of this curve gives the variation of force with extension $(x - x_0)$.

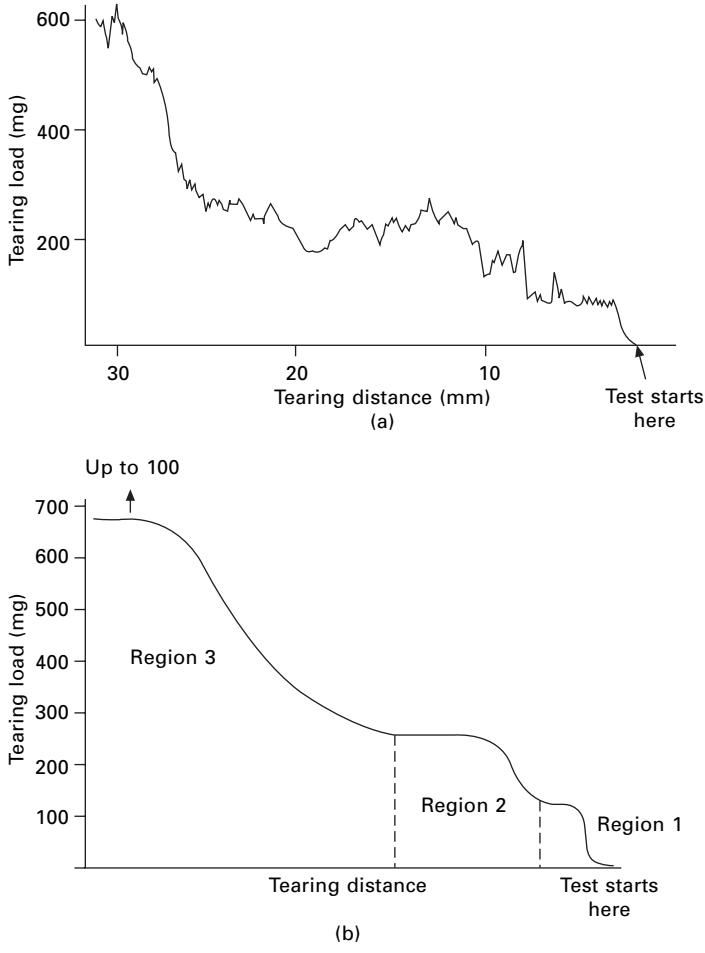

19.19 (a) Tearing force for Kevlar 49 filament, (b) Schematic representation. From Law and Mukhopadhyay [9].

The maximum value F, which is the 'theoretical' strength, occurs at the point of inflection on the energy curve. It will be high when there are strong covalent bonds between the atoms, weaker with intermediate attractions, such as hydrogen bonds and dipoles, and least with weak van der Waals interactions. However, the theoretical predictions of the shape of the variation of U with x are not exact, especially in terms of the precise position and slope of the inflection point. More commonly, an approximate value of F is estimated from the linear construction shown in Fig. 19.22(c), which demonstrates that the theoretical strength should equal the modulus times a strain level e_c, related to the position at which the energy curve is expected to go through its inflection. Generally, the maximum strength is expected to be about 0.1 times its modulus.

Among the factors that lower modulus, disorientation and slip at the ends of molecules will also lower strength, but the removal of crumpled disorder at low

Table 19.1 Loads required to cut fibres [12]

Fibre type	Fibre diameter (μm)	Wire diameter (μm)	Cutting load (N)	Estimated principal strains (%)	
				Axial	Lateral
Nylon	20	200	2.2	6	86
	20	400	3.7	–	–
	40	200	5.0	12	81
	40	400	8.0	–	–
Polyester fibre	20	200	2.0	6	114
	20	400	3.5	–	–
	40	200	4.2	15	107
	40	400	8.5	–	–
Wool	20	200	0.5	–	–
	20	400	0.7	–	–
	40	200	2.2	10	47
	40	400	3.3	–	–

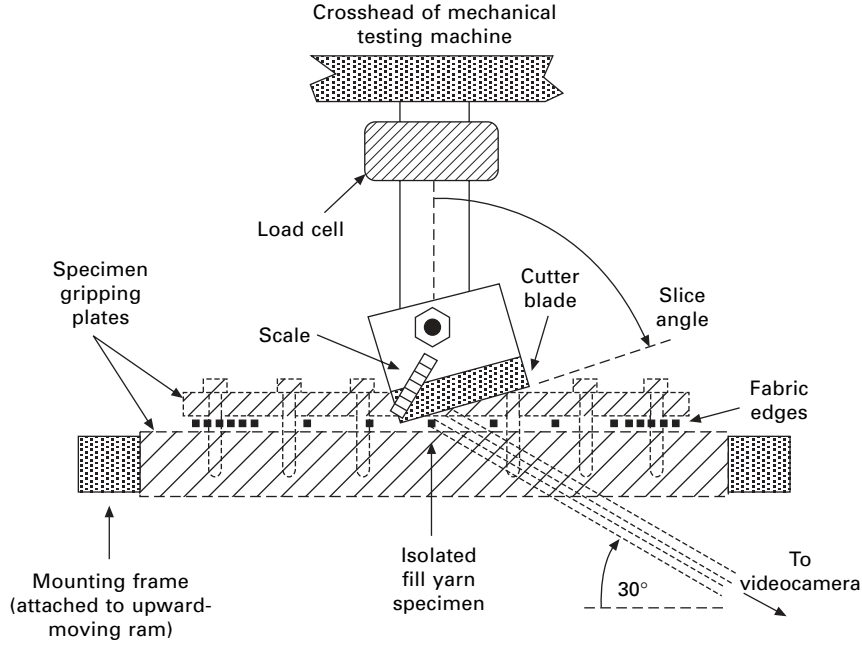

19.20 Cut testing. From Shin *et al.* [13].

strains will not. Any non-uniformity in the distribution of stress between different parts of the structure will lower strength.

Failure is a competitive phenomenon, determined by extreme value and not central value statistics, and will always occur in whichever way is easiest. Even at the theoretical level of a perfect crystal, this means that rupture may occur not under tensile stress across the plane AB in Fig. 19.22(a) but under some other stress, such

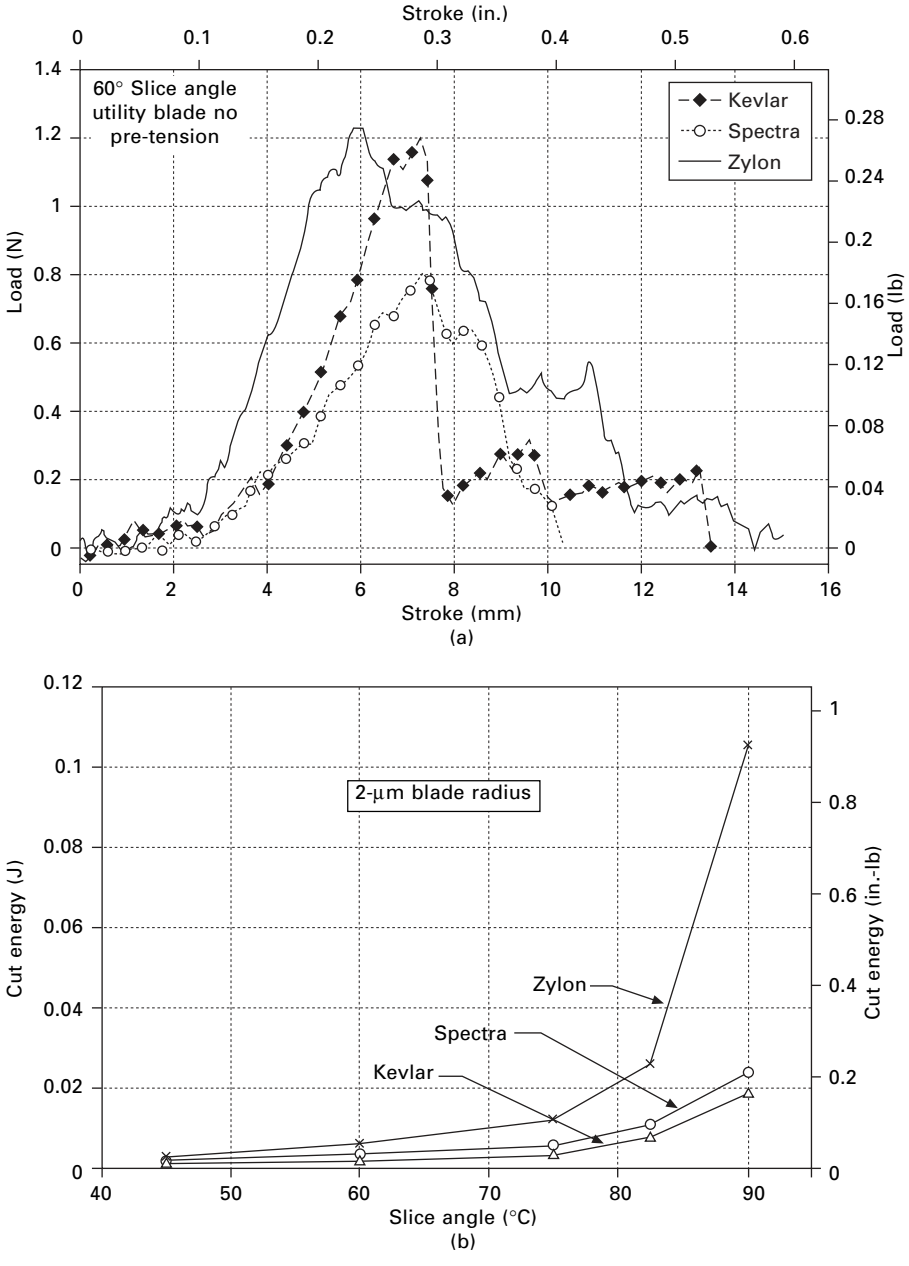

19.21 Cut test results: (a) force-stroke plot; (b) effect of slice angle. From Shin *et al.* [11].

as the resolved shear stress across CD. At the practical level, there are all the complications of local variations in stress due to gross structural differences, of stress concentrations at microscopic defects, and of uneven sharing of load at the molecular level in an imperfect structure. As indicated above, the interaction of defects with

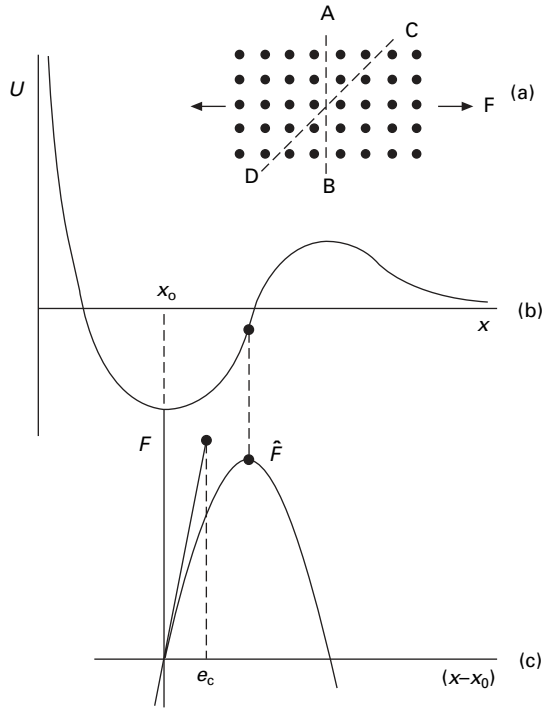

19.22 Simple theory of tensile strength: (a) perfect crystal under tensile force *F*; (b) variation of internal energy *U* with spacing *x*; (c) variation of force *F* with elongation $(x–x_o)$.

very high anisotropy leads to completely different modes of failure in the oriented linear polymer fibres. The simple argument also ignores the time-dependence associated with thermal vibrations, which allows jumps over the point of inflection as discussed in Sections 20.2.1 and 20.7.2.

The role of defects is critical. The foundations of fracture mechanics were laid by A. A. Griffiths in 1921. He emphasised the role of flaws either on the surface or internal, which led to stress concentrations. A direct approach models the stress distribution round a defect. The crack will propagate when the stress at its tip exceeds the fundamental value of the strength as discussed above. A more useful approach depends on the relation between the elastic energy released by crack growth and the increase in surface energy d*S*. The crack will propagate when $dE > dS$. The deeper the defect, the greater the stress concentration or energy release, so that once the inequality is reached the crack will continue catastrophically across the fibre.

The classical theory applies well to brittle fibres such as glass, where the deformation is purely elastic. When there is also plastic deformation, the situation is more complicated. If there is a small, localised, plastic zone, an additional energy term can be added to d*S* without altering the basic analysis. Modifications can be made when the plastic zone is large compared with the crack depth. The mechanics of the ductile fracture of nylon and polyester fibres raises more difficulties. As indicated by the tensile break of a polyester film in Fig. 19.23, the plastic deformation would extend

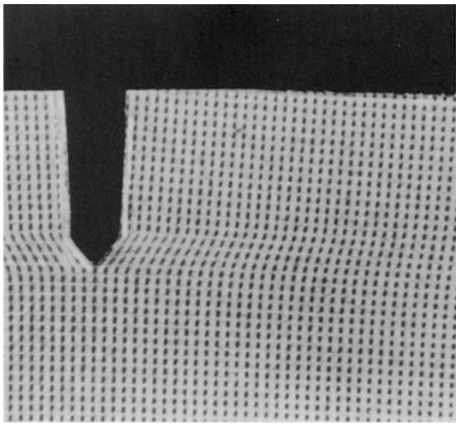

19.23 Tensile break of a marked polyester film.

right across the fibre and for a considerable length along the fibre, where it is linked to the unstressed region in line with the crack by a shear zone.

The mechanics of this complexity has not been analysed. It should be noted that the material across from the crack is under a higher stress than unaffected remote parts of the fibre length and is extended by larger amounts than the measured break extension of the fibre. The stress-strain relation at these stresses is unknown.

Michielsen [12, 13] has studied the fracture toughness of nylon 66 monofilaments. Applying fracture mechanics, he derives a value of 17 kJ/m^2 for the energy release rate at 65% r.h., rising to 31 kJ/m^2 at 0% r.h. and falling to 16 kJ/m^2 at 100% r.h.

In other forms of break, granular, axial splitting, fibrillar, the stress concentrations that lead to failure are distributed in more complex ways. However, the fundamental principle that cracks will propagate when it leads to a reduction of energy remains valid. The problem is how to calculate the energy terms.

19.3 Tensile fatigue

The classic definition of fatigue, as found, for example, in metals, is of failure under cyclic straining at a level that would not cause failure if applied as a constant strain. There has been a search for similar effects in fibres.

One of the problems has been that in simple extension-cycling, the load progressively decreases owing to stress relaxation: failure does not occur unless the imposed extension is very close to the usual breaking extension. Most fatigue testers therefore operate on the principle of cumulative-extension cycling, with the slack removed at the end of each cycle. This work has been reviewed by Hearle [14]. However, as shown in Section 15.7.3, a common result of such a test at larger imposed extensions is a climb up the stress–strain curve to the normal breaking point. At low imposed extensions, failure does not occur. There have been some indications that fatigue effects might be important over a narrow range of imposed extensions.

Table 19.2 gives a comparison of the behaviour of fibres in such a cumulative-extension test.

Table 19.2 Median number of cycles to break for various yarns in cumulative-extension test (from Booth and Hearle [15])

	Imposed extension (%)					
Fibre	$2\frac{1}{2}$	5	$7\frac{1}{2}$	10	$12\frac{1}{2}$	15
Viscose rayon	†	79		6		
Acetate	32 000	58		6		
Nylon			$>5 \times 10^5$	11 000	220	12
Polyester fibre		$>5 \times 10^5$	16 000	18	7	

†Four out of ten had failed at 5×10^5 cycles.

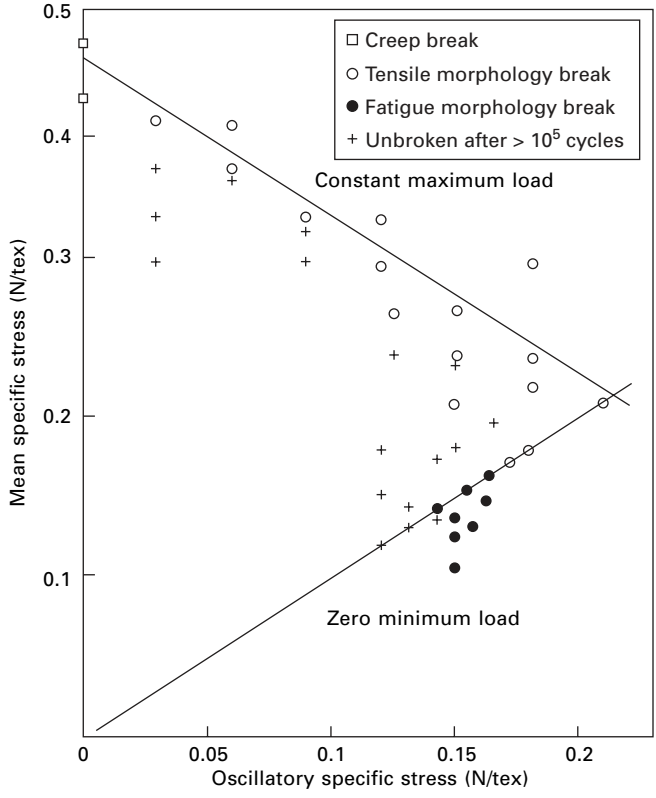

19.24 Failure conditions in fatigue-testing of nylon [17].

More interesting results have been obtained with a controlled-load fatigue tester operating at 50 Hz [16]. The specimen is cyclically strained by a vibrator acting on one end of the fibre, and the clamp at the other end is driven through a servo-system to maintain the peak load constant.

Studies of nylon by Bunsell and Hearle [17] showed that, at high maximum loads, failure occurred in the same time and the same mode as in a creep test. This gives the failures about the line of constant maximum load in Fig. 19.24. Under these conditions,

the cyclic nature of the loading has no effect, and the behaviour could be predicted from studies of creep failure.

However, at much lower maximum loads, between one-half and two-thirds of the equivalent creep breaking load, failure occurred provided that the minimum load in each cycle was zero. This gives the breaks about the line of zero minimum load in Fig. 19.24. At an intermediate state, with higher maximum and minimum loads, failure did not occur.

The fracture morphology is also different. In creep failure, and at the high maximum loads, the fracture showed the V-notch typical of tensile failure, as in Fig. 19.3. But the fatigue failures, at zero minimum load, were quite different in appearance. One end showed a long tail, which had stripped off the other end, as shown in Fig. 19.25. The sequence of events is that an initial transverse crack appears (Fig. 19.26(a)), and this then turns and runs along the fibre, to become gradually wider and deeper (Fig. 19.26(b)), until final failure occurs with a tensile break across the reduced cross-section. The angle of the crack in nylon is about 10°, so that the tail is about five fibre diameters long.

In more recent work, Oudet and Bunsell [18] have shown that zero minimum load was not an absolute criterion for tensile fatigue failure in nylon fibres. For a particular sample of nylon, fatigue failures were found with a small positive minimum load. They were still present, together with some creep failures, when the minimum load was 4% of breaking load but were absent when it was increased to 6%.

A similar tensile fatigue failure is found in polyester fibres [19, 20], though the fatigue lifetime is greater than that in nylon. Another difference is that the axial crack in polyester fibre runs almost parallel to the fibre axis and leads to extremely long tails (Fig. 19.27(a)). The other end shows where the material is stripped off (Fig. 19.27(b) and in this example the final failure has occurred where there is a weak

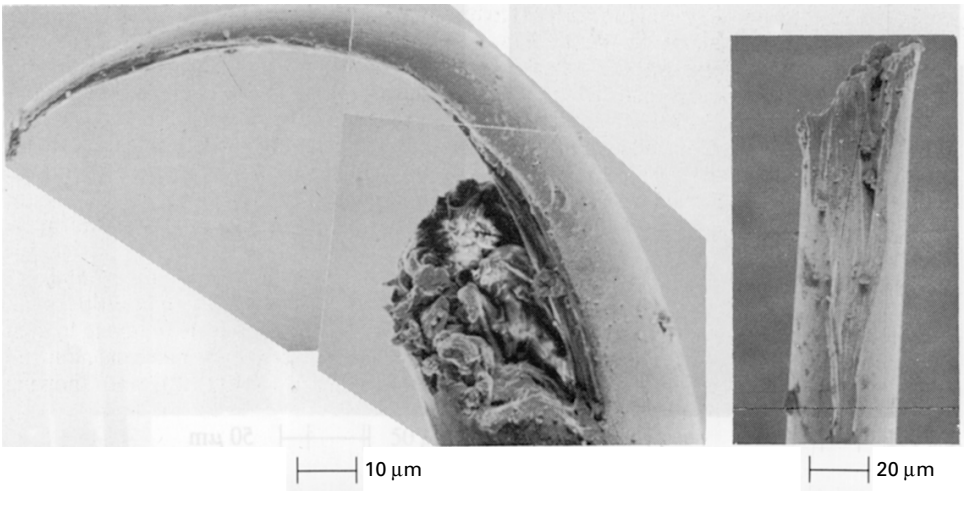

19.25 Opposite ends of break of nylon 66 fibre after 62 000 cycles at 50 Hz between zero load and 71% of normal break load.

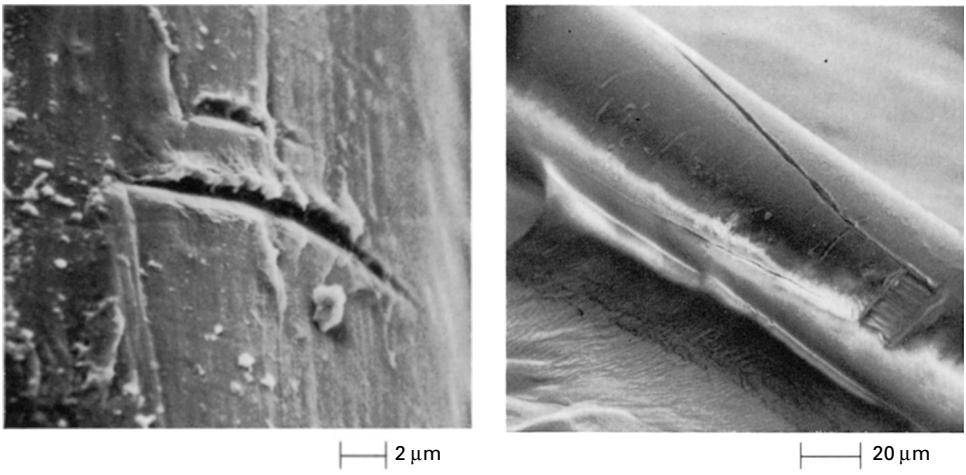

19.26 (a) Initial transverse crack in tensile fatigue. (b) Shear crack runs along the fibre.

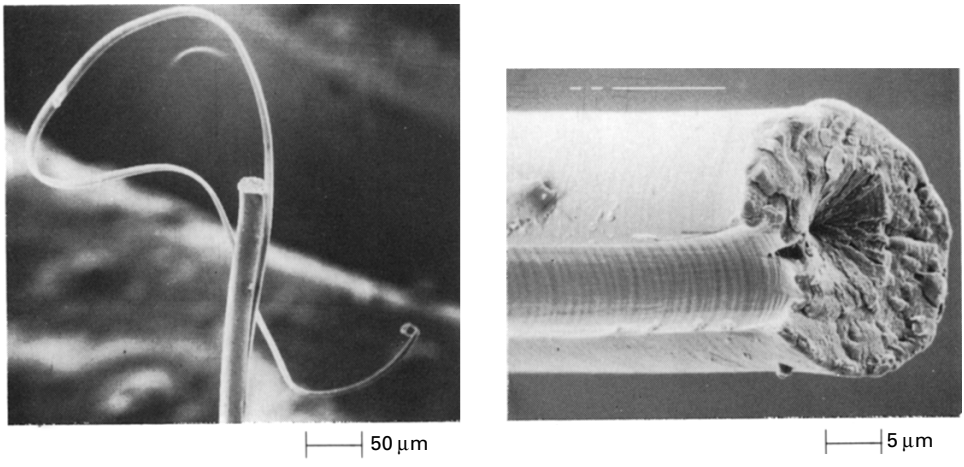

19.27 (a) Break of polyester fibre after 83 000 cycles at 50 Hz between zero load and 65% of normal break load. (b) Final break of a polyester fibre by tensile fatigue.

place due to an internal defect in the fibre. Although the long axial splits eventually lead to complete fibre rupture over the remaining cross-section in a single-fibre test, they would not necessarily do so in an assembly in which the fibres are held together by twist or other means and mutually support one another.

Bunsell and his colleagues have continued to study tensile fatigue failures in nylon and polyester fibres. In nylon 6 and 66, final rupture occurs when the crack reaches a point where the reduced cross-section leads to tensile failure, but in polyesters, PET and PEN, it is by creep at a point further back along the crack [21]. The transverse

cracks, which initiate the failure, are attributed to hard inclusions, which may be introduced as catalysts, antioxidants or flame retardants, at the interface between skin and core about 1 μm below the surface [22]. In a study of the effect of temperature on seeral mechanical properties, a threefold decrease in fatigue lifetime was found for polyester fibres [23].

In the meta-aramid fibre *Nomex*, tensile fatigue occurs in a similar form to that in nylon [19]. In an acrylic fibre *Courtelle*, tensile fatigue causes failure by axial splitting, but there is no requirement that the minimum load should be zero in order to promote this mode of fatigue failure. A comparison of typical tensile fatigue failure conditions is given in Table 19.3. The breaking extension in the fatigue tests is lower than that in the tensile tests. This confirms that a special fatigue mode of failure is occurring and provides a means of differentiating from a creep failure after repeated cycling, which occurs at the same breaking extension as in a tensile test.

In the para-aramid fibre *Kevlar*, tensile–load cycling causes a much greater degree of axial splitting but no appreciable loss of strength [24]. In order to achieve failure in around 10^5 cycles, it is necessary to go to at least 90% of the normal breaking load, which is within the range of normal variability.

19.4 Torsional fatigue

Twisting, as discussed in Section 17.3, is the second easiest mode of load–deformation response to study in the laboratory, provided that only a single test to break or a few cycles of deformation and recovery are needed. However, fatigue testing, which requires a large number of cycles at relatively high speeds, is not so easy. For example, a typical test on a 1 cm test length twisted to half the breaking twist might involve a million revolutions, reversing every 50 revolutions. In these circumstances, it is easy to wear out a mechanical drive. Some studies of torsional fatigue, which were carried out before SEM was available to examine fracture morphology, were reported by van der Vegt [25] but these were made under rather severe conditions, which led to failure in less than 1000 cycles, with twist angles ranging from about 11° for rayon to 45° for nylon. There have been few later investigations.

Goswami and Hearle [26], as part of a comparative study of forms of fracture, carried out some torsional fatigue on a 1 mm length of a 16.7 dtex nylon fibre, vibrated to a twist angle of 45° at 5 Hz. Rupture occurred after about 16 hours. The

Table 19.3 Tensile fatigue failure conditions [21]

Fibre type	As percentage of breaking load		Fatigue life cycles	Breaking strain (%) in:	
	Minimum load	Maximum load		tensile test	fatigue test
Nylon 6.6 (MT)	0	62	0.8×10^5	36	25
Nylon 6.6 (HT)	0	55	0.5×10^5	17	11
Polyester fibre	0	65	2×10^5	20	12
Nomex	0	70	0.2×10^5	20	14
Courtelle	20	65	$0.04–2.6 \times 10^5$	55	45

failure started with the development of several splits running along the fibre, which led to the breaking away of chunks of material. Duckett and Goswami [27] have described a multi-station torsional fatigue tester, which has been used for studies of fibre failure related to pilling in fabrics [28].

Toney and Schwartz [29] report a linear decrease log(cycles to failure) with increase of surface strain.

19.5 Flex fatigue

19.5.1 Test method

The simplest way of repeatedly bending a fibre is to pull it backwards and forwards over a pin under sufficient tension to cause the fibre to follow the curvature of the pin surface as illustrated in Fig. 19.28. If the tension is applied by a hanging weight, the fibre is free to turn round, so that the application of tension on the outside of the bend and compression on the inside occurs rather irregularly on different parts of the fibre. It is therefore preferable to apply the tension by means of an elastic string [30] and to mount a card to check that there is no rotation. A simple, approximate description of the test would then be that a length of fibre, equal to the reciprocating stroke of the drive vibrator, is subject to an alternation between a straight and a bent form.

Application of classical bending theory, as given in Section 17.2.1, predicts that, in the bent state, the fibre strain would increase from zero at the centre plane to a maximum tensile strain e_b on the outside of the bend, and a maximum compressive strain $-e_b$ on the inside. Depending on the position within the fibre, the material would oscillate between zero strain and the maxima in tension or compression. The value of e_b is given by:

$$e_b = \frac{r}{R + r} \approx \frac{r}{R} \tag{19.1}$$

where r = fibre radius and R = pin radius.

In reality, there are a number of complicating factors, which will be discussed in more detail in Section 19.5.4. Firstly, there is the additional strain due to the applied tension. Secondly, the fibre cannot change abruptly from finite curvature on the pin to zero curvature off the pin, since there must be a zone of varying curvature with resulting shear stresses. Thirdly, friction on the pin will generate surface shear stresses.

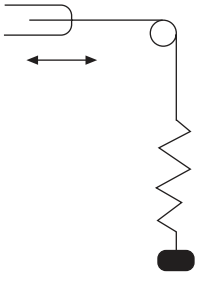

19.28 Flex fatigue over a pin.

These three effects are inherent in the mechanics of the test method and would be present even if the fibre were ideally linear elastic (Hookean). But, in fact, most fibres have non-linear stress–strain curves and, as shown in Section 17.2.4, yield more easily in compression than in tension. Consequently, a fourth complication is that the neutral plane shifts away from the geometric centre of the fibre, the maximum tensile strain is reduced, and the maximum compressive strain is increased. An exception to this rule occurs in wool and hair, which yield more easily in tension. Although the 'bending strain' e_b is thus not strictly a measure of maximum strain, it is a convenient quantity to quote as an indicator of the severity of bending in a flex fatigue test.

Temperature and moisture conditions are found to have a considerable influence on flex fatigue, and the apparatus has therefore been modified so that four test positions are enclosed within a box under controlled atmospheric conditions [31]. A complete statement of test conditions should include: bending strain, tension, temperature, humidity, and the state of the pin and fibre surfaces.

19.5.2 Modes of failure

The bending of fibres with yield in compression causes the appearance of kink-bands as illustrated for polyester fibre in Fig. 19.29. A single bend causes no detectable damage to the fibre. If tension is applied, the kink-bands are pulled out, and there is no loss of strength. However, fatigue tests [1, 30, 32] show that repeated flexing leads to failure. Three forms of damage occur in cycling over a pin. Initially, Fig. 19.30(a), there is some surface wear due to rubbing on the pin. This is an artefact not directly related to flexing and is discussed in Section 19.7. In addition, there are kink-bands, which have started to break up into a fibrillar or crazed formation and some incipient cracking. A complete crack, which would be on the compression side of the fibre, is shown in Fig. 19.30(b). Shear at the tip of the transverse crack has led to an axial crack. When the compression side of the fibre has failed, it ceases to be effective, and

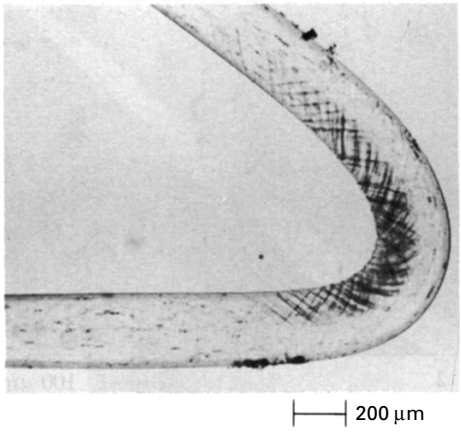

19.29 Kink-band, visible in polarised light, formed on the inside of a bent polyester fibre.

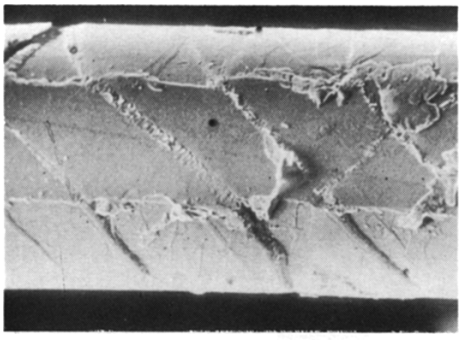

(a)

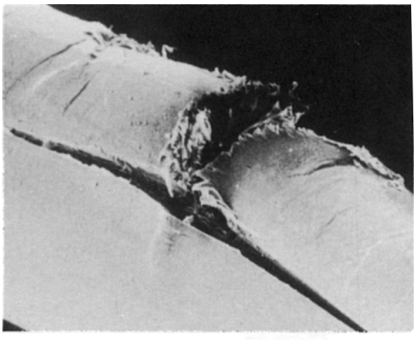

(b)

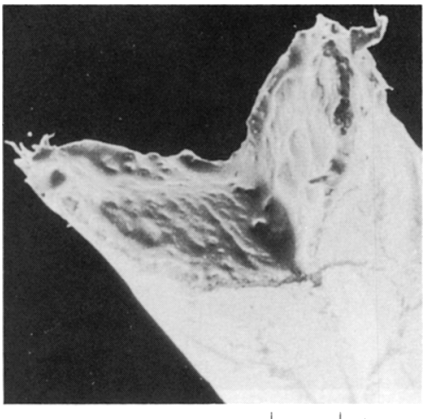

(c)

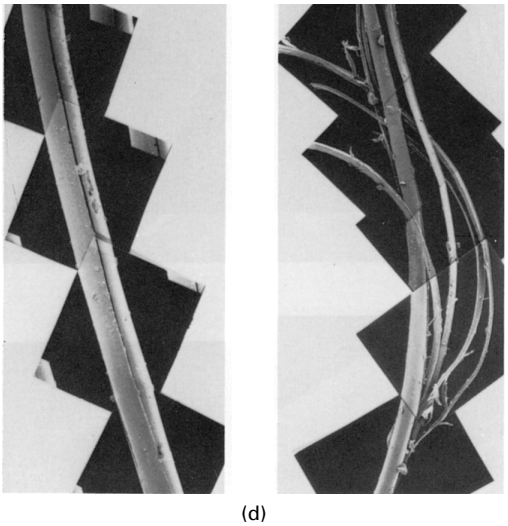

(d)

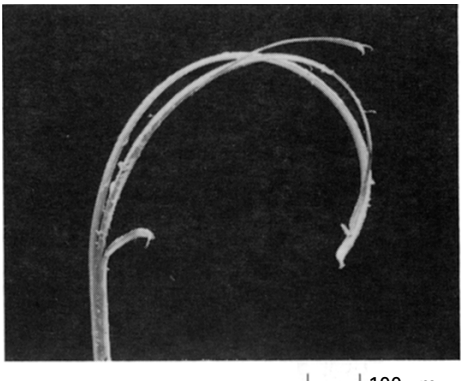

(e)

19.30 Forms of damage in flex fatigue over a pin: (a)–(c) polyester (PET) at 65% r.h., 20 °C; (d) nylon 66 at 60 °C, 30% r.h.; (e) polyester (PET) at 80 °C, 5% r.h.; (f) nylon 6 at 100 °C, dry air.

the other half of the fibre then bends independently, so that the same mechanism can repeat itself, with the formation of more angular cracks, which constitute this mode of failure in flex-fatigue tests. In tests in which the fibre is allowed to rotate, kink-bands will come in from all sides and a final break occurs along the angle of kink-bands (Fig. 19.30(c)). This mode of flex fatigue failure, which is directly related to the compression that occurs in bending, is found in some examples of wear in use [1]. However, another mode of failure can also occur. Variable curvature results in shear stresses, which lead to single or multiple splits, Fig. 19.30 (d, e). As the fibre is pulled over the pin, the region of shear stress will travel along the fibre and cause long axial splits. Failure by multiple splitting is the commonest mode of failure in use, but may result from twisting, bending or a combination of both.

Observations of the development of damage in flex fatigue testing is reported by Hearle and Miraftab [33].

19.5.3 Flex fatigue lifetimes

The statistical variability of fatigue tests of fibres is usually fairly high, and the results are most conveniently expressed by survivor diagrams. Typical examples are shown in Fig. 19.31 for nylon and polyester fibres flexed over a pin with a diameter of 0.25 mm under standard atmospheric conditions (65% r.h., 20 °C). The mechanical conditions are similar, but not identical, as indicated in Table 19.4 [31], which also includes some statistical data on lifetimes. The median is the most convenient measure to quote, since it avoids large errors due to a few abnormally large or small values.

Flex fatigue has been found to be very dependent on conditions of temperature and humidity. A set of results obtained by Miraftab [32] for the 22 dtex nylon 6 fibre, under the same conditions as given in Table 19.4, are shown in Fig. 19.32. The median lifetime ranges between about 30 000 cycles at 5% r.h., 20 °C and 600 000

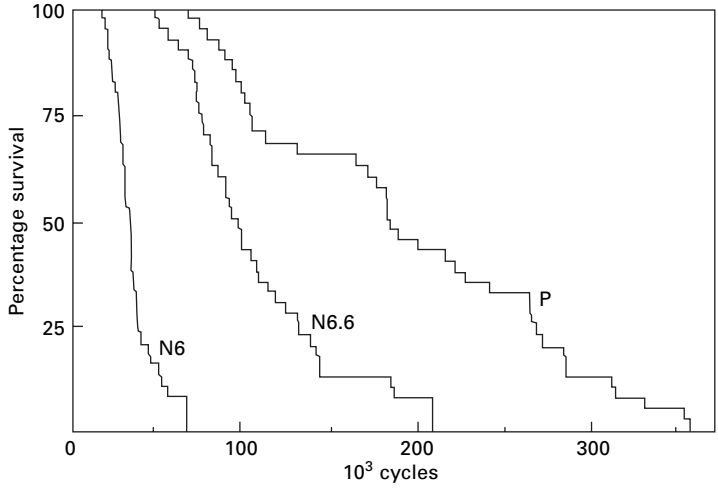

19.31 Survivor diagrams for nylon 6 (N6), nylon 6.6 (N6.6) and polyester (P) fibres flex-fatigued under conditions shown in Table 19.4 [32].

Table 19.4 Flex fatigue tests at 65% r.h., 20 °C [34]

Fibre	Linear density (dtex)	Bending strain (%)	Specific stress (mN/tex)	Fatigue lifetimes in cycles		
				Mean	Median	Coefficient variance (%)
Nylon 6	22	16.1	54	35 825	34 725	32
Nylon 6.6	13.6	13.5	73	104 807	98 050	34
Polyester	13.3	12.4	75	194 616	187 825	44

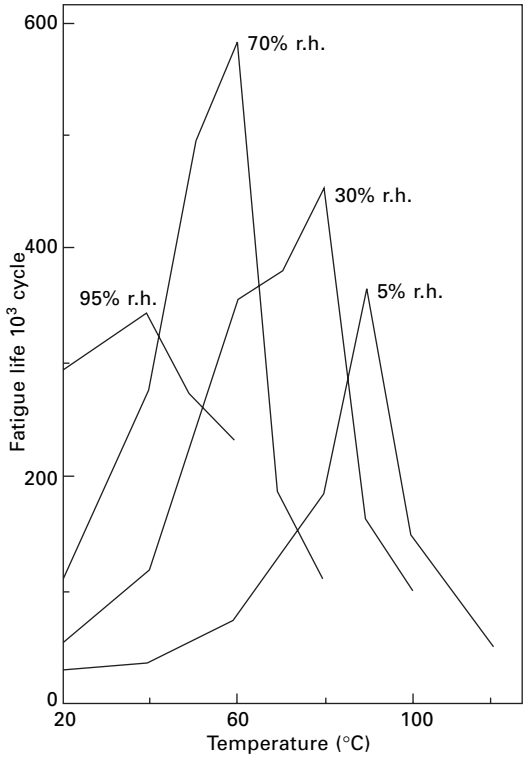

19.32 Effect of temperature and humidity on median-flex fatigue life of nylon 6, with test conditions as in Table 19.4 [31].

cycles at 70% r.h., 60 °C. The peak lifetime positions are remarkably similar to the peaks in the loss modulus, as shown in Chapter 18. The closest comparison in terms of temperature and humidity is with Fig. 19.33, though this is for nylon 6.6, but the tan δ peaks in nylon 6 are similarly located (see Section 18.3.1). Miraftab's flex fatigue results for nylon 6.6 show the same trends, but the curves are shallower, and the only sharp peak is at 60 °C and 70% r.h. For the polyester fibre, the peak lifetime at 5% and 30% r.h. occurs at about 65 °C. The absence of an effect of humidity is expected in this material, but the temperature is lower than for the peak in tan δ. At higher humidities, the plots of flex fatigue life against temperature are almost flat.

The reasons for the association between a high flex fatigue life and dynamic loss

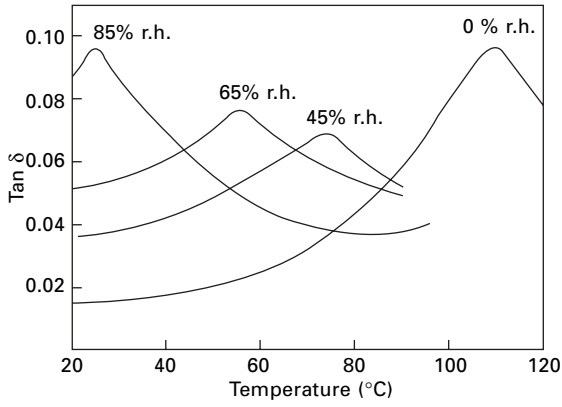

19.33 Effect of temperature on tan δ for nylon at various humidities. From Meredith [34].

in deformation are not clear. Furthermore, the test is complicated by the fact that a number of properties of fibres are affected by temperature and humidity. In addition to the bulk mechanical properties, the fibre friction will change and so alter the stress pattern. Effects may be masked because one mode of breakdown takes over from another as the mode with the shortest life. Miraftab [32] found that the dominant forms of failure were as follows: kink-bands, type (9) in Fig. 19.1, at lower humidities and temperatures; axial splits, type (10), at intermediate values; and surface wear, type (12), at higher values.

Sengonul and Wilding [35, 36] studied the flex fatigue of *Dyneema* gel-spun HMPE fibres. Figure 19.34 shows the fatigue life dependence on (a) tensile stress and (b) temperature. Failure is by multiple splitting.

19.5.4 Mechanics of the flex test

A perfectly flexible fibre, with no resistance to bending, would follow the curvature of the pin surface and then run straight to the clamps, as shown in Fig. 19.35(a). If we ignore any deviations from this geometry, neglect the tension applied to the fibre, and assume that the material follows Hooke's law, there will be zero stress in the straight part, and the analysis given in Section 17.2.1 will apply to the bent part. On the central neutral plane, the stress and strain will be zero, but along the contact with the pin there will be a compressive strain $-e_b$ given by equation (19.1), and a corresponding specific stress $-Ee_b$, where E is the tensile modulus of the fibre, and at the opposite extremity there will be a tensile strain e_b and a stress Ee_b.

Most fibres, as discussed in Section 17.2.4, have non-linear stress–strain relations and yield more easily in compression. Consequently, the neutral plane moves out in order to balance the moments on either side (or minimise the deformation energy), the compressive strain is increased, and the tensile strain is reduced. On the basis of this model, it follows that if the fibre is not allowed to rotate, the material will oscillate between zero strain and a magnitude of tensile or compressive strain determined by the distance from the neutral plane. The compressive effect will be more damaging

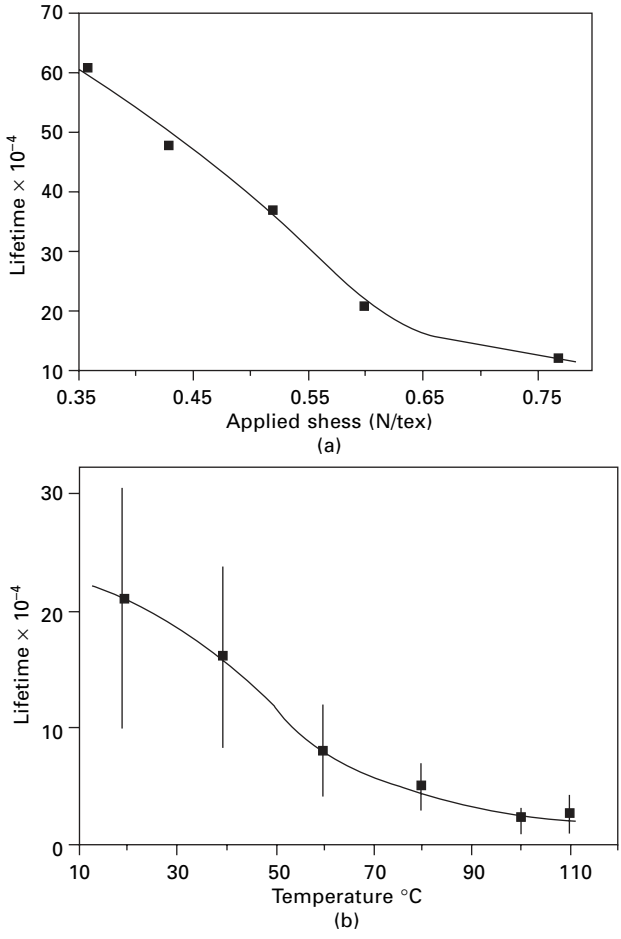

19.34 Flex fatigue at 50 Hz of HMPE fibres at nominal bending strain of 4.95%: (a) effect of applied stress at 20 °C; (b) effect of temperature at 0.6 N/tex. From Sengonul and Wilding [36].

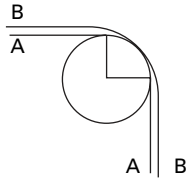

19.35 Comparison of fibre paths over a pin: A, perfectly flexible; B, real.

than the tensile in an oriented linear-polymer fibre, and thus the kink-band mode of failure can be expected. In wool and hair, the strain distribution, but not necessarily the damage, will be reversed because yield occurs more easily in tension.

In reality, the forms are not as simple as indicated above, and other stresses will also be present. Firstly, some tension is needed to hold the fibre in contact with the

pin. For the curved portion of the fibre, this superimposes a small tensile strain as a correction to the strains indicated above, and the plane of zero stress is displaced slightly inwards. However, it does mean that the straight part is under tension, and it may well be that an oscillation between compression and even a small tension will cause a greater disturbance of the fibre structure than one between compression and zero tension.

Secondly, there will be normal and frictional forces at the contact between the fibre and the pin. The most obvious effect of this is to add alternating shear stresses in the material close to the contact point, and these can promote surface-peeling and wear. However, a full analysis of contact stresses may show up other damaging features.

In well-designed experiments, these two effects can be regarded as minor corrections. The tensile stress is kept small, and, if necessary, the frictional effects can be reduced by allowing the pin to rotate. However, there is a third feature, which is more fundamental. The assumption that the fibre changes abruptly from curved to straight implies a discontinuity in bending moment, which cannot occur in practice. In reality, the length in contact with the pin is reduced and there is a zone of gradually reducing curvature, as shown in exaggerated form in Fig. 19.35(b).

Miraftab [32] has shown that, for a fibre with flexural rigidity B, under a tension T, the contact length on the pin is reduced at either end by an amount l_0 where l_0^2 equals B/T. For the maximum curvature to be determined by the pin radius, the applied tension must be large enough to make less than the nominal contact length for a perfectly flexible fibre. Away from the ends of the contact region, the curvature is given by:

$$c = c_0 e^{-l/l_0} \tag{19.2}$$

where l is the distance from the pin contact and c_0 is the curvature of the pin surface, equal to the reciprocal of the pin radius.

Standard textbooks on strength of materials, such as that by den Hartog [37], show that the change in bending moment in variable curvature is balanced by a shear force, S given by:

$$S = B\frac{dc}{dl} = -B\left(\frac{c_0}{l_0}\right)e^{-l/l_0} \tag{19.3}$$

The standard theory also shows that, for a Hookean material, the shear stress in a fibre of radius r is a maximum, equal to $(4S/3\pi r^2)$ at the centre plane of the fibre and reduces in proportion to $[1 - (y^2/r^2)]^{1/2}$ with the distance y from the central plane.

For the fibre over the pin, the highest shear stress will occur on the centre plane at the point at which the fibre leaves the pin and will be given by $-[4(B/T)^{1/2}\, c_0/3\pi r^2]$. The shear stresses will decrease with the distance from the centre plane and with the distance from the pin contact. However, it is these shear stresses that can cause the fibre to fail by splitting.

A qualitative summary of the stress pattern is presented in Fig. 19.36, which is at least a second approximation to reality, because there will be other complications arising from localised stresses and from the non-linear and inelastic properties of fibres. The lines in the diagram show how the major contributions to the stress at the

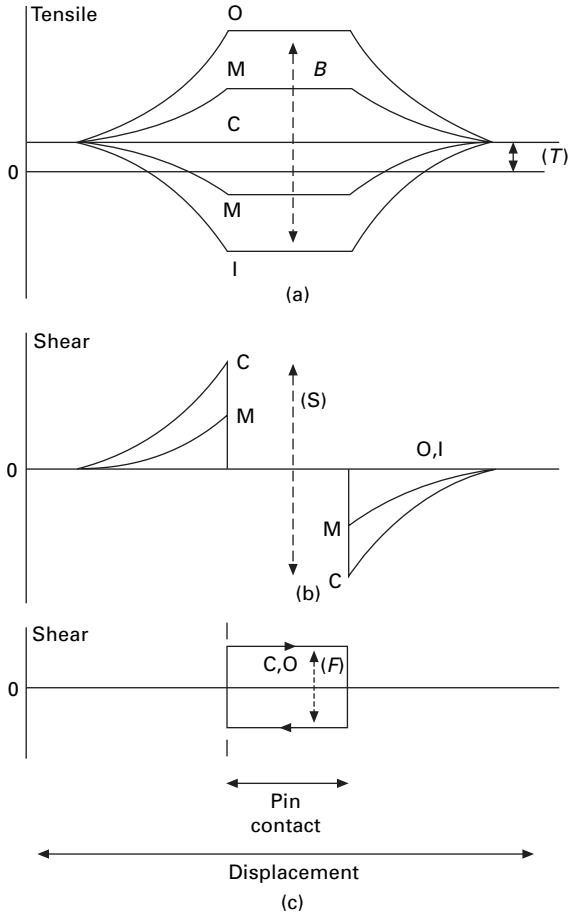

19.36 Main stresses in a flex fatigue test: C, on centre plane; I, on inner surface in contact with pin; O, on outer surface; M, intermediate positions. (a) Tensile stress due to bending (B) plus the constant tensile stress (*T*): note that zero-stress line will move out for a fibre that yields easily in compression. (b) Shear stress (*S*) due to change of curvature: there will be a shift associated with displacement of the neutral plane. (c) Frictional shear stress (*F*), alternating in direction as the fibre moves in opposite directions.

centre plane and extremities of the fibres vary along the fibre. Under normal test conditions, the axial displacement of the fibre by the drive mechanism will be much longer than the nominal contact length over the pin and so will be longer than the length over which the stresses are varying appreciably. Consequently, the material will move backwards and forwards through the stress field, given by summation of the components shown in Fig. 19.36, as the fibre is cycled.

19.5.5 Reduction in tensile strength after flex cycling

Hearle and Miraftab [33] report the loss of tensile strength due to flex fatigue. Figure 19.37(a) shows that change in the stress–strain curves of nylon 6.6 fibres after various

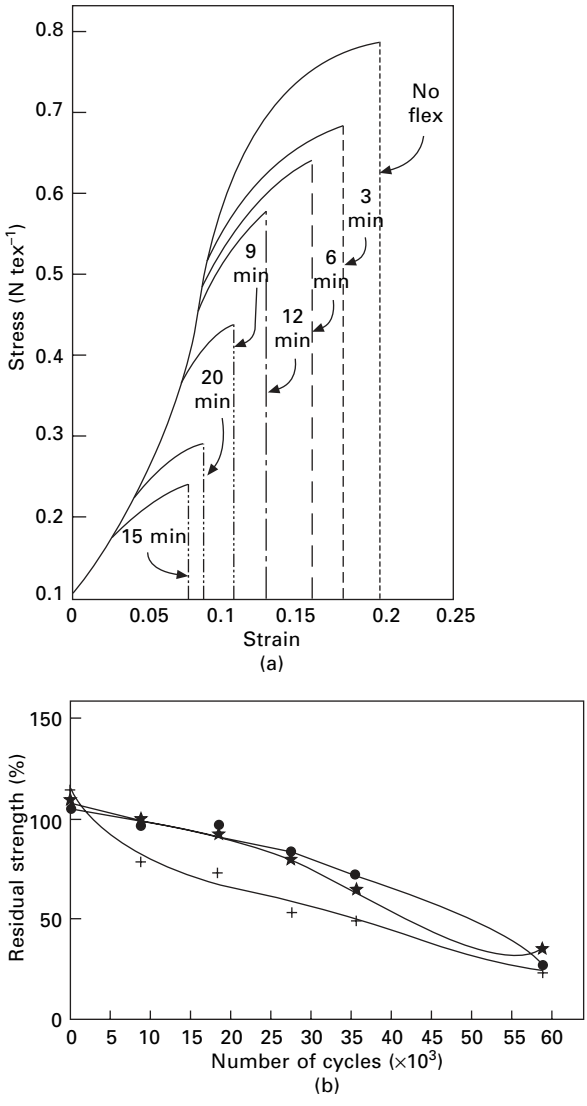

19.37 Tensile testing of fibres after flex fatigue cycling at 50 Hz, so 10 mins = 30 000 cycles: (a) stress–strain curves of nylon 6.6 fibres; (b) residual strength; * nylon 6.6, 6 ● nylon polyester [33].

times of flex cycling. The initial part of the stress–strain curve is unchanged, but only a fraction of the tensile test covered the part of the fibre that was subject to flexing over the pin. However, this zone provides a substantial yield section before breakage. Nylon 8 has a similar behaviour, but polyester follow an unchanged curve up to the reduced break point, except for the fibre fatigued for the longest time. Figure 19.37(b) shows that the rate of loss of strength is similar for all three fibre types. The nylon fibres typically show two V-notch breaks separated by a central split. Polyester fibres showed more multiple splitting.

19.6 Combined bending and twisting: biaxial rotation

19.6.1 Test methods

For coarse monofilaments, Lyons [38] introduced a method of studying bending fatigue by biaxial rotation, as illustrated in Fig. 19.38(a). However, this method, which was also used by Hearle and Vaughn [39] is not convenient for textile fibres because it would be necessary to miniaturise the rotating and clamping arrangements in order to achieve a high enough curvature and to control fine fibres. Nevertheless, the mode of failure by multiple splitting is very similar to that found in many examples of wear in use, so it was desirable to find a way of adapting it for testing fibres. The solution is to concentrate the curvature by passing the fibre over a pin under a small tension, as shown in Fig. 19.38(b) and (c). Surface wear, as a result of rubbing on the pin, has not proved to be a problem, except in fibres such as wool and *Kevlar*, which are highly susceptible to this form of damage. The friction will impose a drag and generate torque and twist in opposite senses in the portions of fibre on either side of the pin. Even in the tests on monofilaments without a pin, the splits followed helical lines in opposite senses in each half of the test length, which indicated false twist about the centre point, as shown in Fig. 19.38(a). As explained below, this is due to hysteresis ('internal friction'), and means that, in addition to the cyclic bending as the fibre is rotated, torque also promotes failure.

In the first version of rotation over a pin [26, 40], indicated in Fig. 19.38(b), the fibre rotation was driven from one end, with a weight hanging from the other end. Although this method gave interesting results, some of which will be quoted later, the fibre was not well controlled, and there were unwanted inertial forces from the rotation of the weight. Consequently, a change was made to driving from both ends, as shown in Fig. 19.38(c). Various different instrument designs were tried [41–44] with different drive methods to the fibre ends and different methods of applying tension to the fibre. The best method of tensioning consists of mounting the pin on a holder that is free to slide up or down a guide. The mechanical design is simplified if the drive shafts can be parallel, and the form used in one multi-station tester designed by Clark [44], which proved satisfactory for fairly coarse textile fibres, is shown in Fig. 19.39(a).

In later work [45], it was found that this apparatus was unsuitable for finer fibres. The first problem was purely mechanical. The frame holding the pin was too heavy, and, if it was made lighter, it tended to stick on the two guide bars. This problem was cured by having the pin mounted on a rod sliding in a tube, as shown in Fig. 19.39(b).

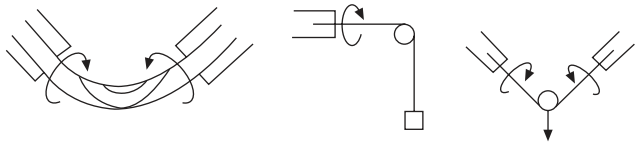

19.38 Forms of fibre biaxial rotation: (a) without a pin; (b) over a pin, driven from one end; (c) over a pin driven from both ends.

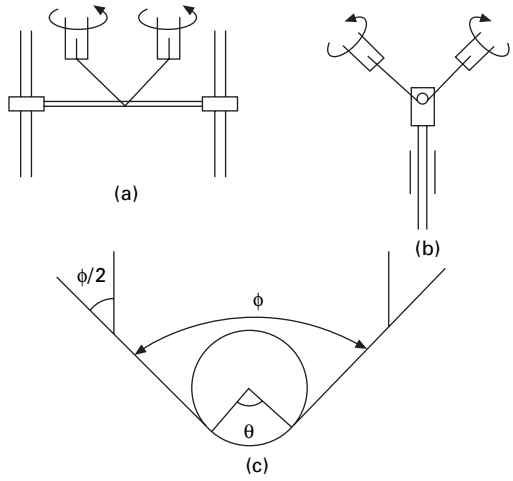

19.39 Arrangements in multi-station testers: (a) first type, with pin mounted on a beam sliding on two shafts; (b) second type, with pin mounted on holder sliding through single collar; (c) test angle, ϕ and wrap angle θ.

The other problem involved the mode of fibre failure and depended on the test angle, ϕ, as defined in Fig. 19.39(c). The fibre is bent through an angle $\phi/2$ where it is clamped to the drive shaft If ϕ is too large, jaw breaks, which are not determined by conditions at the pin, can result. If ϕ is too small, the angle of wrap, $\theta = (\pi - \phi)$, round the pin becomes large. Under these conditions, it was found that anomalous failures, called 'direct breaks', could occur after a small number of cycles and before the false twist had fully developed [46]. Direct breaks appear to be associated with an irregular motion of the fibre as it rolls and slips over the pin before reaching a steady motion, with the torque fully developed and overcoming the external and internal friction. Direct breaks show evidence of the fibre softening and melting, with localised deorientation, contraction to form bulges, and the formation of voids seen in the broken fibres. The detail of how this happens is not understood. For the coarser fibres being studied by Clark and Hearle [43], it was possible to find suitable intermediate values of ϕ that avoided both direct and jaw breaks. However, this was not possible in the later work of Liolios [45] on finer fibres, and a new multi-station apparatus was made with the drives aligned, as in Fig. 19.39(b), so that there was no bend where the fibres were clamped, and jaw breaks were eliminated. With $\phi = 90°$, the occurrence of direct breaks was negligible.

19.6.2 The form of failure

In biaxial rotation without a pin, two zones of splits, which twist in opposite direction, join in a more intense damage zone, which eventually ruptures (Fig. 19.40(a–c)). In fairly thick textile fibre, the two regions with helical splits are separated by an undamaged zone, which covers most of the length in contact with the pin (Fig. 19.40(d)). Rupture occurs at one of the positions at the end of splits. In finer fibres,

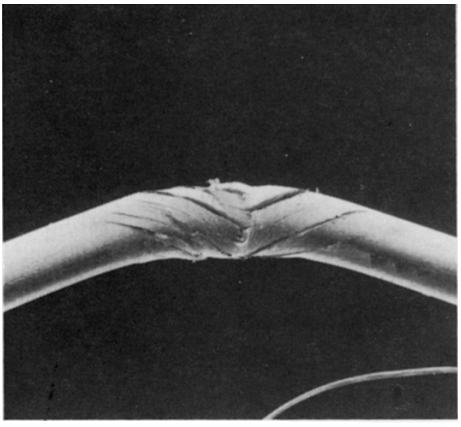

100 μm

(a)

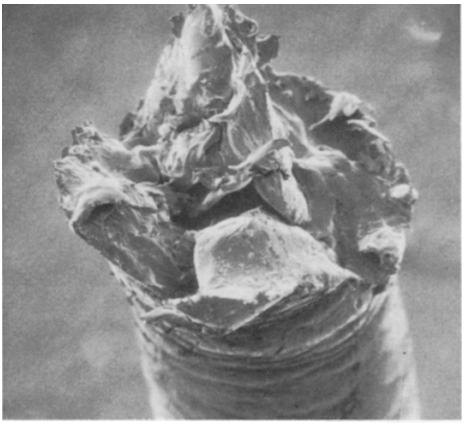

50 μm

(b)

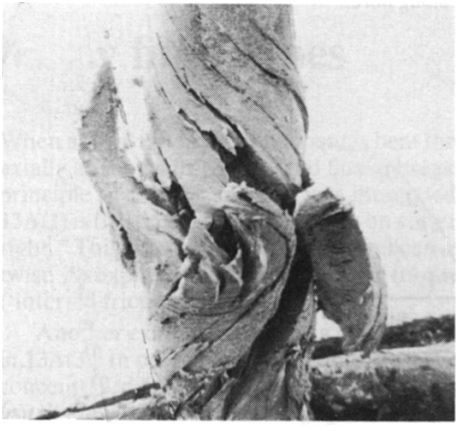

100 μm

(c)

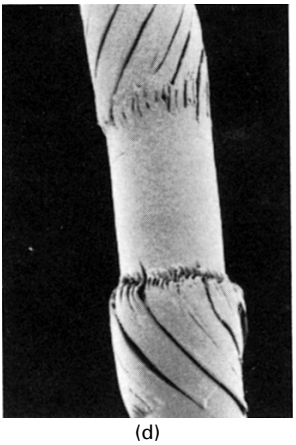

(d)

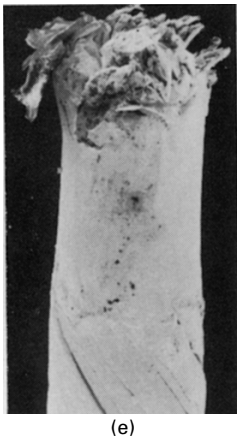

(e)

(f)

19.40 (a) Nylon monofil, 67 tex, in biaxial rotation without a pin. (b) Severe damage zone. (c) Break of the monofil. (d) Polyester fibre, 4.2 tex, after 1503 cycles in biaxial rotation over a pin. (e, f) Opposite ends of break at 2606 cycles.

the helical splits join and there is no undamaged zone [1]. In most fibres, there would be at least ten separate split portions in the final break, giving a brush-like end, but nylon gives fewer and larger pieces. This form of break by multiple splitting is also common in fibres after wear in use, though there can be confusion with splitting due to simple flex cycling or other causes [1].

The sequence of damage and loss of strength in fibres, rotated at 15 Hz over a 0.254 mm diameter stainless steel pin in water at 20 °C, has been described by Calil *et al.* [47]. For an 8.4 dtex polyester fibre, which gives a bending strain of 11%, there is no loss of strength up to about 2000 cycles, and the only visible damage consists of some kink-bands and some surface abrasion. There is then a linear loss of strength with number of cycles, accompanied by progressively increasing splitting, up to failure at about 4000 cycles. The helical splits cover the whole length of bent fibre.

In a thicker polyester fibre, of 42 dtex, with a bending strain of 20%, there were two regions of strength loss, in which the visible damage increased, preceded by two initiation regions (Fig. 19.41(a)). The final break divided into separate zones, both along and across the fibre (Fig. 19.41(b)). The axial separation is associated with the more severe stresses at the points at which the fibre leaves the pin, as discussed below. The transverse separation is due to the neutral plane moving out as indicated in Fig. 19.36. On rotation, this will cause an outer zone to suffer a damaging alternation of tension and compression, which causes splitting in the first period of strength loss. The inner zone will always be in compression in the early stages of the test and does

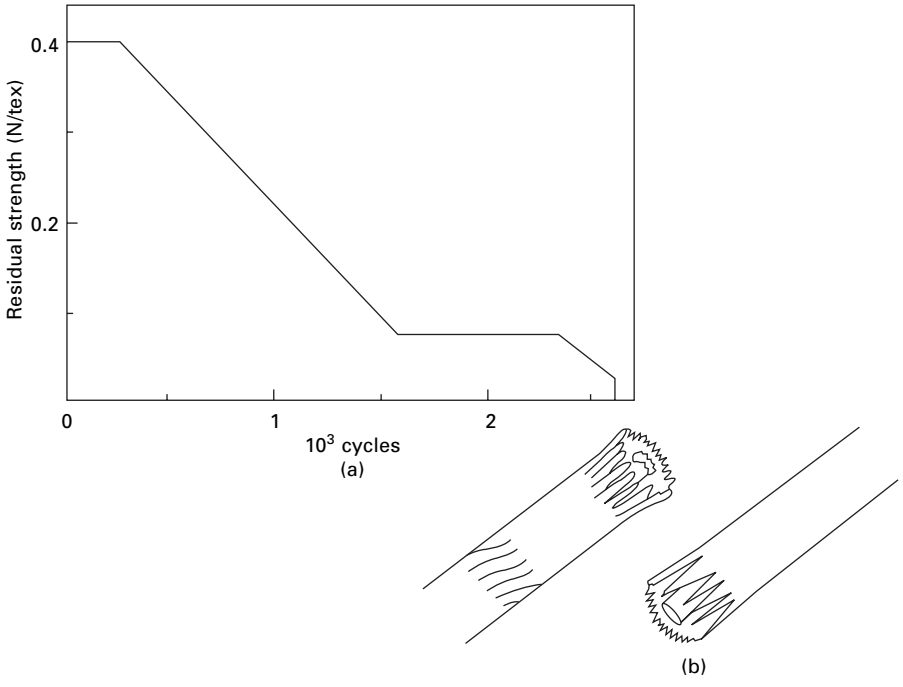

19.41 (a) Variation in retained strength for a 42 dtex polyester fibre subject to biaxial rotation in water at 20% bending strain. (b) The appearance of a fibre broken after 2600 cycles [47].

not start to break up until the outer zone is unable to resist stress and a further initiation of damage has occurred.

19.6.3 Statistics of fatigue failure

Figure 19.42 shows a histogram of the fatigue lifetimes from ten tests on each of ten stations for 17 dtex polyester fibres under typical test conditions in a laboratory atmosphere [48]. It should be noted that the biaxial rotation test operates on a very short length of fibre in contact with the pin (about eight fibre diameters for a 90° wrap at 10% strain). There was no significant difference in the results from different positions on the multi-station tester. The total range from 1878 to 9480 cycles is acceptably low for fatigue testing. The distribution is slightly skewed. The histogram for 17 dtex nylon had a similar shape, and the statistical parameters for both fibres are given in Table 19.5.

In these results reported by Clark and Hearle [48] and in earlier studies by Calil and Hearle [41] and Hearle and Wong [49], it was found that the statistics gave a reasonable fit to a Weibull distribution, as might be expected for an extreme value situation. However, from a practical viewpoint, the agreement was almost as good with a normal distribution of log(cycles to break).

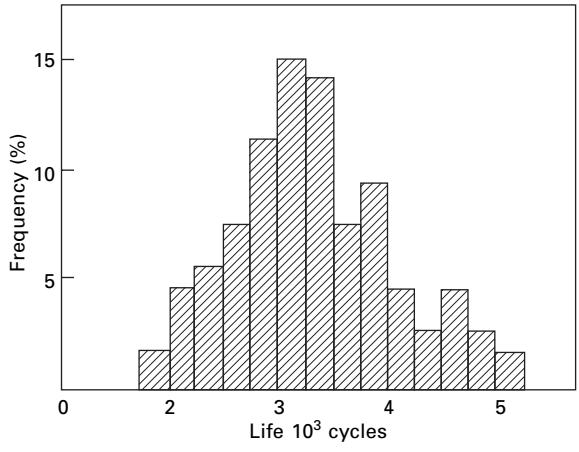

19.42 Distribution of fatigue lifetimes for 17 dtex polyester fibre rotated at 2.5 Hz, with a bending strain of 10% and a tension of 58 mN/tex (0.65 gf/den), at 20 °C, 65% r.h. [48].

Table 19.5 Statistics of fatigue failure [50] (test conditions as for Fig. 19.42)

	17 dtx polyester fibre	17 dtex nylon
Number of tests	100	100
Mean cycles to break	3352	5507
Median	3293	5282
Standard deviation	736	1320
Coefficient of variation (%)	22	24

In order to investigate statistical features, at least 100 tests are needed, but, for comparative testing, about 20 tests are adequate. A survival diagram is the best way to present the results, and the most useful parameters to quote are often the median fatigue life and the coefficient of variation.

19.6.4 Effect of mechanical parameters on fatigue life

There are several geometrical and mechanical parameters that affect biaxial rotation fatigue life. The state of the pin surface is usually not critical, unless it is highly abrasive or the fibre is of a type highly prone to surface wear. Figure 19.43 shows the influence of angle of wrap, as reported for 42 dtex polyester fibre by Clark and Hearle [43]. It can be seen that there is a very sharp change from the short lifetimes ending in direct breaks at high wrap angles to the longer times for fatigue breaks. Provided that the direct break region is avoided, and the jaw break region is not entered, the angle of wrap has only a small effect on fatigue life. As discussed in Section 19.6.1, smaller wrap angles must be used to eliminate direct breaks in finer fibres, and the design of equipment must then be changed to prevent jaw breaks.

The two most important normalised controlling parameters are the bending strain, given in terms of fibre diameter and pin diameter by equation (19.1), and the specific stress in the fibre. The latter is controlled by fibre tension, which, for the preferred form of apparatus shown in Fig. 19.39 is given by:

$$T = {}^{1}/_{2} W \sec(\phi/2) \tag{19.4}$$

where W is the total weight of the pin holder.

The effects of these two parameters are demonstrated in Table 19.6. As would be expected, the fatigue life decreases as the intensity of bending is increased and as the tension in the fibre is increased. Note that, in the second set of results, the specific stress on the fibre is decreasing, so that the effect of bending is under-estimated.

19.6.5 Environmental influences

It is easy to study the effect of different environments in biaxial rotation fatigue by immersing the fibre over the pin in liquid in a trough or by enclosing the whole

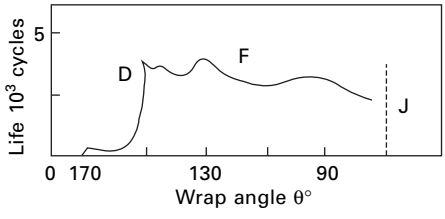

19.43 Change of mean fatigue life with wrap angle, θ (= π–ϕ), for 42 dtex polyester fibre rotated at 5.3 Hz with bending strain of 14% and tension of 86 mN in air regions are: (D) direct breaks, (F) fatigue breaks and (J) jaw breaks [43].

Table 19.6 Effect of bending strain and fibre tension on biaxial rotation fatigue

17 dtex nylon 6.6 rotated from one end with hanging weight [50]

	Median life in thousand cycles							
	In air				In water			
Bending strain (%)	Fibre tension (mN) 58	83	96	121	*58	83	96	121*
14	31	20	9.2	5.1	14	7.3	5.0	3.0
22	8.8	4.7	3.4	1.6	2.4	1.1	1.0	–
28	4.4	2.2	1.3	–	1.7	0.8	0.7	–

*not corrected for buoyancy

Polyester fibre rotated from both ends in air over same pin at 41 mN [43]

Linear density (dtex)	Bending strain (%)	Mean life (thousand cycles)
8	10	9.0
17	14	5.5
27	17	3.0
42	20	2.2

8 dtex Polyester fibre rotated from both ends in water at 10% strain [43]

Fibre tension (mN)	Mean life (thousand cycles)
6	27
20	12
30	10
41	7.8
70	4.0

apparatus in an environmental chamber for gaseous environments. The reduction in the fatigue life of nylon in water compared with air under standard conditions has been shown in Table 19.6. The effect of buoyancy means that the tension is lower in water, so that the effect of the change of environment is slightly reduced. The effect of temperature in the same series of experiments was to reduce the median fatigue life of 17 dtex nylon 6.6, tested in water at 14.5% strain and 108 mN tension, from 4207 cycles at 20 °C to 2356 cycles at 66 °C [50].

A more extensive study of the effects of temperature has been reported by Clark and Hearle [51]. The results for nylon 6 are shown in Fig. 19.44. The trend follows the trend in dynamic loss, tan δ, with the position of the maximum fatigue life increasing in humidity as the temperature is reduced. For polyester fibre, there is little effect of humidity, but, subject to some scatter in the results, the maximum fatigue life appears to decrease as the temperature increases from 0 to 80 °C. There is a linear relation between log(fatigue life) and reciprocal of absolute temperature, as shown in Fig. 19.45. In water, the fatigue lives of both nylon 6 and polyester fibre decreased with increasing temperature. In polyester fibre, the magnitude of the effect was similar to that in air, but in nylon 6 the effect was greater than that for air at 100% r.h.

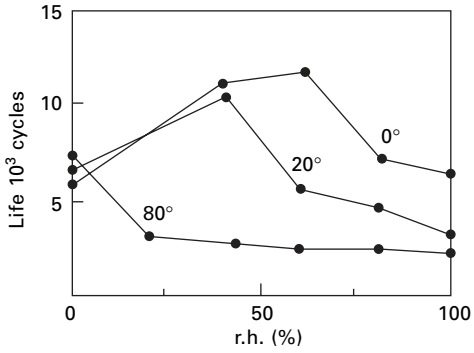

19.44 Variation of mean fatigue life with humidity at, 0, 20 and 60 °C for 17 dtex nylon 6 rotated at 2.5 Hz with a bending strain of 10%, a tension of 100 mN, and a wrap angle of 90°; the plots for 40 and 80 °C are close to those for 60 °C [51].

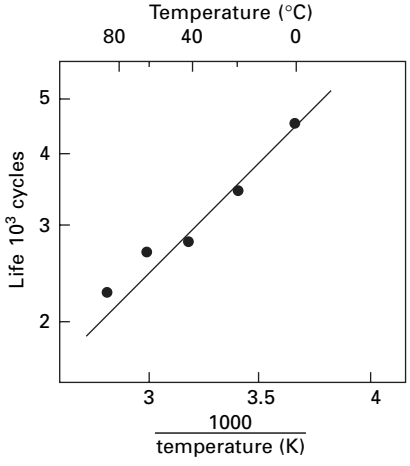

19.45 Relation between mean fatigue life on a logarithmic scale and reciprocal of absolute temperature for 17 dtex polyester fibre, tested under same conditions as for Fig. 19.44 [51].

The effect of changing pH on the biaxial-rotation fatigue of nylon 6.6 is shown in Fig. 19.46 [50]. From alkaline conditions in sodium hydroxide solution down through increasing concentrations of hydrochloric acid, there is no change in life until pH 2 is reached, but there is then a rapid linear decrease. The reduction in fatigue life is proportionately much greater than the reduction in tensile strength.

Clark [52] found that atmospheres of hydrogen, carbon monoxide and methane gave no difference from air in the fatigue life of nylon 6, but small amounts of nitrous oxide (N_2O) or sulphur dioxide (SO_2) caused an appreciable reduction in the fatigue lives of both nylon 6 and polyester fibre. Nitrogen dioxide (NO_2) reduced the fatigue life of nylon 6 to zero cycles but did not have as severe an effect on polyester fibres.

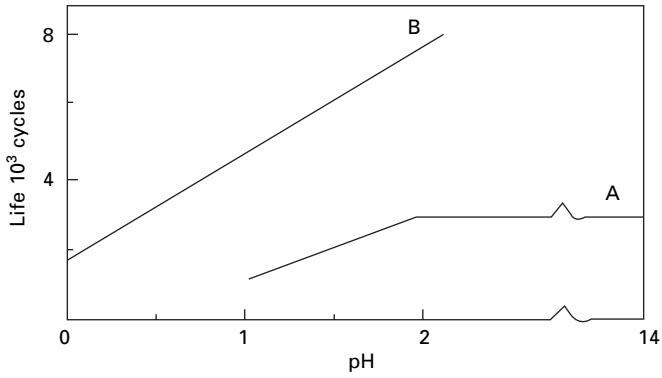

19.46 Effect of pH on median fatigue life for 17 dtex nylon 6.6 rotated from one end over a 273 μm diameter wire: A, with weight of 12 gf; B, with weight of 2 gf [50].

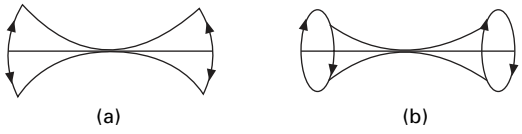

19.47 Cyclic bending: (a) in a plane; (b) by rotation.

19.6.6 Effects in different fibres

Unfortunately, there is not a good set of comparative data for the biaxial rotation fatigue lives of different types of fibre, though similar multiple splitting failures have been found in most general textile fibres. The study of failures in use would suggest that rayon may be an exception [1]. Hearle and Wong [50] report that, in order to obtain broadly similar fatigue lives, in the range from 300 to 8000 cycles, polypropylene fibre will stand more severe conditions than nylon, which in turn is slightly more resistant than polyester fibre, as also shown by the results in Table 19.5. However, as shown above, the results are highly dependent on temperature and humidity.

In natural fibres, comparative results are difficult to obtain because of the variability of fibre diameter. However, observations from experiments on cotton [42] and wool and hair [53] have been reported.

19.6.7 Mechanics of biaxial rotation

The initial rationale for the biaxial rotation test was that it was a means of applying cyclic bending to a fibre, not from straight to bent as in the flex fatigue test described in Section 19.5, but from bent in one direction to bent in the opposite direction. However, this is not done by flexing backwards and forwards in a plane as in Fig. 19.47(a). Instead, the same extreme positions are reached by rotating the fibre, as in Fig. 19.47(b).

In order to understand the mechanics of the test, which is more complex than first appears, we start by considering the simpler situation without a pin, in which a length of fibre is bent into constant curvature, as in Fig. 19.48(a), and then rotated. For a material following Hooke's Law, there will be a central neutral plane, which rotates as indicated in Fig. 19.48(b): the strain variation over the fibre would then be as shown in Fig. 19.48(c), with a phase difference related to the position around the fibre cross-section. If, as is common, the fibre yields more easily in compression, with a stress–strain relation like that in Fig. 19.49(a), the neutral plane will move out, as indicated in Fig. 19.49(b), and during rotation will define a cylinder, within which the material is always in compression. The strain variation with time and position is shown in Fig. 19.49(b). The stresses during the first bending are indicated in Fig. 19.49(a), but the situation for stress, strain and the position of the neutral plane will evolve in successive cycles as the material follows the indicated hysteresis loop.

In the exceptional case of wool and hair fibres, which yield more easily in tension, the above argument will be reversed. The neutral plane will move in the opposite direction, and most of the fibre will be in tension. Effectively, the horizontal axis in Fig. 19.48(b) will be moved downwards instead of upwards.

For a perfectly elastic fibre, as in Fig. 19.50(a), the bending moment will be the only force present. As indicated in Fig. 19.50(b), the maximum stresses coincide with the maximum strains at the top and bottom of the fibre, and they act normal to the plane of the paper in opposite directions on the tension and compression sides. Consequently, the bending moment vector, $\boldsymbol{M}$, acts in the direction shown. On rotation of the fibre, $\boldsymbol{M}$ remains fixed in space, but it changes direction relative to the material. The situation is the same at all positions along a uniformly curved fibre, as indicated in Fig. 19.50(c), in which three mutually perpendicular vectors represent the fibre

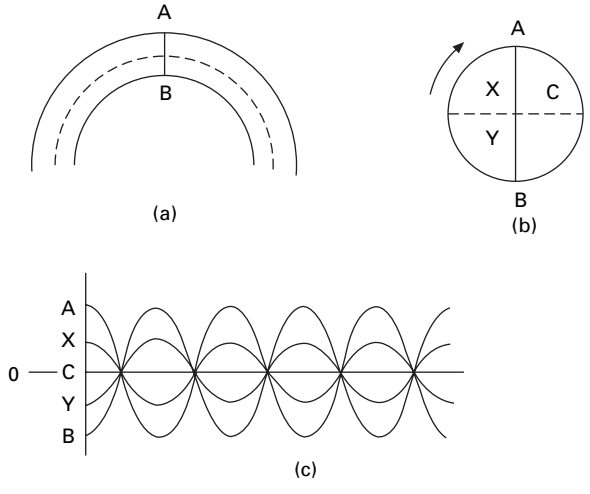

19.48 (a) Linear elastic fibre deformation in uniform curvature, showing neutral plane dotted. (b) Cross-section, showing the line AOB from maximum tension to maximum compression, which rotates during the test. (c) Strain variation with time and position in the fibre.

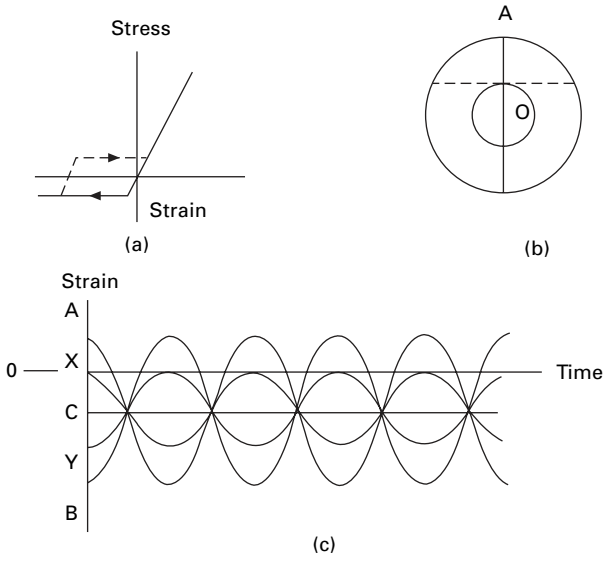

19.49 (a) Idealised stress–strain relation with yielding in compression: the hysteresis recovery path is shown dotted. (b) Fibre cross-section showing displacement of neutral plane. (c) Strain variation in the fibre.

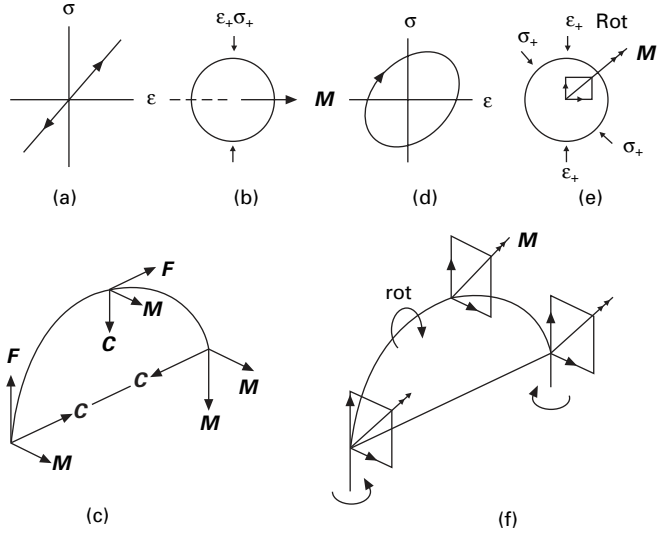

19.50 (a) Elastic stress–strain relation. (b) Fibre cross-section showing positions of maximum stress and strain and bending moment vector. (c) Changing directions of fibre direction ***F***, curvature direction ***C***, and constant direction of bending moment ***M***. (d) Stress-strain relation with hysteresis. (e) Fibre cross-section with stress leading strain and changed direction of bending moment vector. (f) Translation of the bending-moment vector from the centre of the fibre to the ends.

direction $\boldsymbol{F}$, the direction to the centre of curvature $\boldsymbol{C}$, and the bending moment $\boldsymbol{M}$, which is always in the same direction perpendicular to the plane of the fibre.

However, if there is hysteresis, as shown in the simplest possible form in Fig. 19.50(d), energy is dissipated in each cycle. The work needed can be supplied only through the drive shafts, which must therefore apply torque to the fibre in opposite senses at either end. At the centre point, there will be zero torque, but this will increase with distance from the centre as energy has to be supplied to increasing lengths of material. The torques will cause the fibre to be false-twisted about the centre point, just as if there were an external frictional drag.

The situation, in terms of forces and moments, is explained by noting that when there is hysteresis, stress and strain are not in phase. Consequently, the position of maximum stress will lead the position of maximum strain, and the bending moment vector will change direction, as shown in Fig. 19.50(e). Considering effects along the fibre, as shown in Fig. 19.50(f), it can be seen that a component of the bending moment vector, which is in the vertical direction in the cross-sectional plane at the centre point, must be balanced by an axial component at the ends, which is the direction of a torque vector. However, Fig. 19.50(f) is oversimplified, except at the centre point, because the moment vector will really have components in all three directions, owing to the combination of in-phase and out-of-phase bending moments and increasing torque.

The energy argument is not only simpler in qualitative terms; it is also the best basis for quantitative estimates of the magnitude of the torque. An approximate analysis has been made by Calil *et al*. [54] and a more precise treatment by Waterman [55]. In the approximate treatment, we consider a length of fibre, $2x$, bent in uniform curvature through an angle θ, as in Fig. 19.51(a). If the fibre were bent backwards and forwards in a plane between $+\theta$ and $-\theta$ through $\theta = 0$, in the manner of Fig. 19.47(a), the relation between bending moment and bending angle could be represented as in Fig. 19.51(b). The energy loss per cycle would be $M_b d\theta$, and we can assume that it will be similar in value when the bending cycle is caused by rotation, as in Fig. 19.47(b). At each end, there is an energy input per cycle of $2\pi M_t$ from the drive torque, M_t. The sum of the two inputs must equal the energy loss. A generalised form of the equation for different lengths and variable bending would have the form:

$$2 \times 2\pi M_t = \int_{-x}^{x} \oint M_b \, d\theta \, dx \tag{19.5}$$

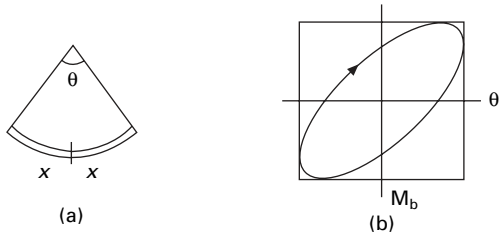

19.51 (a) Fibre bent through an angle θ. (b) Hysteresis loop between bending moment and bending angle.

The torque must increase from zero at the centre point to a maximum value at the ends. For constant curvature through a total angle θ, the value is given by:

$$M_t = (1/4\pi) \oint M_b d\theta \tag{19.6}$$

If f is the ratio of the area of the ellipse in Fig. 19.50(b) to the area of the circumscribing rectangle, ranging from zero for a perfectly elastic material to π/4 for a completely lossy viscous material, Calil *et al*. [54] derived the following equation by the use of the standard bending theory given in Section 17.2.1:

$$M = \frac{\eta f E c^2 \theta}{4\pi^2 \rho R} = \frac{\eta f E c^2 x}{2\pi \rho R^2} \tag{19.7}$$

where η is the shape factor (1 for a circle), E is the specific modulus, c is the linear density, ρ is the density and R is the radius of curvature.

The form of stress–strain relation given above would be applicable to a linear viscoelastic material. The reality, with the more complicated non-linearity of yielding, will be somewhat different but will be similar in principle.

For rotation over a pin, the friction between the fibre and the solid surface will also contribute a torsional drag. The total torque M will be given by:

$$M = M_t + {}^1/_2\, Fr \tag{19.8}$$

where M_t is given by equation (19.7), F is the total frictional force over the whole length on both sides of the centre point and r is the fibre radius.

The variation in torque along the test length is indicated in Fig. 19.52. By putting in what seemed to be reasonable values of the various parameters, Calil *et al*. estimated that the torque due to hysteresis ('internal friction') would be at least ten times as large as the torque due to surface friction. For a 42 dtex polyester fibre with a wrap angle of 90°, the torque was estimated to be in excess of 1 μN m, which would produce in excess of 1 turn/mm. This is in reasonable agreement with the angles of the helical splits found in fatigue failures by biaxial rotation. Clearly, the torque contributes in an important way to the failure of the fibres, which will have been weakened by the tension/compression action in cyclic bending.

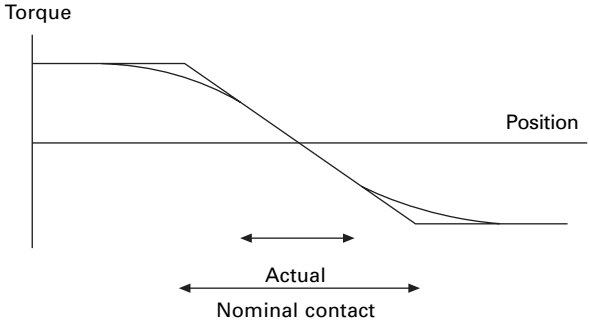

19.52 Variation of torque along the fibre in biaxial rotation test: the line with a sharp discontinuity is for the fibre path A in Figure 19.35; the smooth curve is for an actual path like B.

The increase in torque with wrap angle is probably a cause of the change from fatigue breaks to direct breaks, described in Section 19.6.

For rotation over a pin, there will also be the complications of variable curvature, which were discussed in 19.5, since the fibre will follow the path illustrated in Fig. 19.35(b). The stresses due to bending, tension and shear will be the same as in Fig. 19.36, but the frictional force will be acting circumferentially instead of axially; and the stresses will rotate within the fibre, instead of moving along the fibre. In addition, there will be the torque shown in Fig. 19.52.

The most highly stressed part of the fibre will be where it leaves the pin because at that point the bending stresses have not reduced, the shear stresses have abruptly appeared, and the torque has reached its maximum value. As in the flex test, the normal and frictional contact stresses may also influence fibre failure, particularly in fibres that are prone to surface wear.

19.7 Surface wear and peeling

Another mode of fibre failure, which has been found to occur often in use [1], consists of splitting and peeling of fibre surfaces when they are subject to abrasion. The observed forms vary in appearance, but they are grouped in one poorly defined class, type 13 in Fig. 19.1. Unfortunately, there is little information in the literature on the experimental or theoretical fibre physics of these effects. Recent papers on yarn-on-yarn abrasion [56–58] using the apparatus shown in Fig. 19.53 give some comparative information and show that in wet conditions nylon does not last as long as polyester fibres. The nature of the fibre finish is major determining factor. But the method is complicated by the yarn structural effects. As mentioned in Section 19.5.2, the flex fatigue test, in which a fibre is pulled backwards and forwards over a pin, can lead to failure by surface wear.

In order to avoid the effects of repeated flexing, another method that has been tried is wear of fibres held under tension over a rotating pin. The commonest form of wear is a progressive peeling of the surface (Fig. 19.54(a,b)). This is eventually leads to break over a reduced cross-section (Fig. 19.54(c)). Alternatively, the break may from a long taper (Fig. 19.54(d)).

This form of failure clearly results from the contact forces. In external application, these consist of a normal load, acting at right angles to the surface, and a frictional force, acting tangentially in opposition to the relative motion. The direct effects of these forces will be a transverse compressive stress and an axial shear stress within the fibre near the surface, as shown in Fig. 19.55(a). This can lead to formation of a crack developing from the surface (Fig. 19.55(b)). However, the internal stress distribution resulting from contact stresses can become much more complicated, especially when there is hysteresis [59]. High subsurface shear stresses can be present and cause internal cracks (Fig. 19.55(c)). These cracks lead to peeling of slivers from the surface and a reduction of the cross-section until a tensile break occurs. Alternatively the shear stresses may lead to angled cracks crossing the fibre (Fig. 19.55(e)), to give a tapered end. In *Kevlar*, surface wear eventually led to a break with multiple splitting [1].

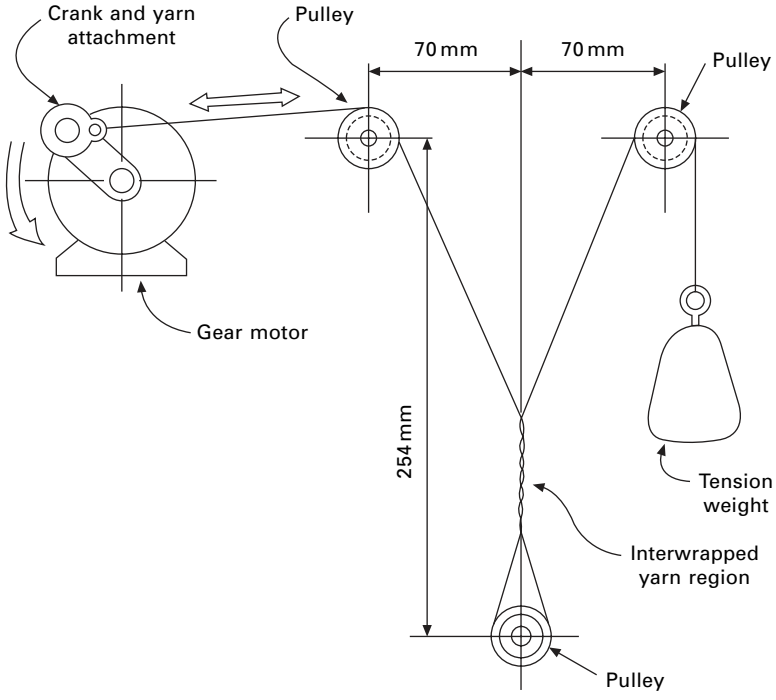

19.53 Yarn-on-yarn abrasion tester.

19.8 Abrasion and wear

Other information on the failure of fibres can be obtained from studies of yarn and fabric wear. Fibres in use are subject to a variety of different forces, which are repeated many times until finally the fibres wear out. The abrasive wear of materials depends to a considerable extent on the construction of the yarn or fabric, and no way has been found to eliminate the influence of these factors and calculate a basic fibre property, if indeed this exists at all. Wear resistance is more likely to be a complex of several properties, whose relative influence is different in different uses.

It is, however, true that simple tensile tests of fibre properties do not give an exact indication of resistance to wear. On the other hand, there is general qualitative agreement between the results of various types of abrasion test and of tests of wear in actual use. It is therefore not completely unreasonable, in the absence of further knowledge, to consider abrasion resistance as a fibre property.

Table 19.7 gives some results obtained in practice, reduced so as to give nylon the value 100 in all tests. These tests were carried out as follows:

A Taber Abrader, in which rubber-emery wheels are rubbed over a yarn sheet. The figure gives the relative number of cycles for 60 loss in strength (Hamburger [60]).
B As A (Hicks and Scroggie [61]).
C As A, on fabric (Hicks and Scroggie [61]).
D Laboratory wear test (Schiefer *et al.* [62]).
E Yarn-on-yarn abrasion (du Pont [63]).

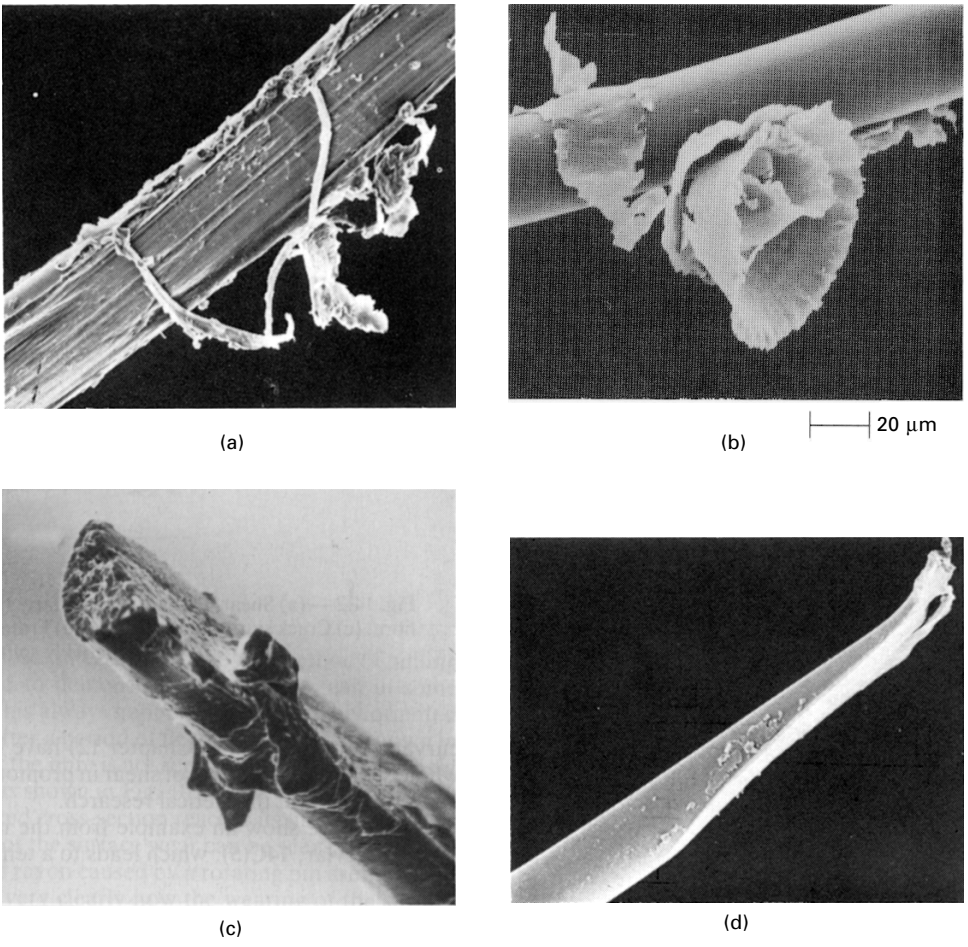

19.54 Wear of fibres over rotating pin: (a) nylon; (b) polyester; (c) wool, (d) nylon.

F Walker Abrader, in which yarn is twisted round a guide, and then round itself–mainly yarn-on-yarn abrasion. Relative number of cycles to break. Staple-fibre yarns (Abrams and Whitten [64]).
G As F – continuous-filament yarns (Abrams and Whitten [64]).
H Stoll flex and abrasion test. Yarn folded and rubbed over a bar. Staple-fibre yarns (same as in F) (Susich [65]).
I As H – continuous-filament yarns (same as in G) (Susich [65]).
J As H – wet fabric (Dennison and Leach [66]).
K Flexing test. Cycles to break (Thomson and Traill [67]).
L Flex cycles to failure (du Pont [63]).
M Flex cycles to failure (Schiefer *et al.* [62]).
N Service-wear test on men's socks. Days of wear (Schiefer *et al.* [62]).
The fibres have been arranged in the order of ranking found in most tests. The exceptions are in italics, but it will be seen that there are few of these.

Table 19.7 Abrasion and wear – relative values

Fibre	Conditions													
	A	B	C	D	E	F	G	H	I	J	K	L	M	N
Nylon	100	100	100	100	100	100, *4*	100	100, *73*	100	100	100	100	100	100
Terylene, Dacron polyester fibres					42	*696, 249, 21*	33	77, 57	62	62				
Wool				20		*28, 13*		*29, 17*			100	11.6	64	33
Cotton						*32, 5*		44, 30			16		25.6	33
Silk							6		8.3		9, *1.8*			
Orlon acrylic fibre	41	28	19		3.0	18,*3*	2.6	14, 12	*9.7*	13		*83*		
High-tenacity rayon		25	17				2.7		16		4.7	1.32	31.3	
Viscose rayon	17	10, 15	13, 15	6	1.6	6	*3.2*	9.1	*18*	3.7	3.3, 0.7	0.66	0.28	12
Acetate	17	7.5	9.3	4.5		3	0.31	5.3	7.2	2.2	0.5	0.053		5
Casein				1.5			*0.45*		1.9		0.12			1.8

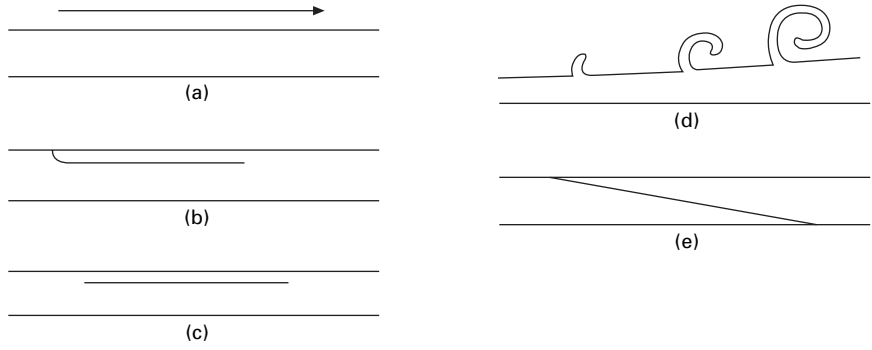

19.55 (a) Shear stress in fibre over a rotating pin. (b)–(e) Various consequences.

Another form of damage occurs within twisted ropes if a component yarn cycles between tension and compression [1]. This is axial compression fatigue, with failure at kink bands, similar to those in flex fatigue. Guidance design limites are 2,000, 40,000 and 100,000 cycles for aramid, HMPE and polyester fibres respectively [68].

19.9 References

1. J. W. S. Hearle, B. Lomas and W. D. Cooke. *Atlas of Fibre Fracture and Damage to Textiles*, 2nd edition, Woodhead Publishing, Cambridge, 1998.
2. J. W. S. Hearle and P. M. Cross. *J. Mater. Sci*., 1970, **5**, 507.
3. S. Simmens and F. Howlett. *J. Text. Inst.*, 1949, **40**, T590.
4. R. J. E. Cumberbirch, J. Długosz and J. E. Ford. *J. Text. Inst.*, 1961, **52**, T513.
5. L. Konopasek and J. W. S. Hearle. *J. Appl. Polymer Sci.*, 1977, **21**, 2791.
6. J. W. S. Hearle and J. T. Sparrow. *Text. Res. J.*, 1971, **41**, 736.
7. K. R. Makinson. *J. Text. Inst.*, 1970, **61**, 151.
8. A. R. Haly. *Text. Res. J.*, 1970, **40**, 965.
9. S. J. Law and S. K. Mukhopadhyay. *J. Textile Inst*., 1999, **90**, 137.
10. G. E. Settle and S. L. Anderson. *J. Text. Inst.*, 1963, **54**, T28.
11. H.-S. Shin, D. E. Erlich, J. W. Simons and D. A. Shockey. *Textile Res. J*., 2006, **76**, 607.
12. S. Michielsen. *J. Materials Sci. Letters*, 1992, **11**, 982.
13. S. Michielsen. *J. Appl. Polymer Sci*., 1994, **52**, 1081.
14. J. W. S. Hearle. *J. Mater. Sci*., 1967, **2**, 474.
15. A. J. Booth and J. W. S. Hearle. In '*Proceedings of Fourth International Congress of Rheology*', Interscience, New York, 1965, p. 203.
16. A. R. Bunsell, J. W. S. Hearle and R. D. Hunter. *J. Phys. E*, 1971, **4**, 868.
17. A. R. Bunsell and J. W. S. Hearle. *J. Mater. Sci*., 1971, **6**, 1303.
18. Ch. Oudet and A. R. Bunsell. *J. Mater. Sci*., 1987, **22**, 4292.
19. J. W. S. Hearle and A. R. Bunsell. *J. Appl. Polymer Sci*., 1974, **18**, 26.
20. Ch. Oudet and A. R. Bunsell. *J. Mater. Sci. Letters*, 1984, **3**, 295.
21. C. Lechat, A. R. Bunsell, P. Davies and A. Plant. *J. Materials Sci*., 2006, **41**, 1745.
22. Le Clerc, A. R. Bunsell, A. Plant and B. Monasse. *J. Materials Sci.*, 2006, **41**, 6830.
23. Le Clerc, A. R. Bunsell and A. Plant. *J. Materials Sci*., 2006, **41**, 7509.
24. L. Konopasek and J. W. S. Hearle. *J. Appl. Polymer Sci.*, 1977, **21**, 2791.

25. A. K. van der Vegt. *Rheol. Acta*, 1962, **2**, 17.
26. B. C. Goswami and J. W. S. Hearle. *Text. Res. J.*, 1976, **46**, 55.
27. K. E. Duckett and B. C. Goswami. *Text. Res.* J., 1984, **54**, 43.
28. B. C. Goswami, K. E. Duckett and T. L. Vigo. *Text. Res. J.*, 1980, **50**, 481.
29. M. Toney and P. Schwartz. *J. Appl. Polymer Sci.*, 1992, **B46**, 2023.
30. B. C. Jariwala. PhD Thesis, University of Manchester, 1974.
31. J. W. S. Hearle and M. Miraftab, *J. Mater. Sci.*, 1991, **26**, 2861.
32. M. Miraftab. PhD Thesis, University of Manchester, 1986.
33. J. W. S. Hearle and M. Miraftab. *J. Materials Sci.*, 1995, **30**, 1661.
34. R. Meredith. In *Proceedings of Fifth International Congress of Theology*, University of Tokyo Press, Tokyo, Japan, 1969, Volume 1, p. 43.
35. A. Sengonul and M. A. Wilding. *J. Textile Inst.*, 1994, **85**, 1.
36. A. Sengonul and M. A. Wilding *J. Textile Inst.*, 1996, **87**, 13.
37. J. P. Den Hartog. *Strength of Materials*, McGraw-Hill, New York, 1949.
38. W. J. Lyons. *Text. Res. J.*, 1962, **32**, 750.
39. J. W. S. Hearle and E. A. Vaughn. *Rheol. Acta*, 1970, **9**, 76.
40. J. W. S. Hearle and B. S. Wong. *J. Phys. E: Sci. Instrum.*, 1977, **10**, 448.
41. S. F. Calil and J. W. S. Hearle. *Fracture 1977, ICF4 Conf.*, Waterloo, Canada, 2, p. 1267.
42. J. W. S. Hearle and N. Hasnain. In *Cotton in a Competitive World*, (P. W. Harrison Editor), The Textile Institute, Manchester, 1979, p. 163.
43. I. E. Clark and J. W. S. Hearle. *J. Phys. E: Sci. Instrum.*, 1979, **12**, 11.
44. I. E. Clark, J. W. S. Hearle and A. R. Taylor. *J. Phys. E: Sci. Instrum.*, 1980, **13**, 516.
45. K. Liolios. PhD Thesis, University of Manchester, 1988.
46. I. E. Clark and J. W. S. Hearle. *J. Text. Inst.*, 1980, **71**, 87.
47. S. F. Calil, I. E. Clark and J. W. S. Hearle. *J. Mater. Sci.*, 1988, **24**, 736.
48. I. E. Clark and J. W. S. Hearle. *J. Text. Inst.*, 1983, **74**, 168.
49. J. W. S. Hearle and B. S. Wong. *J. Text. Inst.*, 1977, **68**, 155.
50. J. W. S. Hearle and B. S. Wong. *J. Text. Inst.*, 1977, **68**, 127.
51. I. E. Clark and J. W. S. Hearle. *J. Text. Inst.*, 1982, **73**, 273.
52. I. E. Clark. PhD Thesis, University of Manchester, 1980.
53. J. W. S. Hearle, B. C. Jariwala, L. Konopasek and B. Lomas. *Proc. Int. Wool Text. Res. Conf.*, Aachen, 1975, II-370.
54. S. F. Calil, B. C. Goswami and J. W. S. Hearle. *J. Phys. D: Appl. Phys.*, 1980, **13**, 725.
55. H. A. Waterman. *J. Phys. D: Appl. Phys.*, 1983, **16**, 227.
56. J. F. Flory, M. Goksoy and J. W. S. Hearle. *J Text. Inst.*, 1988, **79**, 417.
57. M. Goksoy and J. W. S. Hearle. *J. Text. Inst.*, 1988, **79**, 432.
58. M. Goksoy and J. W. S. Hearle. *J. Text. Inst.*, 1988, **79**, 443.
59. K. L. Johnson. *Contact Mechanics*, Cambridge University Press, Cambridge, 1985.
60. W. J. Hamburger. *Text. Res. J.*, 1945, **15**, 169.
61. E. M. Hicks and A. G. Scroggie. *Text. Res. J.*, 1948, **18**, 416.
62. H. F. Schiefer, L. Fourt and R. Kropf. *Text. Res. J.*, 1948, **18**, 18.
63. E. I. du Pont de Nemours and Co. Inc. Cited by E. R. Kaswell. *Textile Fibers, Yarns, and Fabrics*, Reinhold, New York, 1953.
64. E. Abrams and H. P. Whitten. *Text. Res. J.*, 1954, **24**, 980.
65. G. Susich. *Text. Res. J.*, 1954, **24**, 210.
66. R. W. Dennison and L. L. Leach. *J. Text. Inst.*, 1952, **43**, P473.
67. R. H. K. Thomson and D. Traill. *J. Text. Inst.*, 1947, **38**, T43.
68. Tension Technology International and Noble Denton, *Deepwater Fibre Moorings*, Oilfield Publications, Ledbury, 1999.

20

Theories of mechanical properties

20.1 Introduction

20.1.1 A variety of approaches

The wide range of materials and phenomena concerned in the study of the mechanical properties of fibres leads to a variety of useful theoretical approaches. A study of changes in structure at various levels gives the best general scientific understanding of the observed effects. One approach is to treat polymer fibres as composites of crystalline and amorphous regions, even though, in dealing with regions of the order of 10 nm (100 Å) in size, atomic and molecular effects must be borne in mind.

The chief technological interest is in deriving relations that will describe mathematically the macroscopic properties of the material: the stress–strain curves, recovery behaviour, creep, relaxation of stress, and so on. There are two main schools of thought: the analytical and the integral. Analytical theories aim at breaking down the behaviour into that of a combination of ideal elements. This may be done empirically, but the more sophisticated theories are based on fundamental reasoning. Integral theories aim at a single relation to fit the experimental results. An alternative mathematical approach is the application to the problem of thermodynamics, dealing with the changes of energy and entropy involved in deformation. The various theories are neither exclusive nor completely separate, and there is a crosslinking of ideas. Inorganic fibres are very different in structure and require different theoretical treatments.

20.1.2 Basic theory

Polymer fibres contain material in three main forms: crystalline; rigid amorphous below the glass transition temperature; rubbery amorphous above the glass transition. The behaviour will also be affected by the extent of secondary bonding, e.g. hydrogen bonds, in amorphous regions. It is useful to give a brief account of the basic mechanical theories for the three types of material.

Crystalline lattices are bonded by covalent, electrovalent or weaker intermolecular bonds. In the simple case, shown by the full line in Fig. 20.1(a), increasing strain gives a rise in energy up to a maximum value and then an asymptotic approach to a reference level. Differentiation of the free energy curve results in the stress–strain curve (Fig. 20.1(b), giving Hooke's Law for small strains.

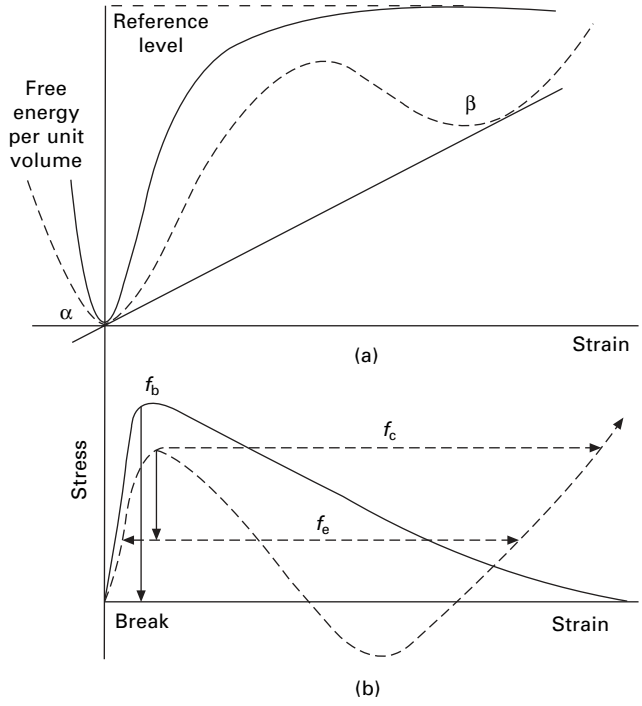

20.1 Crystal lattice deformation. Full lines: a crystal which extends to rupture. Dotted lines: a transition between different α and β forms. Note that in reality the full lines would go to much higher values of free energy and stress than the dotted lines. Following the transition, the dotted line would continue in the form of the full line to give rupture of the β-lattice. (a) Free energy versus strain. (b) Stress versus strain.

$$f = \frac{\mathrm{d}U}{\mathrm{d}e} = Ee \tag{20.1}$$

where f = stress (or specific stress), U = free energy per unit volume (or per unit mass), e = strain and E = initial modulus.

Owing to the strength of the bonding, a crystal is a high-stiffness material. Typical moduli are of the order of 100 GPa for extended chain crystals dominated by bond stretching, but are much lower with helical lattices when bond bending and twisting can occur. The maximum stress occurs at the point of inflection on the free energy curve. For uniform straining, the stress would then fall and approach zero as the free energy reaches its asymphotic level with complete separation of parts of the crystal. In practice, a local instability will lead to a catastrophic rupture at the point of maximum stress, or earlier if there are stress concentrations or, for small crystals, thermal vibrations leading a jump over the energy barrier.

The dotted lines in Fig. 20.1 relate to materials in which there can be a transition from one crystal lattice to another, such as the α↔β change from helices to extended chains in keratin. For uniform deformation, the stress curves go into negative stress before increasing again, but, in practice, an instability will lead to a jump from one

form to the other at a critical stress f_c. The stress drops to the equilibrium stress f_e, which is given by the slope of the common tangent to the two troughs in the free energy curve.

The energy and stress relations for glassy polymers are similar to the full lines in Fig. 20.1. In addition to bond stretching and bending, a major cause of the stiffness is resistance to bond rotation. Polystyrene has a modulus of 3 GPa. In the simplest case, the transition from glass to rubber is due to thermal vibrations becoming strong enough to allow free rotation around main chain bonds (Fig. 20.2). There may be secondary transitions associated with side chains or with intermolecular bonds. In particular, in nylons, there are two major transitions, one due to bond rotation and the other to mobility of hydrogen bonds. There is a similar effect in polyesters and the consequences are discussed in Section 20.3.1.

The classical theory of rubber elasticity [1] is based on the assumption that there are no changes in internal energy, so that the resistance to deformation depends only on changes in entropy. The greatest number of possible conformations of a chain of N freely orienting links, and hence the maximum entropy, occurs when the two ends of the chain are closest together. As the chain extends, the number of possible conformations decreases. The change in entropy, which can be related to the tension in the chain, depends on the change in probability of chain ends being separated by a distance r. An approximate solution, which is not valid at high extensions, for a random chain gives a Gaussian function for the probability P(r):

$$\mathrm{P}(r) = \left(\frac{4b^2}{\pi^{1/2}}\right) r^2 \mathrm{e}^{-b^2 r^2} \tag{20.2}$$

For large extensions, getting near to a fully extended chain, it is better to follow a derivation by Flory [2, 3]. This depends on the fact that for a link of a length a at an angle ψ, the length x along the chain axis is (a cos ψ). If the tension on the chain is F, there is an associated potential energy of $(-Fx)$[1]. According to the

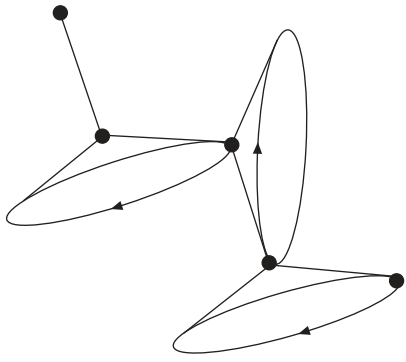

20.2 Freedom of rotation around main chain bonds.

[1]The negative sign results from an increase in x lowering a notional weight on the end of the chain and hence a reduction in potential energy.

Maxwell–Boltzmann law, the probability of a value between x and $(x + dx)$ is $\exp[-(-Fx/kT)]dx$. This leads to a mean value of x of $a[\coth(Fa/kT) - (Fa/kT)^{-1}] = a\mathcal{L}(Fa/kT)$, where $\mathcal{L}$ is the Langevin function, which first appeared in the theory of the alignment of dipoles. The total end-to-end length l of the chain is N times the mean value of x and the fully extended chain length L is Na. Hence:

$$l = N\left[a\mathcal{L}\left(\frac{Fa}{kT}\right)\right] = L\left[a\mathcal{L}\left(\frac{Fa}{kT}\right)\right] \tag{20.3}$$

$$F = \left(\frac{kT}{a}\right)\left[\text{arc}\,\mathcal{L}\left(\frac{l}{L}\right)\right] = \left(\frac{kT}{a}\right)\left[3\left(\frac{l}{L}\right) + \left(\frac{9}{5}\right)\left(\frac{l}{L}\right)^3 + \left(\frac{297}{175}\right)\left(\frac{l}{L}\right)^5 + \ldots\right] \tag{20.4}$$

The first term is the Gaussian approximation in the entropic derivation and is reasonable to use up to $(l/L) = 0.4$.

Rubbers are a network of flexible polymer molecules. If the chains are long enough and sufficiently entangled, slippage of molecules past one another is inhibited to the extent that a low-modulus plateau appears below the glass transition. However, viscous flow will take place with time and, if the molecules are short, the plateau will disappear. Commercial rubbers are vulcanised to form a network that is covalently crosslinked by $(—S—)_n$ bonds or in other ways. This prevents long-term flow. Rubbers are elastic with very low hysteresis, i.e complete recovery with very small differences between stress–strain curves in extension and recovery.

Energy minimisation provides a means of calculating stress–strain relations [1, 3]. The details are complicated and only a brief account will be given here. The dominant energy term is elongation of the flexible tie-molecules between crosslinks, which is given by integrating equation (20.4) for the changes in l from the initial to the extended lengths. There is also energy associated with change in volume, just as there is in a liquid. Except when there is a large change of hydrostatic pressure, a common procedure is to assume constant volume, which is close enough to give acceptable values of l for most deformations, although paradoxically the stresses to give exact constant volume are not small. A better procedure is to include in the analysis a volume energy term derived from the relatively high bulk modulus[2], and at the end to neglect negligibly small contributions to the stress [3].

Affine deformation[3] relates the changes in lengths of tie-molecules between network points to the external deformation and hence, in principle, enables energy changes to be calculated. The complications arise from the need to take account of different initial lengths, extended lengths and orientations. If the Gaussian approximation is assumed, i.e. only the first term of the series in equation (20.4), an averaging procedure gives an algebraic solution for the shear modulus G:

[2]An advantage of this approach is that it eliminates an indeterminacy in the constant volume theory. Since there can be no volume change, any value of hydrostatic pressure gives the same result.

[3]Affine: the strain matrix for any small element, e.g. as defined by the distribution of network points, is the same as for the specimen as a whole.

$$G = N\,k\,T \tag{20.5}$$

where N = number of tie-molecules per unit volume, which can be related to the density of crosslinks, k = Boltzmann's constant and T = temperature.

A typical value of the shear modulus G is 0.5 MPa. With a Poisson ratio close to 0.5, this gives a tensile modulus of 1.5 MPa, many orders of magnitude less than the modulus of crystals or glasses. The bulk modulus is more than 1 GPa, over 1000 times greater than the shear and tensile moduli and can clearly be neglected in most modes of deformation.

For large strains, which require use of the full equation (20.4), the averaging is more difficult, except by numerical computation. For an analytic solution, a three-chain (XYZ) model can replace the distribution of orientations. This gives the following equation for uniaxial stress f:

$$f = \left(\frac{NkT}{3}\right) n^{1/2} \left\{ \text{arc}\,\mathcal{L}\left(\frac{\lambda}{n^{1/2}}\right) - \lambda^{-3/2}\,\text{arc}\,\mathcal{L}\left[\frac{1}{(\lambda n)^{1/2}}\right]\right\}$$

$$= NkT\left[\lambda - \left(\frac{1}{\lambda}\right)^2\right]\left[1 + \left(\frac{3}{25n}\right)\left(3\lambda^2 + \frac{4}{\lambda}\right) + \left(\frac{297}{6125n^2}\right)\left(5\lambda^2 + 8\lambda + \frac{8}{\lambda^2}\right) + \ldots\right] \tag{20.6}$$

where λ = extension ratio = (1 + axial strain) and n = number of freely orienting links in the tie-molecules between network points.

Treloar (1) quotes the series for two more terms, which go to a sum of five powers of λ. There are interesting features of equation (20.6) illustrated in Fig. 20.3, which

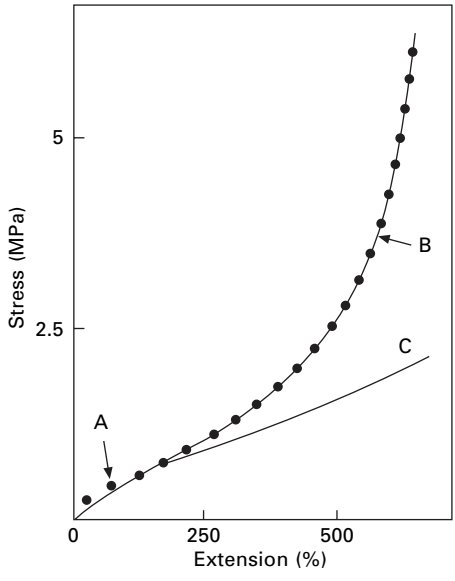

20.3 Stress–strain curves for a typical rubber: A, experimental data, B, inverse Langevin function form; C, Gaussian approximation.

also shows the agreement between experiment and theory. The inclusion of $(1/\lambda)^2$, which also comes into the full treatment of the Gaussian approximation, means that there is some initial curvature of the stress–strain curve. The later terms of the series in λ determine the large strain behaviour with the stress rising more sharply and becoming asymptotic to infinity when the chains are fully extended. The first term in the series, which is the Gaussian approximation, does not include n. The stress depends only on the number of tie-molecules and is independent of the number of links that they contain. However the large-strain behaviour is dependent on n. It should be noted that the number of freely rotating links n = (number of repeat units in a tie-molecule/number of repeat units in a freely rotating link). This differentiates different polymers. For a simple polymer, which can be represented by Fig. 20.2, the freedom is limited to rotation with the angle between bonds remaining constant and a freely rotating link is equivalent to three repeats. However, for different bonds and other interactions, the number varies considerably. For polyisoprene (natural rubber), in which the monomer includes four main chain and contains a double bond, a freely rotating link corresponds to 1.73 monomer units.

Following the first edition of Treloar's classic text in 1949, there were many advances in the theory of rubber elasticity. Some of these dealt with the mathematical approximations, but others dealt with physical differences between the idealised model and real materials. In particular, there are internal energy changes as well as entropy changes. Semicrystalline polymer fibres bring in other effects, but the basic analyses described above can be used in theories for particular fibre types.

20.2 Structural effects in rayon fibres

20.2.1 The extension and recovery of ordinary rayon

Viscose rayon exhibits many features of fibre behaviour that are also shown by other fibres. It is therefore a good example to consider first in qualitative and semi-empirical quantitative theory. The stress–strain curve shown in Fig. 20.4 has three distinct regions: an initial linear portion A, in which recovery is good; a region of easier extension B, in which recovery is incomplete; and, finally, a region of increasing

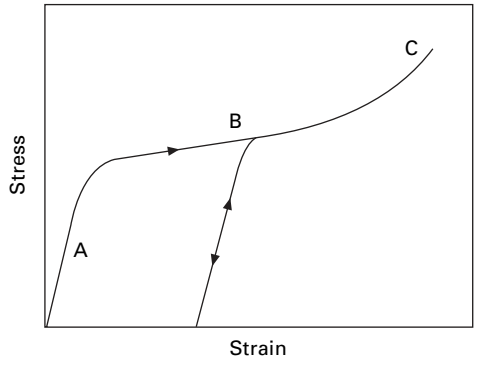

20.4 Stress–strain curve of rayon.

slope C, leading to breakage. This curve may be explained in terms of the structure of the fibres.

When a small force is applied to the fibres, extension will occur for two reasons:

- a slight stretching of the chain molecules themselves;
- a straightening of the molecules in the non-crystalline regions, with a resultant straining of the hydrogen bond crosslinks between them.

The behaviour is thus analogous to that of a bundle of rods held together at irregular intervals by short lengths of elastic. On the application of a force, there may be some stretching of the rods, but there will be a greater stretching of the elastic links, allowing the rods to change position. There will also be some change in bond angles in the main chains.

The magnitude of the distortion of the molecules and crosslinks will be proportional to the applied force, so that the stress–strain curve will be linear. On removal of the force, the molecules and crosslinks will spring back to their original positions, and recovery will be complete. The straining of the bonds occurs at rates comparable to thermal vibrations of the atoms, namely, in times of the order of 10^{-13} second, so that there is no detectable time dependence except at such high rates that inertia effects are also significant.

When the applied force becomes larger, some of the most highly strained crosslinks in the amorphous region will break because they cannot support the force applied to them. This permits a much greater straightening of the molecules and, in turn, puts an increased load on other crosslinks. Consequently, extension becomes much easier. This is the region B. When the force is removed, recovery is incomplete, since many of the crosslinks are now missing and cannot spring back to their original positions or, more probably, hydrogen bonds have re-formed in new positions and are thus tending to stabilise the deformed state. Mechanical conditioning is explained, since the small elastic recovery from the deformed state will be reversible. When the specimen is extended again, no more crosslinks need to break until the original stress–strain curve is reached.

The observed time dependence of this yield region is explained by the fact that the rupture of a crosslink is a statistical phenomenon. The random thermal vibrations of the system give a certain probability that a given crosslink will break in a given time. In the absence of an applied stress, or with a low stress, the probability is almost infinitesimal, and, even when a link does break, the neighbouring links hold the structure in place and prevent any extension or recovery of the fibre. But, as the stress is increased, the most strained crosslinks become less stable and thus are more easily broken by thermal vibrations. The chances of achieving sufficient loosening of the structure to get appreciable localised deformations become significant. The interaction of these two effects, the increasing instability of bonds under stress and the chance fluctuations of thermal vibrations, causes the yield stress to be rate-dependent. At higher rates of extension, the crosslinks have to be raised to a higher level of instability before sufficient chance breaks occur within the timescale of the test; at low rates, the stress does not need to be so great for there to be a sufficient number of random breakages to cause yield.

When put in other ways, the same argument explains secondary creep and stress relaxation. Under constant stress, continued rupture of crosslinks will occur owing to chance fluctuations as time goes on and thus lead to continued deformation or creep. It will be secondary creep without recovery because, when the stress is returned to zero, the structure is so firmly held by the many hydrogen bonds in cellulose that the influence of thermal vibrations is negligible. The rate of creep will slow down with increasing time because the continued rearrangement of the structure tends to remove the most highly strained and unstable crosslinks and leads progressively towards a more uniform sharing of the load among all the chains and hydrogen bonds, with a reducing probability of breakage of crosslinks.

When the fibre is held extended at fixed length, the continued spontaneous breakage of crosslinks relieves the internal stresses in the molecular assembly and thus leads to the lowering of tension, which is termed *stress relaxation*. An oversimplified, but instructive, model of stress relaxation is a set of links that are put under tension by the imposed strain. It is assumed that there is a certain probability that a link will break in a given time and cease to contribute to the stress. The number of crosslinks breaking in a time interval dt will be proportional to the number remaining n. Thus:

$$\frac{\mathrm{d}n}{\mathrm{d}t} = -kn \tag{20.7}$$

where k = constant. But the stress will be proportional to n, the number of effective crosslinks (per unit area), so that:

$$\frac{\mathrm{d}f}{\mathrm{d}t} = -kf \tag{20.8}$$

Integrating and putting $f = f_0$ at $t = 0$, we get:

$$\frac{f}{f_0} = \exp(-kt) = \exp(-t/\tau) \tag{20.9}$$

where $\tau = 1/k$ = relaxation time for the type of bond concerned.

This indicates that an exponential decay of stress is likely, though the situation is more complicated in real fibres for several reasons. There may be various sorts of bond with different relaxation times; there is a complicated distribution of stress over the links; and the effects of breaking a link in the network will not be as simple as in the model. Each break will lead to structural rearrangement.

The small positive slope of the stress–strain curve in the region B can be explained by local variations in molecular packing. The most unfavourable arrangements are disturbed first, and higher stresses are needed to cause further breakage of crosslinks, allowing the molecular chain to straighten and give more fibre extension. However, eventually a point is reached at which some of the molecules are fully straightened. Further extension then becomes more difficult, and the slope increases as at C. During this period, an increasing strain is put on the crosslinks and molecules. Finally, breakage occurs at locally highly stressed or weak points to give a granular break.

Because the yield phenomena are affected by thermal vibrations, they will be influenced by temperature. Creep and stress relaxation will occur more rapidly at the

higher temperatures. Moisture absorption will have a much greater effect. The stress–strain curve in Fig. 20.4 is typical of the behaviour of ordinary rayon at low and medium humidities. In the perfectly dry state, there will be a maximum crosslinking of the cellulose molecules by hydrogen bonds, and the yield stress will be high. As moisture is absorbed, some of these crosslinks are replaced by absorbed water molecules. This loosens the structure and makes yield easier. Consequently, as relative humidity increases, the yield stress falls.

In wet rayon fibres, there is so much moisture absorbed that the non-crystalline regions are virtually free of restrictions on relative movement. The plasticising effect is such that the molecules can be regarded as swimming in a sea of water molecules, held together only by the crystalline micelles. This is why the modulus of standard viscose rayon is so low when wet. In effect, the yield stress can be regarded as having moved down to the origin, the yield slope being left to determine the fibre stiffness.

The loosening effect of absorbed water is such that, at zero stress, spontaneous structural arrangements can occur and the structure will recover to an equilibrium state. This explains swelling recovery (see Section 15.6). A structure that has been left with a 'permanent' extension as a result of being strained while dry will recover when it is loosened up by absorbed water or steam.

20.2.2 A comparison of regenerated cellulose fibres

There is a great diversity of regenerated cellulose fibres with different mechanical properties due to differences in manufacturing sequences (Section 1.5.2). The influence of large-scale structural features is shown by fibres with an asymmetric skin, giving rise to a crimp that has a major influence on the initial part of the stress–strain curve. The all-skin fibres have a finer texture, which leads to lower localised stress concentrations, a more uniform sharing of load among the molecular chains, and thus to higher strengths. These are the high-tenacity rayons. Although not a rayon, cellulose acetate shows behaviour that is qualitatively similar to that of ordinary rayon, except that the weaker attractions between molecules lead to easier yield; the drop in stress that is often observed at the start of yield must be due to the development of an unstable situation once large-scale molecular movement begins.

Finally, there are the very interesting differences between ordinary and high-tenacity rayons in one group and high-wet-modulus or polynosic rayons in another. If orientation effects are ignored, the structure of the high-wet-modulus rayons may be represented by the fibrillar model of Fig. 20.5(a), whereas the ordinary rayons are micellar as in Fig. 20.5(b). If, with some exaggeration, we consider these models as made of glass embedded in rubber, the difference is obvious: the fibrillar model will have almost the stiffness of glass, but the micellar model will have almost the extensibility of rubber.

The fibrillar model (Fig. 20.5(a)), is easily analysed for any combination of material properties because the stress will be the mean stress contributed by the two components at the same strain, weighted to allow for one-third crystalline to two-thirds amorphous. The micellar model is difficult to analyse; but the more extreme lamellar structure of Figure 20.5(c) is again easy to analyse. The behaviour of the composite system is

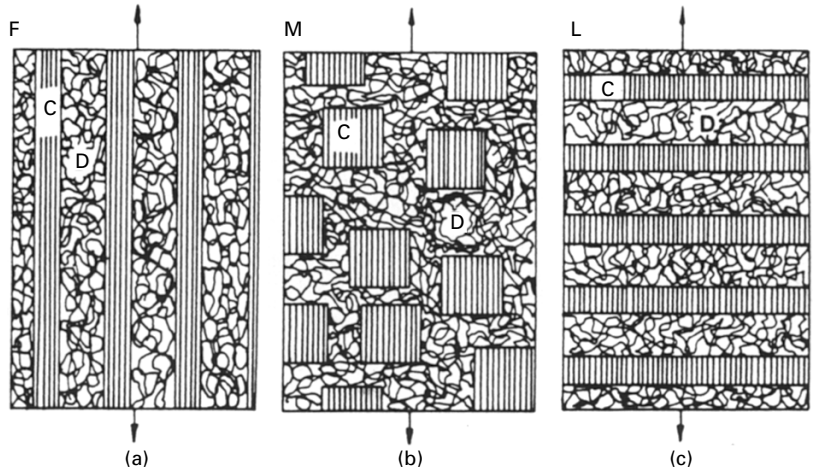

20.5 Structural models – one-third crystalline (C), two-thirds amorphous disorder (D): (a) fibrillar; (b) micellar; (c) lamellar.

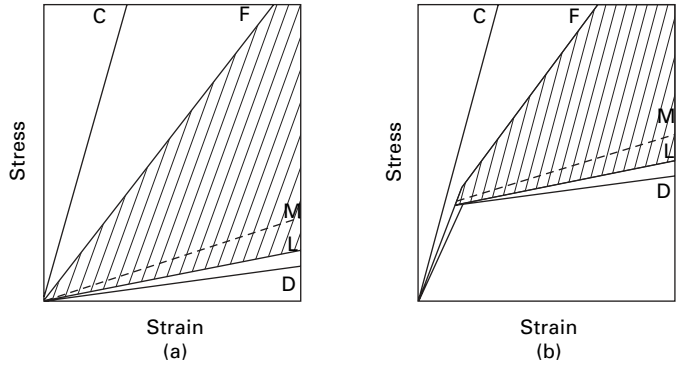

20.6 Idealised stress–strain relations of rayon: C, crystal line; D, disordered; F, fibrillar; M, micellar; L, lamellar; (a) wet; (b) dry.

given by taking the weighted mean strain with the same stress on each component. The micellar structure will give a result between the two extremes and was arbitrarily placed at the mid-point between the fibrillar (F) line and lamellar (L) lines *at a given stress* [4].

Figure 20.6 shows idealised stress–strain curves for the components: a stiff, linear, elastic stress–strain curve, unaffected by water, for the crystalline material, using expected values of the modulus of cellulose crystals; a less stiff, initial linear portion followed by yield for the dry disordered material; and a single region of low slope for the wet disordered material. The arguments for the form of these relations were given in the last section. These combine to give predicted curves, which are then compared with experimental results in Fig. 20.7. The form of the relation for the disordered material was given by fitting to the results for dry standard rayon. There is then good agreement for the other three curves. It is the stiffening effect of the fibrils that causes the high-wet-modulus of polynosic fibres. Lyocell fibres follow the same pattern.

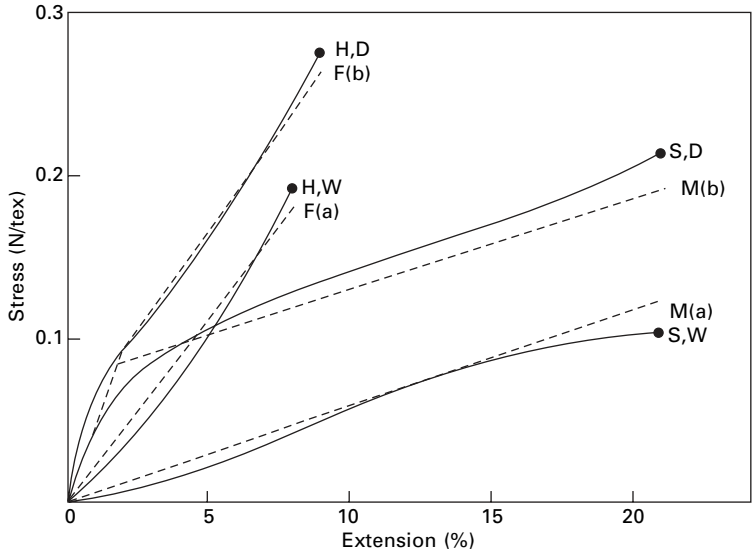

20.7 Comparison of theoretical predictions from 20.6 with experimental results: S, standard rayon; H, high-wet modulus rayon; D, dry; W, wet.

20.2.3 The effect of orientation

The stress–strain curves shown in Fig. 20.8 demonstrate the influence of molecular orientation in raising the stress–strain curve. Intuitively, this is to be expected, since a poorly oriented structure has an opportunity to extend by becoming more highly oriented, but this is not possible in a structure that is oriented to start with. The behaviour is illustrated schematically by the three pairs of diagrams in Fig. 20.9, where the structures in the left-hand pictures have low orientations and can deform to give those in the right-hand pictures. The right-hand pictures can alternatively be regarded as illustrations of the initial states of stiffer structures.

If we consider a simple network of linear elements, as in Fig. 20.9(a), those that lie in the direction of extension will resist deformation more strongly than those lying across it. This is the basis of the influence of fibre orientation on the properties of non-woven fabrics; and the same argument will explain the influence of orientation in the non-crystalline regions of a cellulose fibre. The preferred orientation is produced by stretching during fibre production and stabilised by the pattern of interconnections between crystalline regions. A fibre that has been stretched and permanently set in the dry state will show a further preferred orientation, stabilised by hydrogen bonding.

Crystalline orientation also plays a part. In the micellar structures, the crystalline regions may reasonably be regarded as rigid filler particles with all the deformation occurring in the non-crystalline regions. However, the deformation is easier if the micelles are initially poorly oriented and so are able to swing into alignment and give an added extension with less strain in the non-crystalline matrix, as indicated in Fig. 20.9(b).

In fibrillar structures, with less than perfect orientation as in Fig. 20.9(c), a

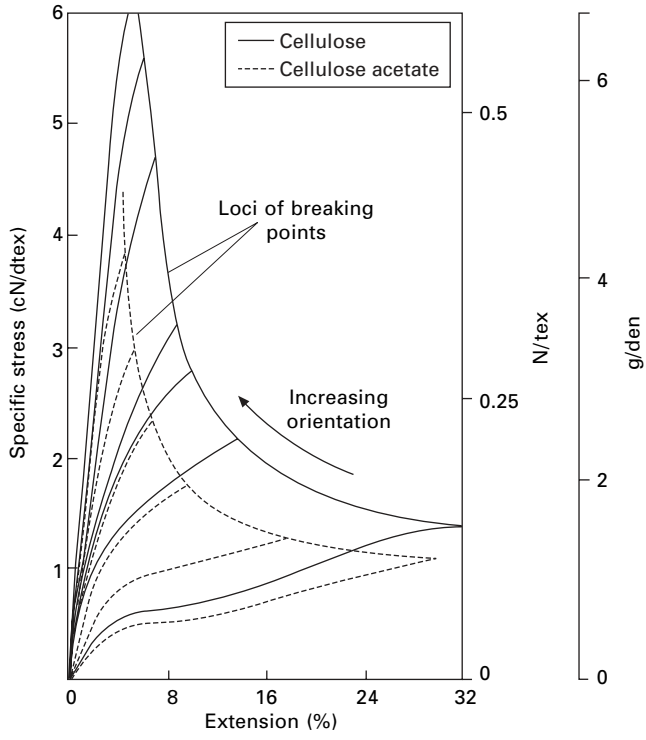

20.8 Stress–strain curves of filaments of varying degrees of orientation. The dotted curves are secondary cellulose acetate and the full curves are cellulose fibres regenerated from acetate. The lowest curve in each set is for unoriented material. From Work [5].

contribution to extension can come from straightening of fibrils, as well as the fibril extension considered in the last section. The less the degree of orientation, the greater is the contribution, and thus the stress–strain curve is at a lower level. A detailed theory of a particular model of this situation has been worked out by Hearle [6] and agrees reasonably with experimental results. It turns out that the major resistance to extension by straightening of fibrils comes not from the bending resistance of the fibrils themselves, but from the resistance to deformation of the disordered material between the curved fibrils.

20.2.4 Ultimate failure

Rupture is, in general, more difficult to explain in detail than earlier deformation behaviour because it is determined by extremes, by the concurrence of abnormal stress concentrations with abnormal structural weaknesses. There has been no special study of stress concentrations in fibres beyond the general recognition that high stresses will occur near cracks, voids and foreign particles. Places of particular weakness, which can be a nuisance in processing even when they occur only at intervals of thousands of kilometres, can probably be attributed to major defects of this sort. But

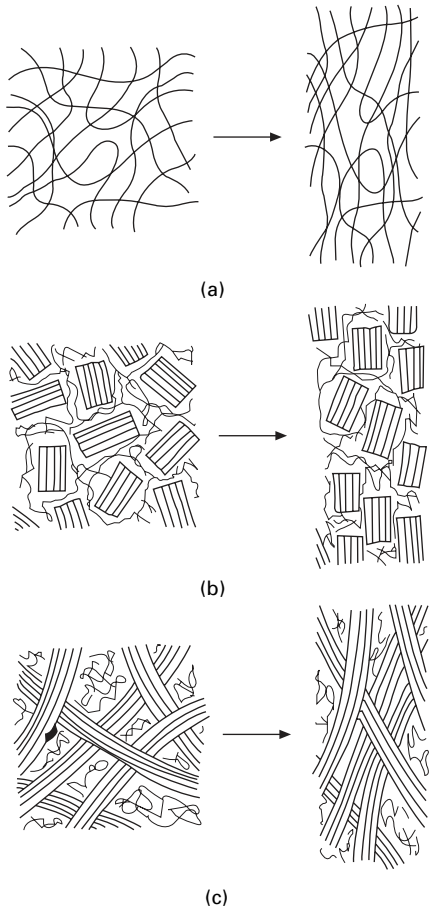

20.9 Schematic representation of effects of orientation: (a) network; (b) micelles; (c) fibrils.

the occurrence of tensile fracture of rayon in a laboratory test, with a test length of a few centimetres, appears to involve multiple initiation and development of fracture at many places within the fibre. Thus, while there will be an influence of the statistical coincidence of points of weakness and of fibre irregularity, the fibre strength will be related to the general ultimate strength of the material structure.

It is simplest to consider first wet rayon, with a structure composed of crystalline regions, linked together by tie-molecules (strictly, better called tie-segments of molecules) passing through non-crystalline regions, as illustrated in Fig. 20.10. The structure will fail and part when all the links along some line such as AB, which represents a surface in the real three-dimensional structure, are broken.

Free ends emerging from a micelle will contribute nothing to the strength. The influence of total chain length (degree of polymerisation or molecular weight) is therefore apparent, since the shorter the chains the more free ends there will be. In

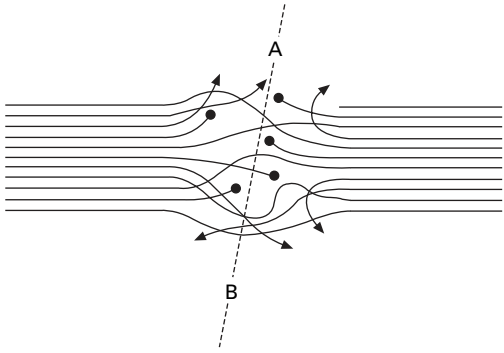

20.10 Schematic representation of chain molecules emerging from micelles, showing chain ends, tie-molecules between the two micelles, and links to other micelles. The line AB continues between other micelles.

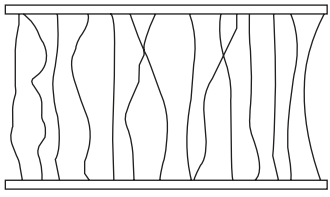

20.11 Tie-molecules of varying length between micelles.

typical rayon fibres, about one-third of the chains emerging from a micelle will be free ends[4].

The other factor that is important is the distribution of segment lengths between micelles as illustrated in Fig. 20.11. As the structure is extended, the shortest segments will break first, but there will still be enough others to take up an increased load. Eventually, however, as the peak of the distribution of segment lengths is approached, there will be insufficient segments left to support the load, and catastrophic failure will occur. The situation is similar to that of a fibre bundle discussed in Section 14.4.

A detailed theory along these lines has been worked out by Cumberbirch and Mack [7, 8], using rubber chain conformation theory to obtain the distribution of chain lengths. There is good agreement with experimental results, and Fig. 20.12 shows the variation of wet strength with degree of polymerisation and orientation.

Both the experimental and the theoretical results demonstrate that, up to a certain level, care in maintaining a high degree of polymerisation (DP) of the cellulose is valuable in improving strength. But there is little advantage to be gained by having a DP greater than about 500, since the number of free ends has then become negligible. Other work shows that it is important to pay attention to the distribution of chain lengths, as well as to the mean value. Any appreciable number of short chains is undesirable.

[4]Owing to the stiffness of cellulose molecules, it is reasonable to assume that there is no chain folding at the ends of crystallites. This is not true for more flexible polymers.

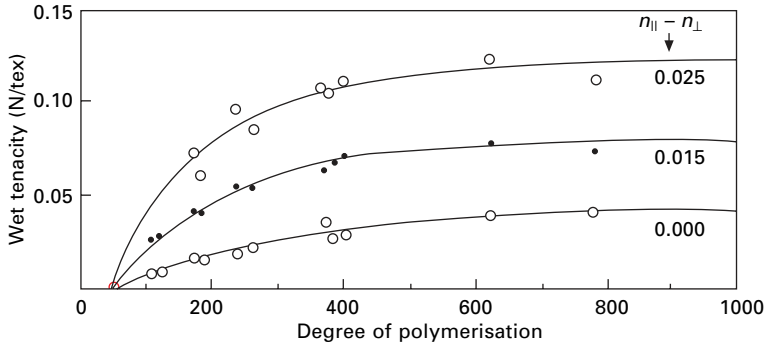

20.12 Theoretical prediction of variation of strength of wet rayon with degree of polymerisation, compared with experimental results, at varying degrees of orientation given by birefringence ($n_{\parallel} - n_{\perp}$). From Cumberbirch and Mack [8].

In dry rayon, including rayon at medium humidities, the tie segments will be linked together by hydrogen bonds. One consequence of this is that the free ends contribute to holding the structure together, so that the strength is increased. The shorter the chains, the greater will be the increase; or, conversely, the decrease in strength on wetting will be greater in ordinary rayon than it will be in better quality rayon with a higher degree of polymerisation. It is also possible that some of the weakening effect due to the range of tie-segment lengths may be mitigated in the crosslinked network.

20.2.5 Torsion

In torsion, shear forces are between the molecules. Deformation in this way is much easier than in tension, just as it is easier to twist a bundle of rods than to stretch it. Consequently, the shear modulus should be less than the tensile modulus. This is found in practice (see Section 17.3.3), the difference being greatest for the most highly oriented fibres.

Water has a great effect on the intermolecular forces, so it is not surprising that it has a great influence on fibre torsional rigidity, as shown in Fig. 20.13.

20.2.6 Creasing

Creasing and crease resistance may be explained on a molecular theory. If a structure, such as the one in Fig. 20.14(a), is bent into a crease, there are two possibilities. The crosslinks may break, and re-form in new positions, as in Fig. 20.14(b). On removal of the load, there will be no recovery, and a crease will be left. Alternatively, the crosslinks may be strained without breaking, as in Fig. 20.14(c). Under these conditions, there will be a recovery on removing the load, and no crease will result.

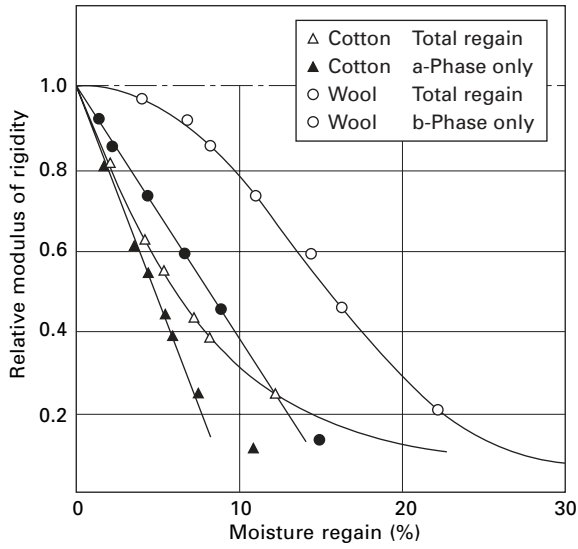

20.13 Modulus of rigidity (relative to value when dry) plotted against moisture regain.

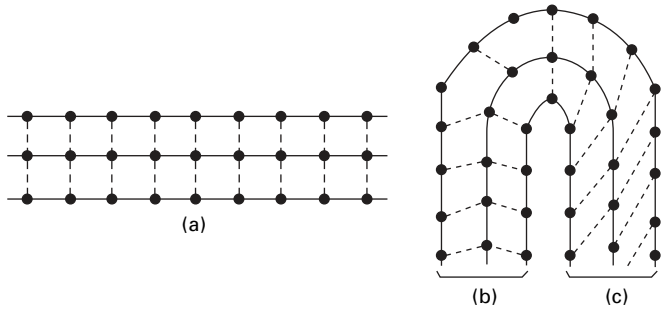

20.14 Creasing and crease-resistance: (a) schematic representation of structure with crosslinks; (b) formation of new crosslinks, giving a crease; (c) straining of crosslinks, leading to crease recovery.

20.3 Nylon, polyester and similar fibres

20.3.1 Molecular responses and fine structure

Polyamide and polyester molecules have important differences from cellulose molecules, which contribute to their superior properties in manufactured fibres. In nylon 6, there is an alternation between five —CH_2— groups and —CO·NH— groups. Nylon 66 is similar, except that the repeat is twice as long with alternately four and six —CH_2— groups. Polyester (PET) has an aliphatic sequence —CO·O·CH_2·CH_2·O·CO—, which with six main chain bonds matches the —CH_2— sequences in polyamides, alternating with benzene rings. These similar structures, or near versions of them, are ideal for synthetic fibres for general textile uses. At room temperature, the aliphatic sequences

in amorphous regions provide a freedom that gives extensibility and the interactions of the —CO·NH— groups or benzene rings in amorphous and crystalline regions give stability, strength and suitable stiffness to the structure.

Figure 20.15 illustrates how the fibres respond to change in temperature. In the unimportant range below about –100 °C, energy barriers prevent freedom of rotation around main chain bonds in the aliphatic sequences. The —CO·NH— groups are strongly hydrogen bonded. The material is fully glassy with high stiffness. Above –100 °C, the thermal vibrations are large enough to overcome the barriers and allow free rotation, as shown in Fig. 20.2. The aliphatic sequences thus act as short rubbery links. The change at around –100 °C is the first half of a glass-to-rubber transition, as suggested in Fig. 20.16. At around 100 °C[5], the thermal vibrations become large enough for hydrogen bonds in nylons and phenolic interactions in polyesters to become mobile. The glass-to-rubber transition is completed. There is some softening of nylon 66 and PET at temperatures near 200 °C with a mechanism that is not well understood but allows for permanent heat setting. Finally, somewhere above about 250 °C, the crystals melt and the material becomes a spinnable liquid, which can be extruded to form fibres. Softening melting temperatures are lower in nylon 6.

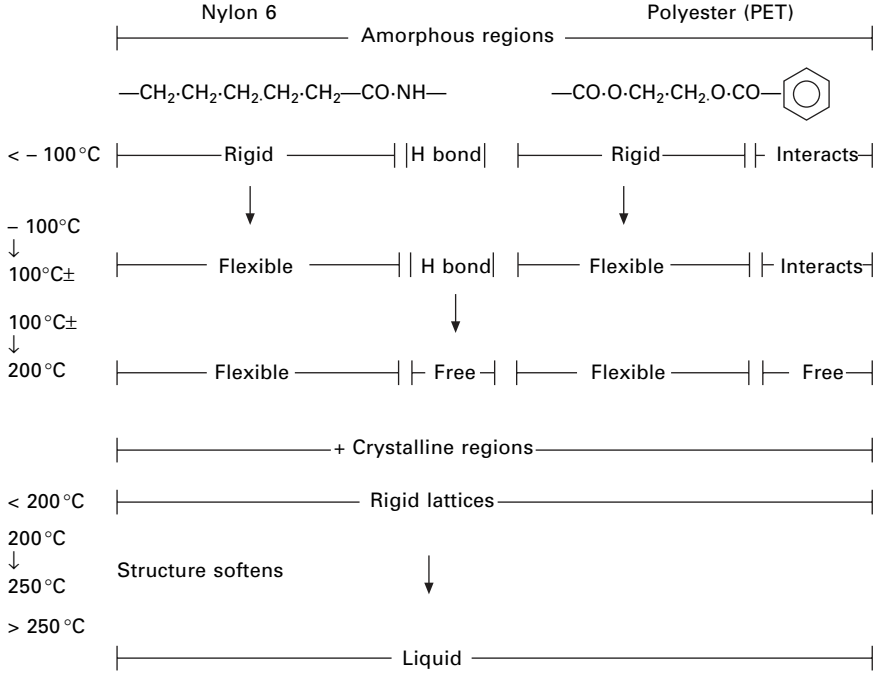

20.15 Polyamide and polyester molecular structures and their thermal transitions. Note that temperatures are approximates within ± 25 °C, and are less in nylon 6 than in polyester (PET).

[5]As discussed in Chapter 18, the transition temperature is lower in wet nylon, is a bit higher in polyesters, and is time dependent.

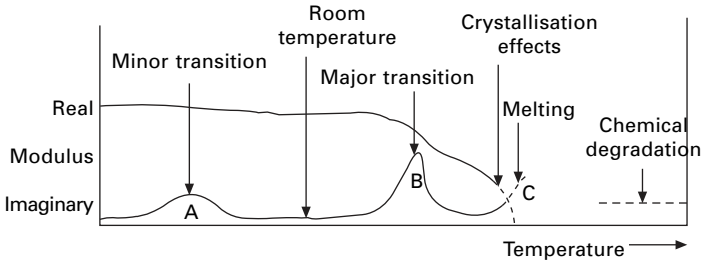

20.16 Transitions in an 'ideal' fibre. From Hearle [9].

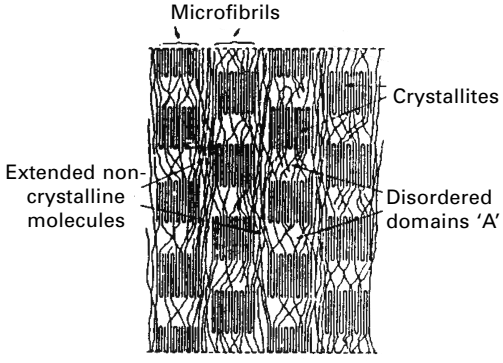

20.17 A model of the fine structure of a polyester fibre, as proposed by Prevorsek *et al.* [10].

A version of a common working model, by Prevorsek *et al.* [10], for the fine structure of polyester (PET) fibres is shown in Fig. 20.17. They have a similar model for nylon 6, except that they place the crystallites in register and not staggered as in Fig. 20.17. Although such views are probably a reasonable representation of the real structure, they suffer from being 2D pictures of a 3D network and there remains much uncertainty about the details of the structure. A simplified model, which will be used in a theoretical derivation, is shown in Fig. 20.18. Other views of roughly cuboid crystals, with a mixture of chain folding and emerging tie-molecules at the ends of crystallites, are shown in Figs 20.19(a,b). Typically, there will be about 100 molecules in the cross-section of a crystallite and the width will be 5–10 nm. There is some indirect evidence suggesting that the ratio of length to width in polyester crystallites is greater than in nylon. In some circumstances the distinction between crystalline and amorphous regions may be less sharp, as indicated in Fig. 20.19(c). The crystallinity is typically about 50% when the fibre has had some exposure to heat or drawing.

20.3.2 A network model

The modelling of a fringed micelle structure in Section 20.2.2 is based on mixture laws applied to a composite of crystalline and amorphous regions. However, it is clear that the model is arbitrary. If the micellar line in Fig. 20.6 had been placed

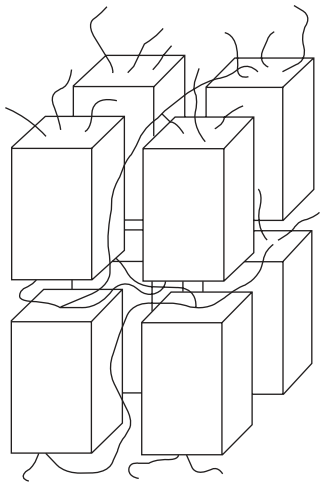

20.18 Simplified model for theoretical analysis, showing a regular array of crystallites linked by tie-molecules, of which only a few are shown.

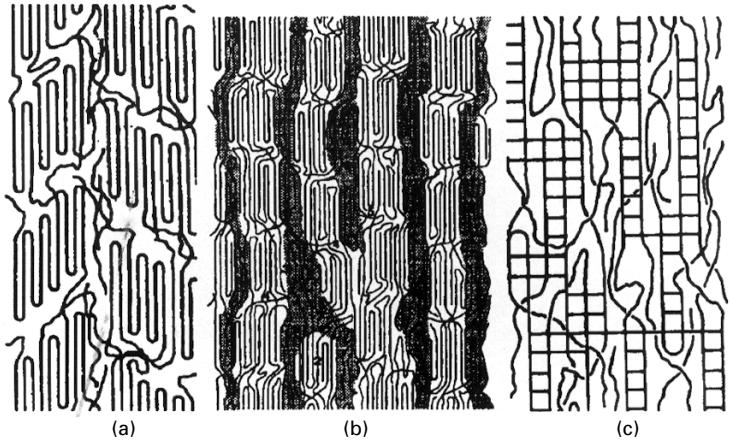

20.19 Views of fine structure of nylon fibres. (a) A common working model proposed by Hearle and Greer [11]. Angled ends are based on small angle X-ray diffraction pattern of nylon 66. (b) From Murthy *et al.* [12], based on X-ray diffraction studies of nylon 6. (c) An alternative form, from Hearle [13].

between the lines for fibrillar and lamellar forms at the same strain, it would have been much higher. Hearle *et al*. [14] showed that the predictions of a combined series and parallel model could be several orders of magnitude apart depending on whether modulus weighting or compliance weighting was used in combining the series and parallel parts. A simplistic approach is not quantitatively viable. It is possible that a more detailed calculation of stress distributions, e.g. by finite element computing, might give better results.

A network model is a more promising way forward and is particularly applicable above the glass transition temperature when the tie-molecules can be regarded as

flexible chains linking crystallites, which would be large-scale crosslinks in an elastomeric polymer network. A theory [15] of this type has been developed and is outlined by Hearle [16]. The quantitative predictions of stress are too low, but both the methodology and the results are instructive.

The basic premise is that the state of the material is determined by the energy per unit volume U, which is the sum of two terms: the energy of extension of tie-molecules between crystallites and the energy of volume change. The first term is the sum over all tie-molecules of the integral of equation (20.4) and the second depends on the bulk modulus k and the volume strain e_v;

$$U = \Sigma \int_{l_0}^{l} \left(\frac{kT}{a}\right) \left[\text{arc}\,\mathcal{L}\left(\frac{l}{L}\right)\right] + {}^1/_2\, k e_v^2 \tag{20.10}$$

The assumed fine structure is the regular array of orthogonal crystallites linked by tie-molecules, as indicated in Fig. 20.18. The crystallinity determines the division of polymer material between crystalline and amorphous regions. Hence the total length of tie-molecules in the set can be calculated. The length and width of the crystallites and the ratio of axial to transverse separation are geometrical parameters. The summation is over the tie-molecules in unit volume. A representative set is given by all the tie-molecules that emerge from the end of a crystallite, which equals the number of molecules in a cross-section of the crystallite minus twice the number of chain folds. This length must then be divided among the locations of the other ends of the tie-molecules, with a correction for chain ends and loops back to the same crystallite. In the absence of more structural information, arbitrary choices were made with links as far apart as next nearest neighbours. It was assumed that the ratio of actual chain length to the shortest path was constant for all tie-molecules. This gives values of l, which is the end-to-end length along the shortest path, and the fully extended chain length L for all the tie-molecules. The integral is from the initial end-to-end length l_0 of tie-molecules in the stress-free state to the extended length l in a deformed fibre. Affine deformation of the positions of the crystallites changes the spacing between crystallites and enables l to be calculated.

For uniaxial extension, the applied strain determines the change in axial spacing of crystallites, but the transverse spacing is left as a dependent variable to be determined by energy minimisation. This gives a value of the Poisson ratio. The procedure is then repeated with a small change of axial strain. The change in energy per unit volume equals the stress times the change in strain. Hence the stress–strain curve can be computed.

There is a difficulty. There is no guarantee that the parameters used to define the initial geometry relate to the stress-free state. Indeed it would be exceptional if they did. The first step in the computation is therefore to allow both axial and transverse spacing to be dependent variables and use energy minimisation to determine the actual spacings in the stress-free state. This illustrates an important insight. In drawing or looking at models of fine structure, such as those shown in Figs 20.17 and 20.19, it is natural to assume that they are static models in which, if there is no external applied stress, there are no internal stresses. In reality, the thermal vibrations mean that the tie-molecules are under tension, pulling the crystallites closer together against

the resistance of volume reduction. The structure can be likened to an array of bricks linked by stretched rubber strings.

The parameters needed to define the model for computation are listed in Table 20.1. Although some, such as molar mass of repeat unit, are known exactly, others, such as the connectivity, are almost unknown quantities. Indeed the first estimate of connectivity gave an impossible structure. The shortest paths were longer than the total chain length. More structural studies using modern techniques would give more information to test the theory, but the real advance would come from modelling the structure formation from the more-or-less random arrangement in the melt through crystallisation and drawing.

The predicted stress–strain curves are of the right form for nylon above the glass transition temperature but, unless unrealistic values of parameters are used, give too low values of stress. Although there are obvious ways of making the theory more rigorous, by eliminating approximations, major changes seem to be necessary to make valid predictions. If the fundamental approach is valid, there are various possibilities. Constant values are assumed for many features that will have statistical distributions. In particular, low values of the ratio of chain length to shortest path would have a disproportionate effect in generating high stresses. It is also likely that interactions and entanglements within the amorphous regions cause the energy of

Table 20.1 Input quantities for computation of the network model

Features of the polymer	
#	Molar mass of the repeat unit
#	Length of repeat unit in crystal
#	Crystal density
#	Amorphous density, stress-free
#	Number of equivalent free links per repeat
○	Degree of polymerisation
Features of fine structure	
#	Fractional mass crystallinity
#	Number of repeats in crystallite length
#	Number of repeats across crystallite
#	Series fraction of amorphite
○	Fraction of sites with crystallographic folds
○	Fraction of sites with loose folds
○	Length factor for free ends
○	Length factor for loose folds
○	Relative probability of connector types
Other parameters	
*	Bulk modulus of amorphous material
*	Stress at which chains break
*	Temperature
*	Mass of proton
*	Boltzmann's constant

= required to characterise two-phase structure; ○ = required to characterise connectivity;
* = required to analyse mechanics.

chain extension to be greater than given by equation (20.4). Other neglected features, such as extension and rotation of misoriented crystallites, would lead to lower stresses.

For predictions of the stress–strain curve at room temperature, it would be necessary to model a network linked by hydrogen bonds or phenolic interactions. Long and Ward [17] have applied theories of crosslinked rubbers and show that this explains shrinkage forces, which increase with temperature, as expected for an entropic mechanism. In another paper, Ward [18] considers the change from *gauche* to *trans* conformations of the molecules in the drawing of polyester (PET). In PBT (3GT) the behaviour is complicated by a crystal lattice transition and in PEN by crystallisation effects.

20.3.3 A theory for dynamic mechanical properties

A purely series model, which is a simpler variant of the above theory, has been presented by Davis [19]. The crystallites are in series with tie-molecules that follow the inverse Langevin [4] for force on a flexible chain. He recognises that this only applies at higher temperatures when the chains act as freely orienting links and then uses Rouse's theory [20] to introduce viscous drag on chain segments in the transition temperature region. The predicted value of the loss factor is given by:

$$\tan \delta = \frac{N\eta\omega Z}{E} \tag{20.11}$$

where N = number of load-bearing chains per unit area, η = a temperature-dependent viscosity, ω = frequency, Z = a temperature-dependent structural parameter and E = modulus of the amorphous material. Although the model gives useful guidance, it suffers from quantitative limitations similar to those for the network theory.

20.4 High-performance fibres

20.4.1 Simplistic theory of tensile deformation of HM–HT fibres

At a first level of approximation, theoretical understanding of the deformation of HM–HT fibres is easier than for the general textile fibres. The dominant mechanism is elastic deformation of covalent bonds. In the ceramic fibres, the network is three dimensional, so that similar effects occur in all directions. In the highly oriented linear polymer fibres, axial elongation is resisted by the covalent bond deformation, which therefore exerts the major control on tensile properties of the fibre. Transverse and shear deformations are resisted only by weaker inter molecular forces. In HM–HT carbon fibres, the orientation of the graphite planes parallel to the fibre axis causes covalent bond deformation to be the dominant effect in fibre extension; but perpendicular to the fibre axis there is a mixture of covalent bonding in the planes and weak bonding between the planes.

The simplest case to consider is the behaviour of a fibre made of infinitely long polymer molecules, with a simple —C—C— backbone like that of polyethylene, oriented parallel to one another, but not necessarily in crystalline register, as indicated in Fig. 20.20(a). Because of the perfect uniformity of the structure, a tensile strain e

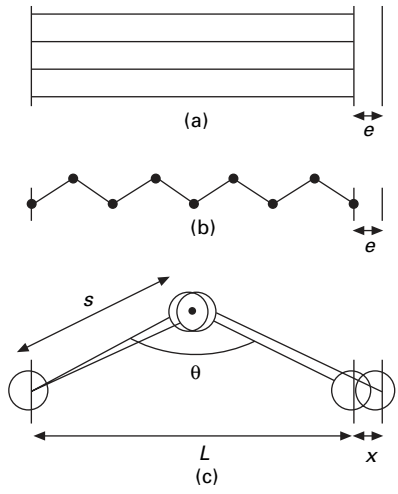

20.20 (a) Perfectly oriented fibre of infinitely long molecules subject to tensile strain *e*; (b) application of strain *e* to molecule; (c) application of strain *e* to repeat unit of molecule.

imposed on the fibre must also occur uniformly along the polymer molecules, as indicated in Fig. 20.20(b), and so to the individual repeat unit in Fig. 20.20(c).

If m is the mass and l is the length of the repeat unit, and U is the change in internal energy associated with an elongation x, then U must be proportional to x^2, in order to give a minimum value at the equilibrium zero-force state with $x = 0$. This leads to the relations, given in terms of a spring constant K as:

$$U = {}^1/_2 Kx^2 \tag{20.12}$$

$$\text{force} = F = \frac{\mathrm{d}U}{\mathrm{d}x} = Kkx \tag{20.13}$$

If we normalise in terms of specific energy $u = U/m$, strain $e = x/l$ and specific stress $f = F/(m/l)$, we can express the relation in terms of a specific modulus E:

$$u = {}^1/_2\, K(l^2/m)e^2 = {}^1/_2\, Ee^2 \qquad f = Ee \tag{20.14}$$

The simplicity of the structure and the small-strain assumption cause the extension to follow Hooke's Law, with a modulus E that is the same for the fibre as for the molecule and is given in terms of basic features of the atomic bonding by $K(l^2/m)$.

The repeat-unit mass m is known from the chemistry, and the repeat length l is given by standard atomic dimensions, or, more exactly, on allowing for some distortion due to neighbouring interactions, by theoretical calculation or measurement on the crystal lattice. The force constant K can be estimated from spectroscopic measurements, which give natural vibration frequencies, or by calculation from interatomic potentials.

In a molecule such as polyethylene, illustrated in Fig. 20.20(c), most of the elongation will come from a change in bond angle θ, with a smaller contribution from change in bond length s. If the energy changes $U(\theta)$ and $U(s)$ due to changes in θ and s are known, including any corrections due to changing interactions with other neighbouring

atoms, then K can be determined. Details of such analyses go beyond the scope of this book, but the following outline indicates the basis of the method.

The geometry is defined by:

$$l = s \sin(\theta/2) \tag{20.15}$$

$$x = \mathrm{d}l = \sin(\theta/2)\mathrm{d}s + {}^1/_2 s\cos(\theta/2)\mathrm{d}\theta \tag{20.16}$$

The energy relations are defined by:

$$U = U(s) + U(\theta) = {}^1/_2 K_s(\mathrm{d}s)^2 + {}^1/_2 K_\theta(\mathrm{d}\theta)^2 \tag{20.17}$$

where K_s and K_θ are the force constants for bond length and bond angle changes, respectively.

Equilibrium will occur at a minimum-energy state given by:

$$\left(\frac{\delta U}{\delta \theta}\right)_s = 0 \qquad \left(\frac{\delta U}{\delta s}\right)_\theta = 0 \tag{20.18}$$

Hence the equations can be solved, and the division of the deformation between ds and dθ determined, together with the value of K in the expression $U = Kx^2$.

There is some uncertainty in the parameters used in the determination of the axial modulus in a perfect polyethylene crystal, and estimates range from 220 to 380 GPa [21], 300 GPa being a commonly accepted value.

Generally, in linear polymers, the modulus of the perfect structure will depend on the molecular geometry, and the calculations are more complicated when there are many atoms in the repeat unit. The most efficient system would consist of a chain of atoms in line, so that the only mode of extension was change in bond length. There is no complete occurrence of this geometry, but, where it occurs in parts of the chain, it will tend to increase the modulus. Zigzag geometry, as typified by the extended polyethylene chain, allows bond angle change to contribute to extension. Nevertheless, the polyethylene molecule is efficient, because most of the mass is in the main chain, with only light hydrogen atoms pendant to it. The modulus will be lower if there are large side groups, which contribute mass but do not help to resist elongation. Modulus will also tend to be lower if some bonds carry a higher than average load, for example, when single-bond connections carry the whole load between rings of atoms, where the load is shared. A major decrease in modulus occurs when bond rotation can contribute to elongation. This occurs in helical chains and is the reason why polypropylene has an inherently low modulus, even in a perfect structure.

On the above basis, the para-aramid molecules have the slight disadvantage from the —CO·NH— links between the benzene rings, possibly offset by the more axial orientation of some groups. The axial modulus has been estimated to be 200 GPa [22]. The influence of molecular geometry is shown by the fact that the corresponding figure for the meta-aramid is 127 GPa.

For a perfectly oriented graphitic fibre, the theoretical treatment would be similar, except that the geometrical deformation occurs in aligned planes. Values close to 1000 GPa are given for the theoretical modulus [23].

Similarly, in three-dimensional crystal structures, extension can be linked to change

in bond lengths and bond angles and the modulus calculated. But many of these materials can also be obtained as large single crystals, so that the modulus is easily measured.

Commercial fibres, of course, do not have the degree of perfection of these simplistic models. Nevertheless, in summary, we can say that, to a first approximation, all the HM–HT fibres are linear elastic, with a tensile modulus E related to the modulus E_c of an appropriately (axially) oriented single crystal by the relation:

$$E = pE_c \tag{20.19}$$

The parameter p is a measure of the efficiency of the structure in utilising the crystal properties and would be the product of a number of factors dependent on deviations from the ideal model. In special cases, such as polydiacetylene, single crystal fibres made by solid-state polymerisation, the value of p will be 1. But, in all cases, it will not be so much less than 1 that it becomes a meaningless quantity, because the deformation mechanisms are completely different, as they are, for example, in a general textile fibre such as nylon.

Some values of E_c together with typical values of E and p, are given in Table 20.2. However, in interpreting this table, it must be remembered that there is some uncertainty in the estimates of E_c and that the experimental values are for typical current fibres, selected as high-modulus variants.

20.4.2 Deviations from the simplistic theory

Table 20.2 shows that real fibres do not achieve the theoretical maximum modulus, so it is necessary to consider the factors that lead to a reduction in efficiency. In addition, the non-linearities of response of the para-aramid and HMPE fibres need explaining. There are several reasons for deviations from the ideal behaviour.

The first is disorientation. The forces between linear polymer molecules or between separate graphitic planes are much weaker than those along the covalent bonding of the chains or planes. This results in a dependence of modulus on direction. Figure

Table 20.2 Approximate tensile moduli of crystals E_c and fibres E

Material	Modulus (GPa)		Specific modulus (N/tex)		
	E_c	E	E_c	E	p
Polyethylene	300		310		
Spectra 1000		175		180	0.50
Para-aramid PPTA	200		140		
Kevlar 149		145		100	0.73
Graphite	1000		550		
Grafil HM-S/12K		400		220	0.39
Silicon carbide	700		250		
Nicalon		200		80	0.29
Alumina	530		130		
FP		380		100	0.72

20.21 illustrates this for the variation of Young's modulus with direction in a graphite crystal: at 8° inclination, the modulus has fallen to about one-tenth of the 0° modulus, and at 45° to almost one-hundredth. Consequently, any disorientation within carbon fibres will lead to a reduction of stiffness, the modulus being an appropriate average of the moduli at the orientations present in the fibre. In the para-aramid poly phenylene terephthalamide (PPTA), the transverse modulus of the crystal is reported to be 4.08 GPa [24], which is one-fiftieth of the axial modulus. In polyethylene, the crystal moduli have been calculated [25] to have values, given in the terminology of Fig. 20.22 as: Y_L = 325 GPa; Y_T = 12–14 GPa; n_{TT} = 6 GPa; n_{LT} = 2–3 GPa. The range of values for Y_T and n_T depend on the particular transverse direction in the crystal. A general theory of the effect of orientation is given in the next section.

A second reason for a reduction in stiffness is what might be termed crumpled disorder of the molecules, or, on a larger scale, defects within the structure. In either case, the initial application of tension leads to a tightening-up of the structure as the buckling of the molecules is pulled out and the structure becomes more compact. This effect will be most pronounced at lower stresses and so will lead to the increasing slope of the stress–strain curve found in para-aramid fibres. The crumpling may be irregular but in the para-aramid fibres is believed to be due to the regular pleated structure shown in Fig. 20.23. As stress is increased, there is progressively less pleat to pull out. The processing that gives the higher-modulus versions changes the structure and reduces the effect. If the compacting of the structure involves the breaking of hydrogen bonds in order that molecules may slip and rearrange, then the extension will be time dependent. This explains the creep.

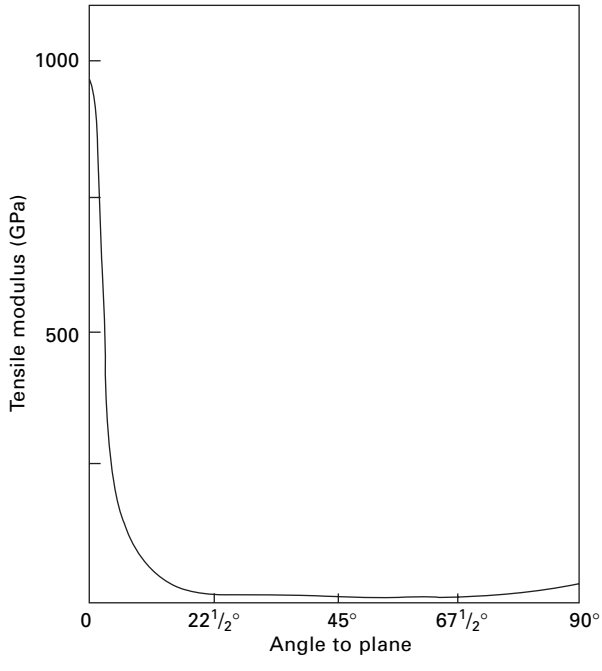

20.21 Variation of modulus of perfect graphite crystal with direction [6].

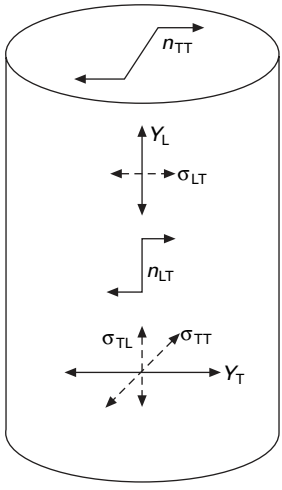

20.22 Elastic constants of a transversely isotropic system.

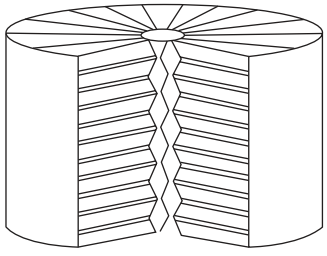

20.23 Radial pleated structure of a para-aramid fibre (Kevlar).

A third reason for the reduction in fibre modulus is slip near the ends of the molecules. At a chain end, the tensile stress must be zero, but it can build up owing to shear forces from neighbouring molecules. A simple analysis [3] shows that this would lead to a factor equal to $1 - {}^1/_2\,[(f/f_b)/AN]$ in the expression for p in equation (20.19), where f is the applied tensile stress, f_b is the bonding shear stress, A is the aspect ratio of a repeat unit, and N is the degree of polymerisation, giving AN as the aspect ratio of the molecule. The important features of this result are (1) that the reduction in modulus is less for a high molecular weight polymer and (2) that the reduction increases with stress and causes the stress–strain curve to soften at high stresses. This explains the behaviour of HMPE. The associated creep would be due to the fact that, even at room temperature, but to a greater extent at higher temperatures, a certain equilibrium concentration of defects, namely kinks of various sorts in the molecules, will be present. Under the influence of thermal vibrations, these will move through the system and allow the slow movement of chains past one another.

Computational molecular modelling is the way forward for more exact predictions of the stress–strain behaviour of HM–HT polymer fibres. Dynamic molecular modelling of thermotropic polyesters has been carried out by Johnson *et al*. [26].

The effects so far described apply to the one- and two-dimensional molecular

materials. The situation is somewhat different in the three-dimensionally bonded ceramic fibres. Here the modulus will be reduced because there are easier modes of deformation in an irregularly bonded material such as amorphous silicon carbide (Fig. 20.24(b)) or glass (Fig. 20.25) than there are in the regular crystal of Fig. 20.24(a). Detailed analysis would require a proper description of the disordered packing of the atoms. In a polycrystalline material, deformation will be somewhat easier at grain boundaries.

20.4.3 Strength

Theoretical analysis of fibre strength and detailed understanding of how and why strengths fall below maximum possible values are not easy. The basic theory of the tensile strength of a perfect crystal was described in Section 20.1.2 and suggests that the maximum strength should be about 0.1 times its modulus. Among the factors that lower modulus, disorientation and slip at the ends of molecules will also lower strength, but the removal of crumpled disorder at low strains will not. Any non-uniformity in the distribution of stress between different parts of the structure will lower strength.

Failure is a competitive phenomenon, determined by extreme-value and not central-

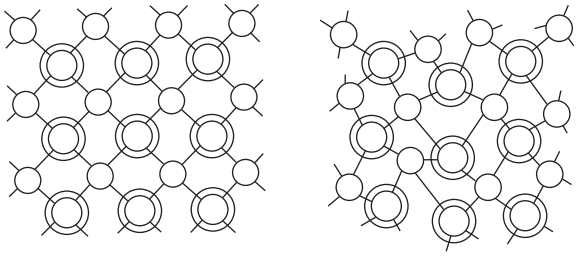

20.24 Schematic two-dimensional representation of the structure of a material such as silicon carbide: (a) crystalline; (b) amorphous. In the actual material, the atoms are distributed over three dimensions, to give a more complicated network.

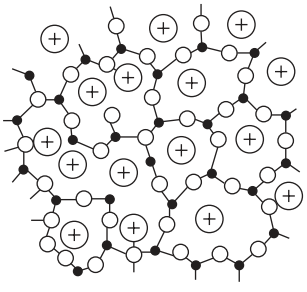

20.25 Schematic representation of the structure of glass, composed of silica, SiO_2, and metal oxides.

value statistics, and will always occur in whichever way is easiest. Even at the theoretical level of a perfect crystal, this means that rupture may occur not under tensile stress across the plane AB in Fig. 20.26(a) but under some other stress, such as the resolved shear stress across CD. At the practical level, there are all the complications of local variations in stress due to gross structural differences, of stress concentrations at microscopic defects, and of uneven sharing of load at the molecular level in an imperfect structure.

The simple argument also ignores the time dependence associated with thermal vibrations, which allows jumps over the point of inflection as discussed in Section 20.7.2. Some detailed modelling by Termonia and Smith [24] predicts the results shown in Fig. 20.27 for the variation of strength of PPTA with temperature, compared with experimental values for *Kevlar*, and of the variation with time at room temperature predicted for PPTA and polyethylene. The predictions are, of course, very dependent on the choice of input parameter used in the computational modelling: there is a major effect of activation energies for bond breakage and a less effect for activation volume. The authors' conclusion that fracture in both PPTA and polyethylene is initiated through primary-bond breakage is not immediately compatible with the explanation of breakage that comes from the morphology.

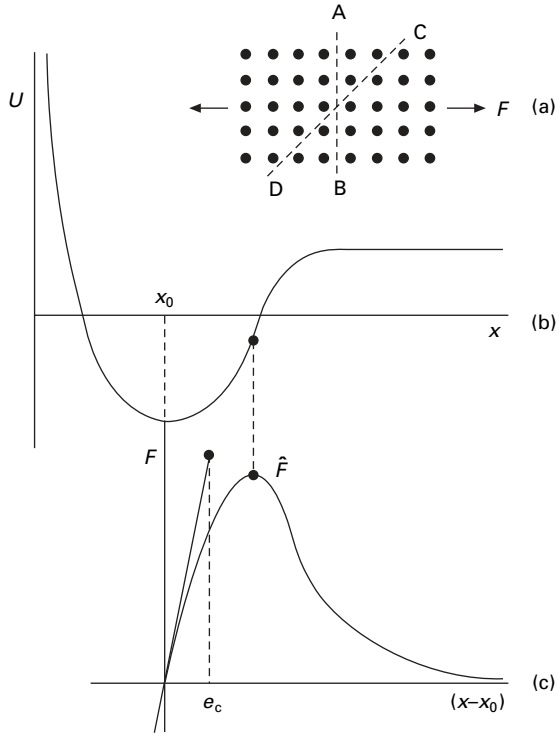

20.26 Simple theory of tensile strength: (a) perfect crystal under tensile force *F*; (b) variation of internal energy *U* with spacing *x*; (c) variation of force *F* with elongation $(x–x_0)$.

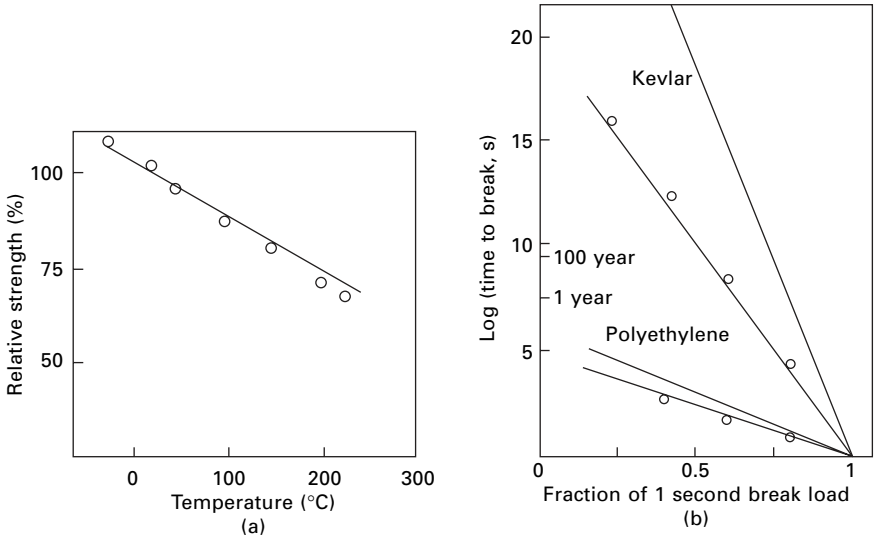

20.27 Theoretical model predictions by Termonia and Smith [24], (a) change of strength of PPTA (*Kevlar*) with temperature (full lines show experimental results); (b) variation of time to break at different stress levels at room temperature for PPTA (*Kevlar*) and polyethylene (full lines indicate range of experimental results).

20.4.4 Elastomeric fibres

At the other end of the performance limits from HM–HT fibres, we have elastomeric fibres, which show good elastic recovery up to high extension. Natural rubber follows the standard network theory described in Section 20.1.2. Spandex fibres, with *Lycra* as one example, are composed of segmented polyurethanes in the form of block copolymers. The hard segments crystallise, and the soft segments provide rubbery linkages between the crystallites. The structure is thus an unoriented fringed-micelle form with the crystallites widely separated by amorphous regions, as suggested in Fig. 20.28. A development of the network theory in Section 20.3.2, which included crystallite rotation, may be applicable.

20.5 A general theory of orientation

Northolt (27) presented a theory of the effect of orientation, which was first applied to predict the modulus of highly crystalline, highly oriented polymer fibres, such as the para-aramid PPTA (*Kevlar*, *Twaron*). The theory has since been developed to be more rigorous (28), to include yield, hysteresis and creep and to be applicable to semicrystalline fibres of cellulose, nylon and polyester (29–32). The full tensor analysis is too long to be given here, but the essential principles can be explained.

The model is assumed to be made up of structural units at angles given by an orientation distribution. In the original version for PPTA, the units were long crystalline blocks, referred to as fibrils, which were variously oriented in the fibre. A particular

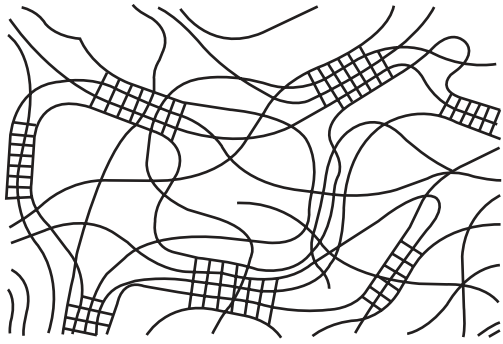

20.28 An unoriented fringed micelle structure with crystallites separated by coiled chains.

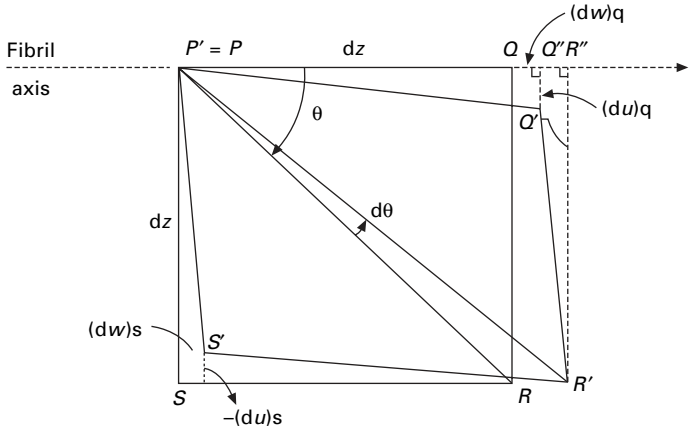

20.29 Deformation of a structural unit, based on a diagram by Northolt and van der Hout [28].

form would be the zigzag pleated structure shown in Fig. 20.23, where all the molecules are locally oriented in the same direction but switch from one direction to another. In other cases, it is necessary to take account of the distribution of orientation and use an appropriate mean value. For the semicrystalline fibres, the units are better viewed as blocks of material with locally parallel crystallite orientation, but different orientations in different blocks. There is evidence that nylon and polyester fibres consist of local domains varying in crystalline orientation, but with a constant orientation in each domain (see Section 1.7.2). The blocks contain quasi-fibrils with an alternation of crystalline and amorphous material. The fibrils are separated by amorphous regions in parallel with the fibrils.

For a fibre subject to uniaxial stress f giving an axial extension and a lateral contraction, Fig. 20.29 shows the deformation of a unit that is at an angle θ to the fibre axis. In addition to its axial strain and lateral strain, the rotation of the unit direction causes a shear strain of the unit. The magnitudes of the strains are expressed by the strain tensor, which depends on the geometry of the deformation. An analysis

shows that the modulus E of the fibre at any strain is given in terms of the axial modulus E_u of the unit, the shear modulus G_u and what is described as an unusual (*sic*) parameter of the orientation distribution [28] by an additive expression for compliances:

$$\frac{1}{E} = \frac{1}{E_u} + \frac{<\sin^2\theta>}{2G_u} \tag{20.20}$$

$$<\sin^2\theta> = \frac{\int_0^{\pi/2} P(\theta)\sin^2\theta\cos\theta\,d\theta}{\int_0^{\pi/2} P(\theta_0)\cos\theta_0\,d\theta} \tag{20.21}$$

where $P(\theta_0)d\theta_0$ is the initial fraction of units with an orientation angle between θ_0 and $(\theta_0 + d\theta_0)$ and $P(\theta)\,d\theta$ and $P(\theta)\,d\theta_0$ gives the fractions after extension.

For highly crystalline fibres, such as the para-aramids, E_u and G_u would equal the crystal moduli E_c and G_c. This would give a contribution to p in equation (20.19) of a factor equal to $(1 + E_c<\sin^2\theta>/2G_c)^{-1}$. As stress increases, the elongation of the specimen causes $<\sin^2\theta>$ to increase and thus to give an increased slope of the stress–strain curve. Fig. 20.30 shows a comparison of the predictions of the theory with experimental data for high- and low-modulus PPTA fibres (*Twaron*) with $E_c = 240$ GPa, $G_c = 2$ GPa and $<\sin^2\theta>$ derived form sonic moduli measured before the second extension. The increasing stiffness is particularly obvious for the more extensible fibre.

In considering the application of the theory to less highly oriented fibres, it should be noted that, owing to the presence of cos θ in equation (20.21), $<\sin^2\theta>$ does not

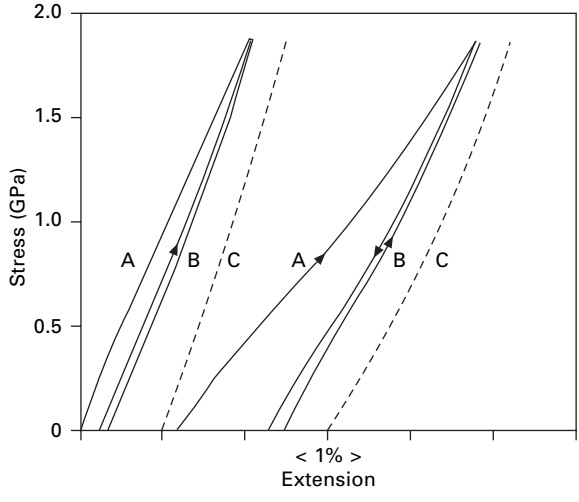

20.30 Comparison of predictions of equation (20.20) for high- and low-modulus PPTA fibres: A, first extension; B, second extension; C, theoretical prediction. The curves all start from zero extension, but are displaced for clarity. From Northolt and Hout [28].

show a simple increase with θ. Some other approximations applicable to highly oriented fibres may not be valid and the full theoretical derivation should be followed.

Figure 20.31 is a schematic representation of the yield process in polyester, cellulose and similar fibres, showing the sequence from zero to increasing stress *f*. The initial distribution of orientations first shows small changes in angle, but then progressively yields to an angle θ_4. The yield theory [31] uses an affine deformation of an isotropic material dependent on draw-ratio λ to give values for $<\sin^2\theta_0>$. If the analysis is simplified to a bundle of parallel units at a constant orientation angle θ_a, given by the average of the distribution, the yield strain e_y is given in terms of the shear yield stress f_g by:

$$e_y \approx \left[\left(\frac{1}{E_u}\right) + \left(\frac{<\sin^2\theta_0>}{2G_u}\right)\right]\left(\frac{f_g}{\sin\theta_a \cos\theta_a}\right) \tag{20.22}$$

For fibres with low and medium orientation:

$$e_y \approx {}^1/_2 f_g \tan\theta_a \tag{20.23}$$

For well-oriented fibres uch as PPTA, the viscoelastic theory [32] gives the following expression for the strain $e(t)$ as a function of time t under a stress f:

$$e(t) = \frac{{}^1/_2 k \log(t) <\sin^2\theta_0> f}{[1 + (f/2G_c)]^3} \tag{20.24}$$

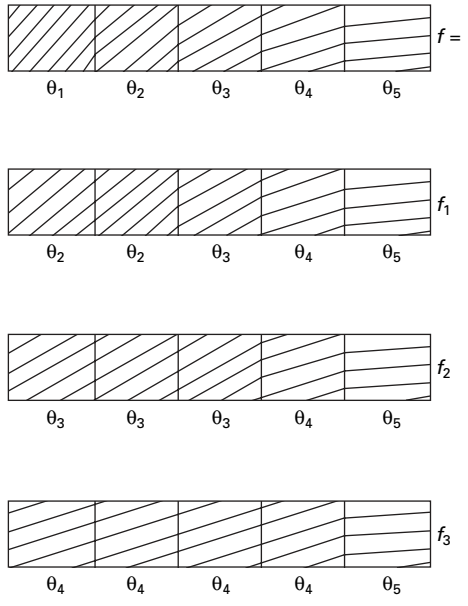

20.31 Schematic representation of yield. After Northolt *et al.* [31].

20.6 Structural effects in natural fibres

20.6.1 Cotton and other plant fibres

Vegetable fibres have a specialised structure of crystalline fibrils spiralling around a central axis. Analysis of the mechanics of such a system has many similarities to that of twisted-yarn mechanics [33]. In such systems, the resistance to extension decreases as the helix angle increases. There are two reasons. For a given axial strain in the system as a whole, the tensile strain in the elements is less at higher angles, and at higher angles, there is a reduced contribution to the total tension. An analysis by Hearle [4], which considers both the extension of the crystalline fibrils and the possible reduction in volume, by means of a minimum energy method, gives the following results for an assembly with a constant helix angle at all radii throughout the fibre:

$$E = E_c (\cos^2\theta - \sigma \sin^2\theta)^2 + K(1 - 2\sigma)^2 \tag{20.25}$$

$$\sigma = \frac{E_c \cos^2\theta \sin^2\theta + 2K}{E_f \sin^4\theta + 4K} \tag{20.26}$$

where E = fibre tensile modulus, σ = fibre Poisson ratio, θ = helix angle, E_c = tensile modulus of cellulose crystal and K = bulk modulus.

Figure 20.32 shows an application of this equation to experimental results for the dynamic modulus of dry stretch mercerised cotton fibres, due to Meredith [34]. The mercerisation has caused the fibre to be a circular cylinder with a helical internal geometry in contrast to the more complicated form of natural cotton fibres discussed below. The assumed value of the moduli, 70 GPa, is of the same order as that

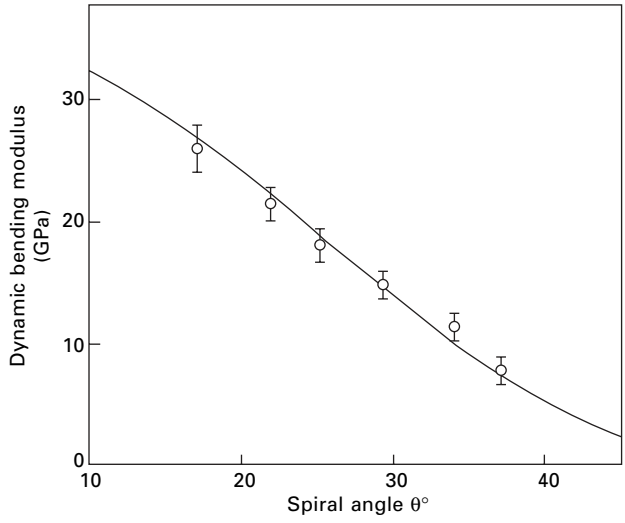

20.32 Comparison of experimental values of dynamic modulus of stretched mercerised cotton fibres at 0% r.h., 20 °C, with theoretical prediction from equation (21.25) From Meredith [34].

calculated theoretically for a crystal lattice of cellulose. Hearle [4] showed that the equation also fitted results for other plant fibres.

The complications that occur with natural cotton fibres are illustrated in Fig. 20.33, which shows how the structural features progressively modify the predicted tensile stress–strain curve. The starting point is the modulus of the crystal lattice of cellulose (A), which gives the properties of the crystalline fibrils. The helical structure in the circular hollow fibre as formed (B) leads to a lowering of modulus as described above. Although there are small changes of helix angle through the fibre, it is reasonable to take a constant value of 21°. However, in cotton, there are reversals of the helices from left-handed to right-handed helices (C). Under tension, a twisted structure will untwist, unless prevented from doing so, and lead to increased length. Free untwisting can occur at the reversals and add to the fibre extension. Finally, there are the convolutions (D), which, as shown in Section 13.5.2, are pulled out under tension. The convolutions provide another mode of extension, which leads to the curvature of the stress–strain curve of cotton. In the dry state, deformation is inhibited by hydrogen bonding between fibrils, but when wet this resistance to deformation due to shear stiffness is reduced leading to lower stresses.

A quantitative theory of the above effects, with some simplifying assumptions has been given by Hearle and Sparrow [35][6]. The simple theory of twisted yarn mechanics

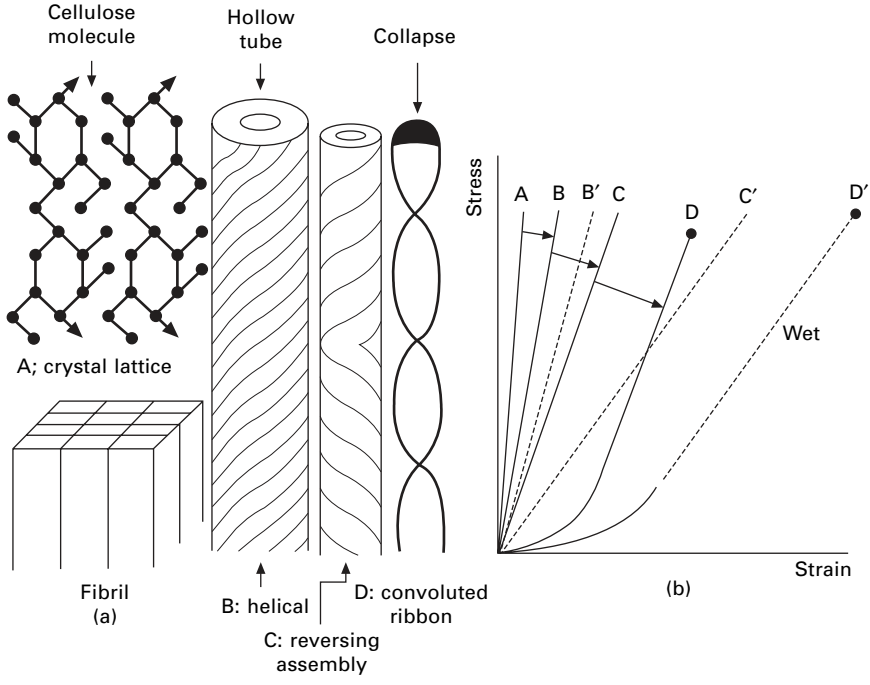

20.33 (a) Structural features of cotton fibres. (b) Development of tensile stress–strain curves. From Hearle [16].

[6]The full analysis includes a volume energy term, but surprisingly energy minimisation shows that extension is at constant volume.

[36] which is the basis for equation (20.25), neglects any resistance to shear, but this is taken into account in a more advanced treatment [37]. For a tensile strain e of the helical structure (B), the crystalline fibrils have a tensile strain e_c and a shear strain s_c, due to change of helix angle, given by:

$$e_c = e\ (\cos^2\theta - \sigma \sin^2\theta) \qquad s_c = -\ e\ (1 + \sigma) \sin\theta \cos\theta \tag{20.27}$$

A fractional rotation ($-\gamma e$) adds additional terms to the tensile and shear strains, so that the total strain energy per unit volume (or unit mass for specific quantities) is given by:

$$U = {}^1/_2\ e^2\ \{E_c\ [\cos^2\theta - (\sigma + \gamma) \sin^2\theta]^2 + G_c\ [(1 + \sigma + \gamma) \sin\theta \cos\theta]^2 \tag{20.28}$$

where G_c = relevant shear modulus of cellulose crystal.

The value of γ, which is found by energy minimisation ($dU/d\gamma = 0$), is given by:

$$\gamma = \frac{E_c - G_c \cos^2\theta}{E_c \sin^2\theta + G_c \cos^2\theta} - {}^1/_2 \tag{20.29}$$

Substitution and differentiation of equation (20.28) gives;

$$f = Ee = \frac{E_c - G_c \cos^2\theta}{E_c \sin^2\theta + G_c \cos^2\theta} \tag{20.30}$$

This is the line C in Fig. 20.33(b). In the wet state, the shear modulus will be lower because fibrils can slip past one another, thus reducing the fibre modulus E. The simple expression would not apply when there is large untwisting. In the limiting state with $G_c = 0$, there would be complete untwisting, which would be determined by geometry.

As convolutions have a major influence on the stress–strain curve of cotton. Hearle and Sparrow [35] modelled the effect by using the converse of a relation given by Timoshenko [38] for the contraction of a ribbon due to twisting:

$$e = -\left(\frac{\phi^2}{2}\right)\left(\frac{b^2}{12}\right) + \frac{f}{E} \tag{20.31}$$

where e = strain, ϕ = twist in radians per unit length, b = ribbon width, f = tensile stress and E = Young's modulus of the material.

It is necessary to take account of the resistance to the untwisting. An approximate analysis of the mechanics gives the following relation between tensile stress f and the strain e_{con} due to untwisting of convolutions, which have an angle of ω:

$$f = k\left[\frac{\tan\omega}{(\tan^2\omega - e_{con}/X)^{1/2} - 1}\right] \tag{20.32}$$

where $k = (\eta\ A\ G_c/\pi\ b^2\ X)$ and η is a shape factor, A is area of cross-section and X is a factor taking account of differences in the shape of a cotton fibre.

Data on cross-sections by House [39] and torsion by Meredith [40] suggest that η

= 0.56, A/b^2 = 0.27 and G = 250 GPa. A plot of breaking strain against convolution angle indicates that X is about 0.67, which gives k = 18 GPa. Owing to differences in cotton types, there will be a wide range of values of k. With k =100 there is little curvature in the stress–strain curve; with k = 5, the curve changes from a low slope to a high slope at around 3% extension. Figure 20.34 shows that the strain due to pulling out of convolutions for different values of ω with k = 20. These can be compared with the curvature in Fig. 20.35. The mechanisms for A, B and C in Fig. 20.33 all give linear plots at the small strains involved; the curvature comes from the convolutions and, as shown in Fig. 20.36 is lost when the convolutions have been removed.

For cotton fibres clamped at short lengths, untwisting at reversals would be prevented and the modulus would be higher.

In considering the tensile failure of cotton fibres, there are three separate modes that can occur. When the fibrils are firmly bonded together, as in completely dry or resin crosslinked cotton, fracture occurs by cracks running across the fibre, which are presumably due to tensile failure of the crystalline fibrils. At medium humidities, splits develop between fibrils and the material between successive turns of the split tears. The fracture extends over a long length, influenced by the geometry of the collapsed fibre. In wet cotton, the fibrils are so separate that they break individually.

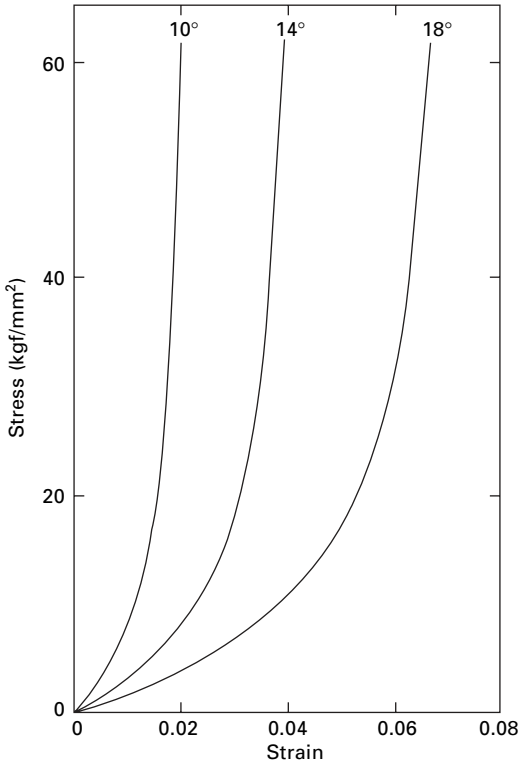

20.34 Strain due to pulling out of convolutions for different convolution angles ω. From Hearle and Sparrow [35].

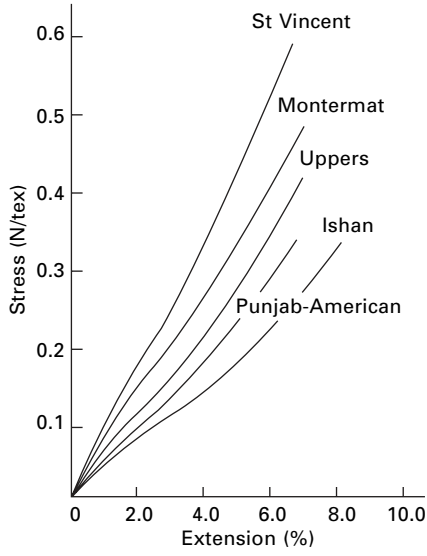

20.35 Stress–strain curves for various cottons. From Sparrow [41].

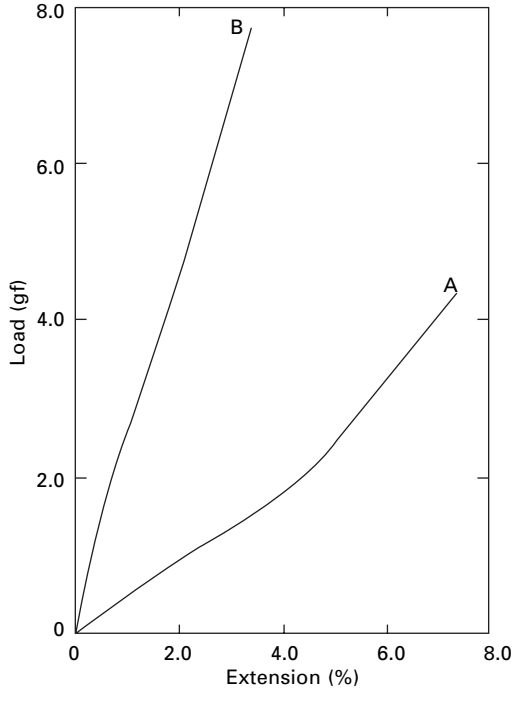

20.36 Load–extension curves of Acala cotton: A Normal fibre, B after stretching wet and drying to remove convolutions.

The reason why wet cotton is stronger than dry is probably mainly the relief of shear stresses that can occur by the untwisting and unbending of the fibre. When the fibrils are bonded together, the complex stresses lead to early breakdown, but when they are free to move and relieve stresses, the fibre is stronger.

Another way of regarding the situation is by considering the sharing of load between molecular chains or fibrils. An analogous system of two elements is shown in Fig. 20.37. With a crosslink present, each element breaks separately, and the strength will be half the value that it would be without the crosslink when both elements have to be broken together. Because the molecules in native cellulose are very long (DP > 10 000), the effect of easier slip at chain ends will be negligible, and thus the main reason why rayon is weaker when wet will not be operative.

20.6.2 Wool and hair fibres

As shown in Fig. 20.38, there are many structural levels from the protein molecules to whole wool and hair fibres[7]. All of these have some influence on mechanical properties. Figure 20.39 shows a scheme for a total mechanical model of a wool fibre. Ideally, the starting point would be computational dynamic modelling of the properties of the protein molecules, but the technology is not yet sufficiently advanced to do this for the complexity of keratin and keratin-associated proteins, though small segments might be modelled. However, there is enough understanding and practical information to model all higher levels, at least to a first approximation, but the programming has not been done [42, 43].

Since the various units of the structure are in parallel, a simple mixture law can be applied in parts of the analysis. The macrofibril assembly and the cell assembly probably have only a small influence on mechanical properties, though slip between cells may be one cause of low strength in some wools [44] and is one likely cause of transverse yielding at low stress, which has been observed in rhinoceros horn and porcupine quill. Prediction of bending and twisting resistance would follow the usual

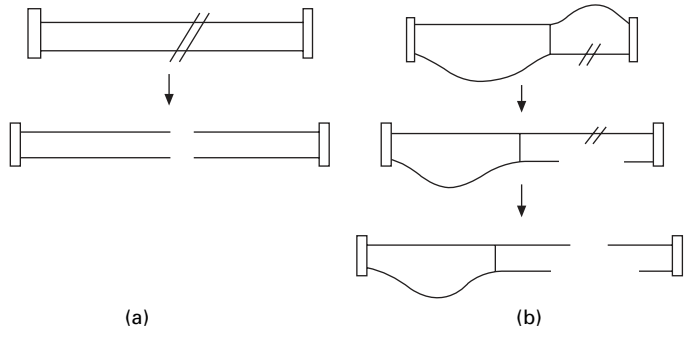

20.37 Rupture of two chains: (a) without link; (b) with a crosslink.

[7]In the remainder of this section the use of the word *wool* also covers in a general way hair fibres, including goat, camel and other hairs used in textiles and human hair.

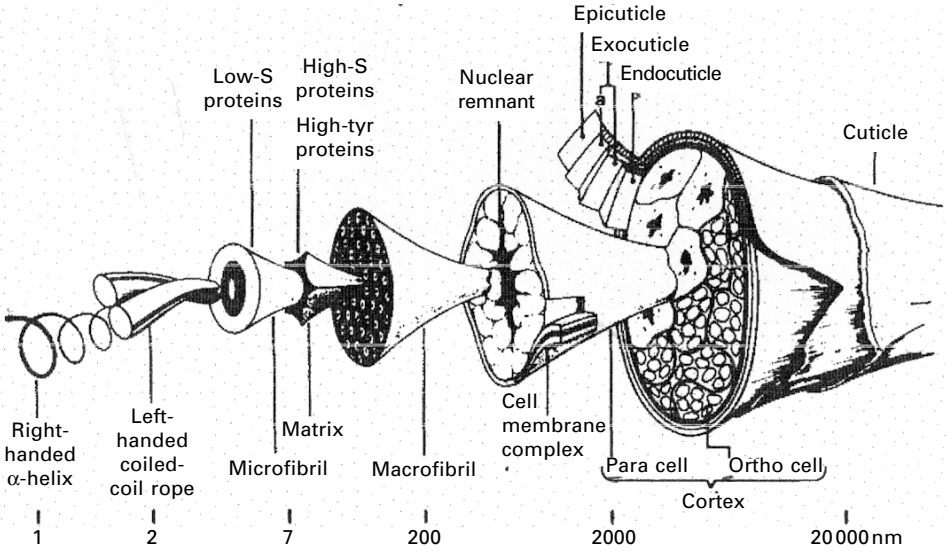

20.38 Structure of wool fibre, as drawn by Robert C. Marshall, CSIRO, Melbourne.

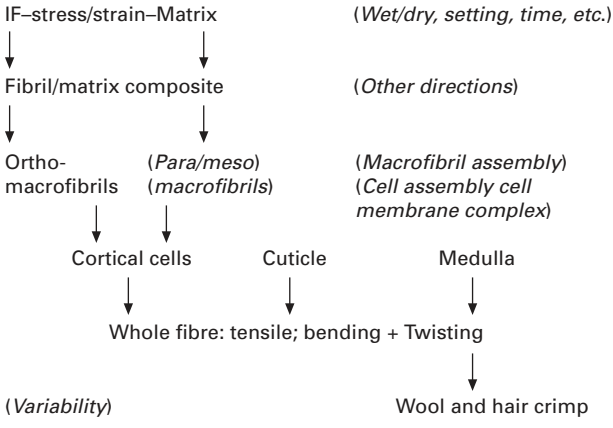

20.39 Scheme for modelling the total mechanics of a wool fibre. Entries in italics in parentheses are supplementary to the main scheme.

treatment for a multicomponent fibre with an increasing influence of outer layers. A three component model of cuticle surrounding the ortho- and para-cortex has been modelled by Liu and Bryson [45]. Unfortunately, knowledge of the properties of the cuticle is limited.

The two parts of the model that are best understood are the tensile stress–strain curve based on the behaviour of the fibril/matrix composite and the explanation of crimp in terms of the difference between the macrofibrils in the ortho- and the para-cortex.

A simple parallel two-phase model (Fig. 20.40) was first proposed by Feughelman

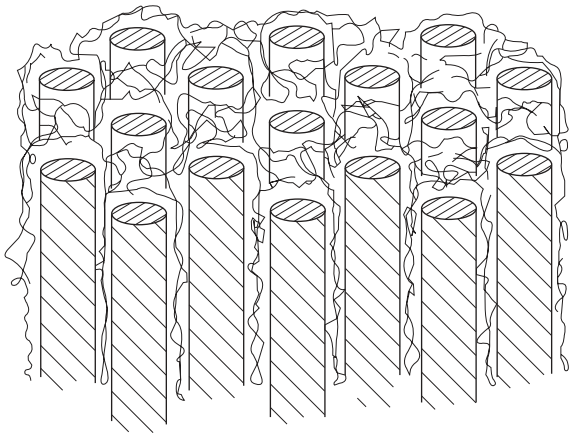

20.40 Simple two-phase fibril–matrix model of fine structure of wool.

[46]. It explains the low strain behaviour, including shear having a lower modulus than extension, and the onset of yield. A model for the whole stress–strain curve in extension and recovery was derived by Chapman [47] and has been shown to be valid in a comparison with two alternative models [48, 49].

The Chapman model represents the two-phase model by crystalline fibrils in the α-helical form linked at intervals to an amorphous matrix[8] (Fig. 20.41(a)). This zonal model was originally used to simplify the analysis, but later research showing that the heads and tails of the keratin molecules protrude into the matrix makes it a better model than one with continuous coupling. The fibrils follow the mechanics shown in Fig. 20.1 for an α↔β transition from a helical to an extended chain form, characterised by an initial modulus, and critical and equilibrium stresses for the transition (Fig. 20.42(a)). In wet wool, the matrix is assumed to be a moderately highly crosslinked rubber. Chapman [49] showed that the matrix stress–strain curve could be derived from the stress–strain curves of supercontracted wool in Fig. 20.42. In the first stage, the crystalline fibrils are disrupted, so that the stress–strain curve is dominated by the matrix. There is some residual stress from the fibrils, which remains after second stage, when it is assumed that the matrix contribution is lost. Subtracting the second stage curve from the first stage curve gives the matrix stress–strain curve, as shown in Fig. 20.43. Up to 35% extension, the curve follows the theoretical rubber elasticity curve given by equation (20.6). At larger extensions, the curves diverge due to breakage of cystine crosslinks, which allows greater extension and eventual break of the network. The matrix stress–strain curve is included in Fig. 20.42(a).

Initial extension is controlled by the elastic modulus of the helical crystals with a small contribution from the matrix (Fig. 20.41(a)). At 2% extension, the critical stress is reached and an α↔β transition starts in one of the zones (Fig. 20.41(b)). The stress in the fibril falls to the equilibrium value and the difference is taken up by an

[8]In the biological literature, the fibrils are referred to as *keratin intermediate filaments* and the matrix is composed of a collection of *keratin-associated proteins*.

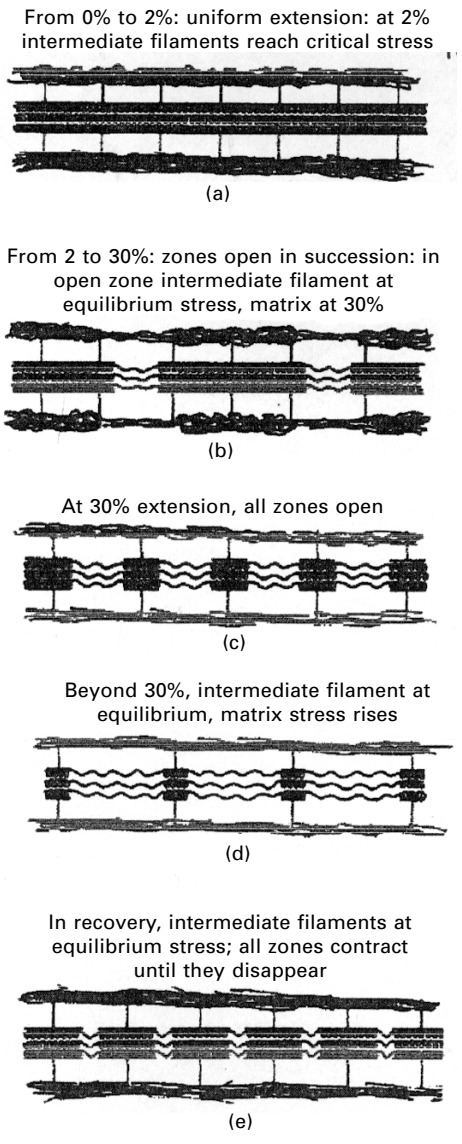

20.41 Sequence of changes in the Chapman model. From Hearle [48].

additional 28% extension of the matrix. The process continues in successive zones until all have been opened at 30% extension (Fig. 20.41(c)). Further extension then follows the line of the matrix curve plus the equilibrium stress in the fibrils (Fig. 20.41(d)). At 40–50% extension, the stress is high enough to cause rupture of the amorphous network and trigger fibre breakage. In recovery, the stress follows the matrix curve down to 2% extension, since the α and β forms remain in equilibrium (Fig. 20.41(e)). Below 2%, the initial curve is rejoined, Fig. 20.41(a). With the controlling parameters listed in Table 20.3, the predicted stress–strain relations, which

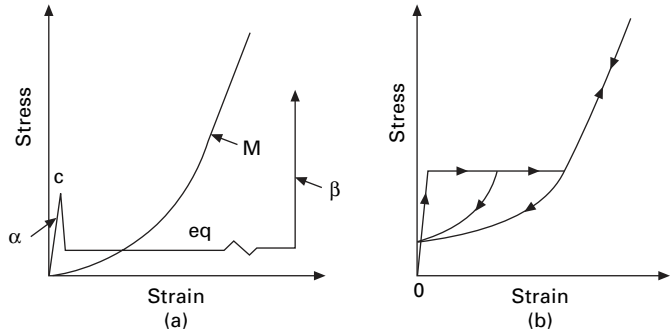

20.42 (a) Stress–strain relations: at a critical stress (c), fibril changes from helical α-crystal to extended chain β-crystal with equilibrium stress (eq); matrix (M), follows a rubber elasticity curve.

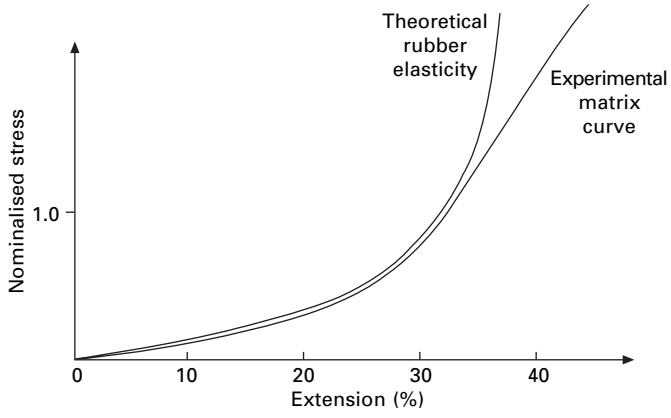

20.43 Matrix stress–strain curve derived from supercontraction experiments compared with rubber elasticity curve. Stress is normalised by stress in wet wool at 15% extension. From Chapman [49].

are shown in Fig. 20.42(b), have good agreement with the experimental results for wet wool in Fig. 20.44. The differences are in some rounding of the sharp changes and a small positive slope in the yield region. Both effects can be explained by variability in wool fibres. The simple Chapman model considers only the fibril/matrix composite and assumes that it is parallel to the fibres axis. In reality, there is a helical orientation in the macrofibrils of the ortho-cortex, which must be taken into account together with other features of the total model for wool.

Developments of the Chapman model explain other features of wool. Hearle and Susitoglu [50] showed that the addition of viscous dashpots would model time dependence. The influence of water and the setting of wool were explained by Hearle *et al*. [51]. As moisture content is reduced, the hydrogen bonds form between peptide and other groups in the matrix. By subtraction of the fibril contribution, the matrix stress–strain curves can be calculated for the initial and post-yield regions and then interpolated for the intermediate regions (Fig. 20.45). The initial stiffening up to a

Table 20.3 Controlling parameters for the Chapman model

Parameter	Value	Determines	Notes
Microfibrils			
α modulus	1.75 GPa	Initial fibre modulus (plus small matrix contribution)	Similar to theoretical calculation
Critical stress α → β transition	35 MPa	Fibre yield stress (plus small matrix contribution)	Reasonable at 2% strain
Equilibrium stress α → β transition	7 MPa	Junction of extension and recover curves	Reasonable on basis of Fig. 13.43
β modulus	1.75 GPa	Additional microfibril extension in post-yield region	Actually higher; negligible effect
α → β strain	80%	Extension in opened zones	From X-ray diffraction experiments; less than ideal α-helix
Matrix			
# Non-linear stress/strain	See Fig. 20.43	Post-yield and recovery curves (plus microfibril contribution)	From supercontraction experiments & rubber elasticity theory
Internal modulus	0.35 GPa	Addition to microfibril tension	Follows from #
Extension at critical stress	30%	End of yield region	Follows from #
Ideal maximum extension	40%	Limiting extension if no crosslink failure	Follows from #
Actual maximum extension	50%	Fibre break extension and strength	Greater than ideal maximum due to cystine bond break

yield point and then following parallel to the curve in the wet state is typical of bonding of an amorphous polymer, as shown in Fig. 20.6 for rayon. Setting of wool depends on rupture of cystine crosslinks in the matrix and their re-formation in new places. It can be assumed to drop the matrix curve to zero stress at the setting strain. Calculated curves for set fibres then show good agreement with the positions of the beginning and end of the yield region in set fibres.

Arai *et al*. [53] presented a theoretical analysis of the rubber-like elasticity of swollen wool and hair fibres based on the inverse Langevin function. They related this to a two-phase structure and make a comparison with experimental results.

Crimp in wool results from the bi-component structure. In the para-cortex (and meso-cortex, if present) the fibril/matrix composite is oriented parallel to the fibre axis, but in the macrofibrils of the ortho-cortex, as discussed in Section 1.6.3, the fibril/matrix composite follows helical paths similar to a twisted yarn. In the wet state, the matrix is swollen by absorbed water. On drying, the fibril/matrix composite shrinks, with the fibrils coming closer together. In the para-cortex, there is no change of length, but in the ortho-cortex the macrofibrils increase in length, owing to their

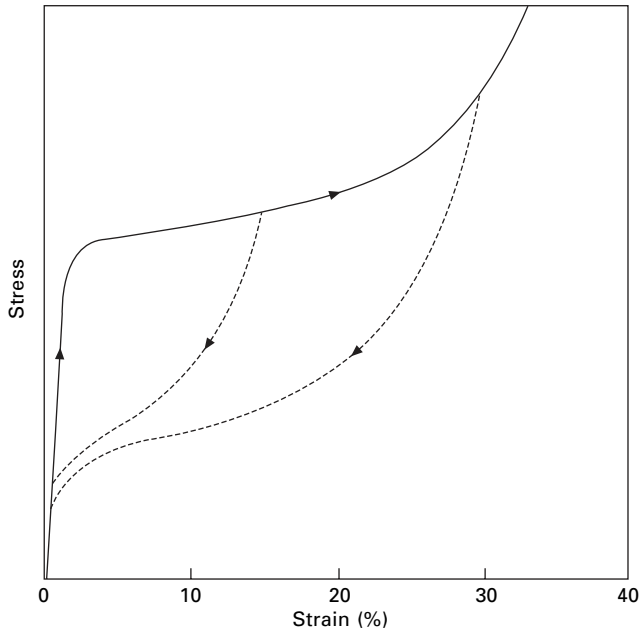

20.44 Stress–strain behavior of wool in extension and recovery. The stress is in arbitrary units.

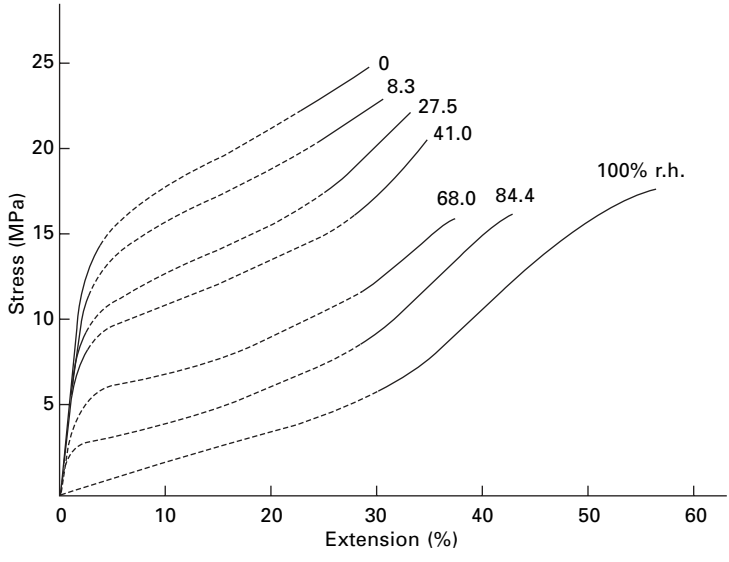

20.45 Matrix stress–strain curves at different humidities calculated by application of Chapman model to experimental data [52].

reduced radius reducing the helix angles. This means that the fibre behaves like a bimetallic strip and develops a crimp with one side increasing in length and the other staying constant. An analysis of the mechanics has been given by Munro and Carnaby [54, 55].

20.7 Theories of time dependence

20.7.1 Ideal springs and dashpots

The mechanical behaviour of polymer fibres is viscoelastic, combining features of both elasticity and viscosity. The use of a parallel spring and dashpot model (or, less conveniently, a series model) in the definition of parameters to characterise experimental results has been described in Section 16.5.2. However, the numerical values obtained relate only to the particular experimental conditions and do not reflect the full complexity of the viscoelastic responses. Analysis can be carried further by the by more complicated combinations of springs and and dashpots and introducing non-linearity.

Ideal springs will follow Hooke's Law, so that stress $f = (E\varepsilon)$, where E = constant and ε = strain, and will show perfect recovery. Ideal dashpots will follow Newton's Law, with stress $f = (\eta\, d\varepsilon/dt)$, where η = constant and $d\varepsilon/dt$ = rate of strain, and will show no recovery. If the spring and dashpot are arranged in series, as in Fig. 20.46, the model will show instantaneous extension of the spring on the application of load, followed by secondary (irrecoverable) creep of the dashpot at a constant rate; it will also show stress relaxation at constant length as the tension in the spring causes continuing elongation of the dashpot. If the units are arranged in parallel, as in Fig. 20.47, they will show primary (recoverable) creep as the extension of the spring is hindered by the dashpot; if held at constant length, there will be an instantaneous drop in tension as the viscous term ceases to contribute but the spring remains extended. The simplest model that shows qualitatively all the features of instantaneous extension, primary and secondary creep, and stress relaxation is the four-element model shown in Fig. 20.48.

It would, however, require a very complicated arrangement of elements to give a complete representation of the behaviour of fibres, exhibiting not only the four effects mentioned, but also dynamic properties, which vary with frequency, and non-linear relations between extension, load and time. This multiplication of the number of

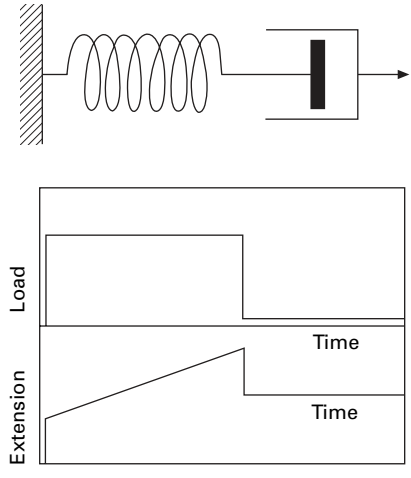

20.46 Spring and dashpot in series.

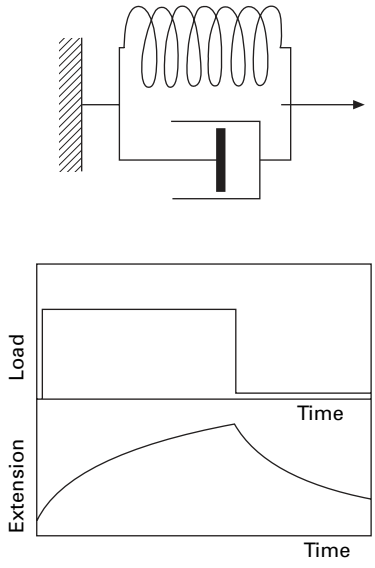

20.47 Spring and dashpot in parallel.

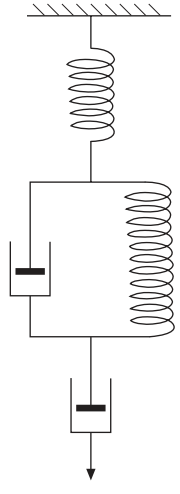

20.48 Four-element model.

elements involved is no simplification of the problem and has led Peirce [56] to say that 'the mechanical analogy in general is an unsatisfactory substitute for direct knowledge of molecular force … there is every reason to allow that imperfect elasticity is a proper characteristic of molecular behaviour, of more physical reality than the end-cases of ideal elasticity and viscosity'.

The use of a combination of springs and dashpots is one way of developing the theory of viscoelasticity, which can be expressed in various other forms. By combining a spectrum of elements, the theory can represent any form of variation with time. Ferry [57] describes the mathematics and its application to eight types of polymer. A

combination of ideal springs and dashpots is necessarily limited to a linear dependence on stress. If all the stress values of a given sequence are doubled, all the strain values will also be doubled. This limitation severely restricts the application of the theory to fibres.

20.7.2 Eyring's three element model: reaction-rate theory

Instead of adding to the number and complexity of arrangement of ideal elastic and viscous elements, one may approach the problem by modifying the properties of the elements themselves. In the three element model put forward by Eyring and his colleagues [58, 59], Fig. 20.49, the springs follow Hooke's Law, but the dashpot shows non-Newtonian viscosity, its behaviour being represented by a hyperbolic sine law of viscous flow:

$$\frac{de}{dt} = K \sinh \alpha f \tag{20.33}$$

where $d\varepsilon/dt$ = rate of strain, f = stress, and K and α are constants.

This means that the rate of strain increases more rapidly with increase of stress than it would do if it were proportional to stress, as in Newton's Law.

There is a justification for the use of an expression of this form in the theory of reaction rates [60]. In its application to the deformation of fibres, we assume that the strain occurs because flow units (which may be chain molecules, segments of chain molecules, or groups of segments of chain molecules) slip over one another from one equilibrium position to another when stress is applied. In order to do this, the flow unit will have to overcome a potential energy barrier, illustrated in Fig. 20.50. This barrier is called the *free energy of activation* for the flow process. In the absence of stress, let its value be ΔF. The frequency with which a flow-unit will surmount the barrier and move to a new equilibrium position is given by statistical thermodynamics as:

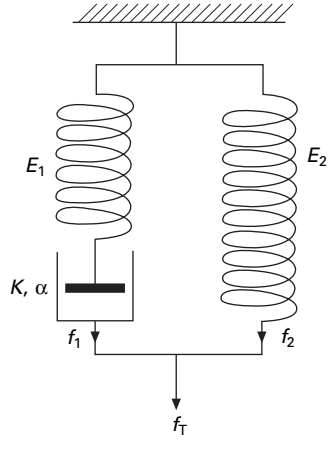

20.49 Eyring's three-clement model.

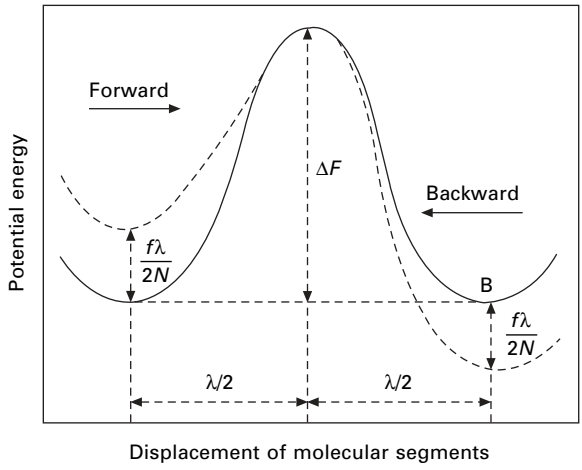

20.50 Potential-energy barrier for flow.

$$\text{number of moves per second} = v\, e^{-\Delta F/kT} \tag{20.34}$$

where v is a thermal vibration frequency ($\approx 10^{13}$Hz), k is Boltzmann's constant and T is the absolute temperature.

Since the two positions are in the same state, in contrast to the different states in Fig. 20.1, their potential energies are at the same level. In the absence of stress, there will be equal numbers of moves in opposite directions in unit time.

However, if a stress f is acting, and is distributed over N flow-units per unit area of cross-section so that the mean force applied to each unit is f/N, then it will contribute to the surmounting of the barrier an amount of work $(f/N)(\lambda/2)$, where λ is the mean distance between equilibrium positions. Conversely, for moves in the opposite direction, this amount of work must be done in addition to ΔF. Consequently, the application of stress may be regarded as equivalent to modifying the potential barrier as shown by the dotted line in Fig. 20.50. Thus we have:

$$\begin{aligned}
&\text{net number of forward moves per second} \\
&\quad = \text{number of forward moves} - \text{number of backward moves} \\
&\quad = v\, e^{-(\Delta F - f\lambda/2kT)} - e^{-(\Delta F + f\lambda/2kT)} \\
&\quad = v\, e^{-\Delta F/kT}\,(e^{f\lambda/2kT} - e^{-f\lambda/2kT}) \\
&\quad = 2v\, e^{-\Delta F/kT} \sinh f\frac{\lambda}{2NkT}
\end{aligned} \tag{20.35}$$

If we multiply the net number of moves forward per second by the distance moved λ, we get the velocity of flow. In order to convert this to a rate of strain, we must divide by λ_1, the mean distance between neighbouring flow units, measured along the direction of flow. This gives:

$$\begin{aligned}
&\text{rate of strain} = d\varepsilon/dt \\
&\qquad = 2\frac{\lambda}{\lambda_1} v\, e^{-\Delta F/kT} \sinh f\frac{\lambda}{2NkT}
\end{aligned} \tag{20.36}$$

This is the full form of equation (20.33), and we see from it that:

$$K = 2\frac{\lambda}{\lambda_1} v\, e^{-\Delta F/kT} \tag{20.37}$$

$$\alpha = \frac{\lambda}{2NkT} \tag{20.38}$$

In addition to the movement of flow units over one another, there will be an initial extension owing to the elastic deformation of the structure. If this is relieved by the flow, then it can be represented by a spring in series with the dashpot. There may also be an elastic deformation that is not relieved by the flow, which must be represented by a spring in parallel. Thus we arrive at the three element model. Various detailed structural interpretations of it are possible. One is that the dashpot represents the flow of segments of chain molecules over one another; the spring in the left-hand arm represents the elastic extension of the molecules; and the spring in the right-hand arm represents an elastic deformation of the molecular network unrelated to the viscous flow.

In the three element model, the springs will follow Hooke's Law with modulus E, so that

$$\text{strain} = \varepsilon = \frac{f}{E} \tag{20.39}$$

$$\frac{d\varepsilon}{dt} = \left(\frac{1}{E}\right)\frac{df}{dt} \tag{20.40}$$

If E_1 is the modulus of the left-hand spring and f_1 is the stress in the left-hand arm of the model, then we have:

$$\frac{d\varepsilon}{dt} = \frac{1}{E}\frac{df_1}{dt} + K \sinh \alpha f_1 \tag{20.41}$$

For the right-hand arm, with a spring of modulus E_2, and a stress f_2, we have

$$\varepsilon = \frac{f_2}{E_2} \tag{20.42}$$

$$\frac{d\varepsilon}{dt} = \frac{1}{E_2}\frac{df_2}{dt} \tag{20.43}$$

The total stress, f_T, is given by:

$$f_T = f_1 + f_2 \tag{20.44}$$

$$\frac{df_T}{dt} = \frac{df_1}{dt} + \frac{df_2}{dt} \tag{20.45}$$

Eliminating f_1 and f_2 from these equations, we get:

$$\frac{d}{dt}[(E_1 + E_2)\varepsilon - f_T)] = E_1 K \sinh \alpha (f_T - E_2 \varepsilon) \tag{20.46}$$

This is the differential equation that gives the relation between stress, strain, and time for Eyring's three element model (incorporating a non-Newtonian dashpot) in terms of the constants E_1, E_2, K, and α. It may be applied to fibre deformation under any loading history. The most straightforward examples are stress relaxation, when ε = constant; creep, when f_T = constant; and the stress–strain behaviour under constant rate of elongation, when $d\varepsilon/dt$ is constant.

20.7.3 Stress relaxation on Eyring's model

For stress relaxation, with $\varepsilon = \varepsilon_c$ = constant and $d\varepsilon/dt = 0$, equation (20.42) becomes:

$$\frac{df_T}{dt} = -E_1 K \sinh \alpha (f_T - E_2 \varepsilon_c) \tag{20.47}$$

On integration, this gives:

$$\frac{\tanh \{\alpha(f_T - f_\infty)/2\}}{\tanh \{\alpha(f_0 - f_\infty)/2\}} = e^{-\alpha E_1 K t} \tag{20.48}$$

where $f_0 = (E_1 + E_2)\,\varepsilon_c$ = initial stress at $t = 0$, and $f_\infty = E_2\,\varepsilon_c$ = final stress at $t = \infty$.

It is convenient to plot this expression in terms of universal variables. The stress is expressed by $(f_T - f_\infty)/(f_0 - f_\infty)$; in other words, the final stress is subtracted from it, and the result is divided by the difference between the initial and final stresses. The time is given in terms of $\alpha K E_1 t$. Curves showing the relation between these two quantities for various values of $\alpha(f_0 - f_\infty)/2$ are given in Fig. 20.51 and are generally similar to those found experimentally. A graph from which numerical values of the constants needed to fit particular experimental curves may be calculated is given by Meredith [62].

If $f_0 >> f_T >> f_\infty$, equation (18.44) reduces approximately to:

$$f_T = f_\infty - \frac{1}{\alpha} \log_e \left(\frac{\alpha E_1 K t}{2} \right) \tag{20.49}$$

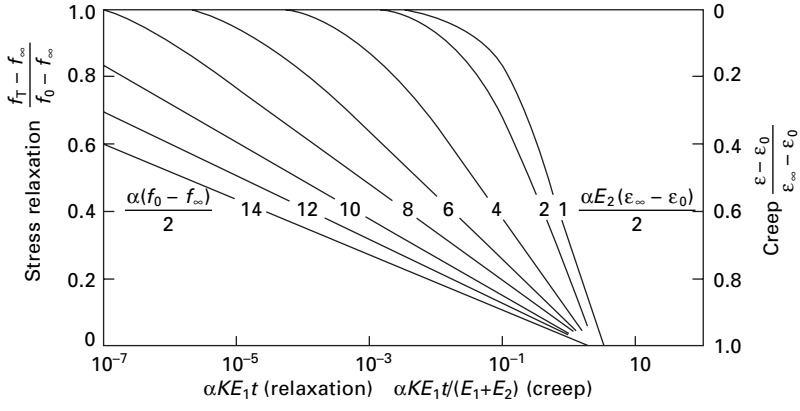

20.51 Graphs of equations (20.44) and (20.47) for stress relaxation and creep [61].

This means that, in the middle stages of the relaxation process, the stress decreases linearly with the logarithm of the time. This is in agreement with experimental results.

By fitting the experimental data to the theoretical equations, values of the constants α and K can be obtained, and then, if one assigns values to λ and λ/λ_1, one can calculate N and ΔF from equations (20.37) and (20.38). Burleigh and Wakeham [63] assumed that in cellulose λ_1 was equal to the length of two glucose units, that is, 1.03 nm; they then found that, for cotton and rayon cords under an initial stress of 78 MPa, N remained fairly constant with values of 3.6×10^{11} and 4.9×10^{11} per mm^2, respectively, over a range of temperatures and humidities. These values correspond to approximately one-eighth and one-sixth, respectively, of the total number of chain molecules per unit area of cross-section.

As the stress is increased, the values of N increase and approach the total number of cellulose chains at a stress approximating to that at which rupture occurs. Burleigh and Wakeham also found that in the wet state there was evidence of the simultaneous occurrence of a second relaxation process. This process was rapid, being completed in 30 s, and gave a value of N equal to the total number of cellulose chains. In other words, all the molecules were moving as individuals.

The values of λ/λ_1 used by different workers [59, 63, 64] range from 2 to 10, according to the assumptions made. However, even this wide range of values has only a small effect (about 6%) on the values obtained for ΔF. Andersen [64] has calculated values of activation energy, ΔF, for cotton and viscose rayon over a range of humidities and initial stresses. He obtained values of about 100 kJ/mol, which varied little with the conditions. However, as Meredith [62] has pointed out, similar values of activation energy will always be found for relaxation processes assumed to be completed in a given time range at a given temperature. To observe other activation energies, experiments must be made at a different temperature or on another timescale.

20.7.4 Creep on Eyring's model

For creep, we have stress = f_T = constant = f_c, and $df_T/dt = 0$, so that equation (20.46) becomes:

$$(E_1 + E_2)\, d\varepsilon/dt = E_1 K \sinh \alpha(f_c - E_2\varepsilon) \tag{20.50}$$

On integration this gives:

$$\frac{\tanh\left[\alpha E_2 (\varepsilon_\infty - \varepsilon)/2\right]}{\tanh\left[\alpha E_2 (\varepsilon_\infty - \varepsilon_0)/2\right]} = e^{-\alpha E_1 K t/(E_1 + E_2)} \tag{20.51}$$

This is similar in form to equation (20.48) for stress relaxation, so that the curves in Fig. 20.51 will also apply to creep. The abscissa will give values of $(\varepsilon_\infty - \varepsilon)/(\varepsilon_\infty - \varepsilon_0)$. It should be noted that this quantity decreases from 1 to 0 as ε increases from ε_0 to ε_∞. More directly applicable to creep is the quantity $(\varepsilon - \varepsilon_0)/(\varepsilon_\infty - \varepsilon_0) = 1 - (\varepsilon_\infty - \varepsilon)/(\varepsilon_\infty - \varepsilon_0)$ shown on the right-hand scale. The ordinate will give values of $\alpha E_1 K t/(E_1 + E_2)$, and the figures on the curves will be values of $\alpha E_2(\varepsilon_8 - \varepsilon_0)/2$. As a consequence of the similarity of form, the same numerical methods may be employed to find the constants to fit the experimental data.

If the stresses involved are small, and the times concerned are less than 10^5 s, it can be shown that equation (20.51) reduces to:

$$\varepsilon = \varepsilon_0 + \frac{\varepsilon_\infty}{\alpha f_c} \log_e (1 + At) \tag{20.52}$$

where $A = \dfrac{\alpha K f_c (1 - \varepsilon_0/\varepsilon_\infty)}{\varepsilon_\infty \log_e \{\coth[\alpha f_c (1 - \varepsilon_0/\varepsilon_\infty)/2]\}}$

Halsey *et al*. [59] applied this equation to Leaderman's creep and creep-recovery data [65] for viscose rayon, acetate and silk and found a good fit over a 10^4-fold range of times. A similar attempt to fit a three element model with a Newtonian viscous element gave a good fit only over a 50-fold range of times. Assuming that $\lambda = {}^1/_2$, they calculated activation energies of the order of 100 kJ/mol.

The alternative three element model shown in Fig. 20.52 has been used by Reichardt *et al*. [66] to analyse Steinberger's data [67] on the creep of acetate. This model is simpler to apply to creep, since the upper spring has a constant extension under constant stress, and only the lower elements vary in extension with time, but it is less directly related to the structural picture. It is mathematically equivalent to the model of Fig. 20.49, though the values of E_1', E_2', K' and α' will be different from those of E_1, E_2, K, and α.

The three element model applies only to primary creep. There is no provision for a non-recoverable extension. Holland *et al*. [68] have tried to allow for this by putting a viscous element in series with the three element model, as in Fig. 20.48. This gives a secondary creep continuing indefinitely at a constant rate, which is not in accord with the usual experimental results. The fourth element must have a more complex response.

20.7.5 Stress–strain curve on Eyring's model

For constant rate of extension, we have $d\varepsilon/dt$ = constant, so that equation (20.46) becomes:

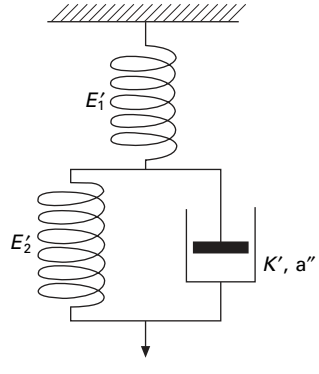

20.52 Alternative three-element model.

$$\frac{\mathrm{d}f_\mathrm{T}}{\mathrm{d}t} = (E_1 + E_2)\frac{\mathrm{d}\varepsilon}{\mathrm{d}t} - E_1 K \sinh\alpha(f_\mathrm{T} - E_2\varepsilon) \tag{20.53}$$

On integration, this gives:

$$f_\mathrm{T} = E_2\varepsilon + \frac{1}{\alpha}\log_\mathrm{e}\left\{\beta + S\tanh\left[\frac{\alpha K S t}{2} + \tanh^{-1}\frac{(1-\beta)}{S}\right]\right\} \tag{20.54}$$

where $\beta = (\mathrm{d}\varepsilon/\mathrm{d}t)/K$ and $S^2 = 1 + \beta^2$.

Methods of fitting this equation to the experimental data and determining the parameter β have been described by Eyring and Halsey [69], Geyer *et al.* [70] and Meredith [62]. The theoretical relations are found to give good agreement with some experimental results for viscose rayon and acetate. A typical example of the application of the theory is shown in Fig. 20.53.

20.7.6 A generalisation of Eyring's model

There are many simplifications in Eyring's application of reaction-rate theory to deformation. One difficulty, about which little can be done, is that there are complicated interactions within a fibre, which cannot really be represented as an assembly of separate flow units.

It is also an approximation to assume that an applied stress merely changes the position of the troughs in the energy barrier, although this is valid provided that the stresses are not too large. A more realistic view of the effect of large stresses is shown in Fig. 20.54. The work done by the applied force changes the whole curve and, if it is large enough, removes the barrier; this would lead to spontaneous deformation or yield. Even before this happens, a thermal fluctuation may cause the barrier to be surmounted. Yield stresses will thus be time-dependent. Chapman [52] has shown that, with parabolic barriers, the effective yield stress $f_{\mathrm{c},t}$ with a time t available is given by:

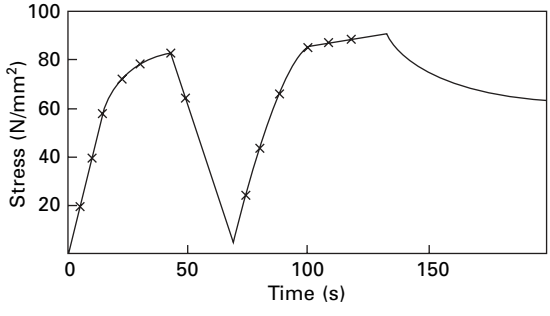

20.53 Application of Eyring's three clement model to the stress–strain relations of acetate at 57% r.h. and 27 °C. The full curve gives the experimental results, and the crosses are calculated from Eyring's theory with parameters derived from the first loading curve. After Reichardt and Eyring [71].

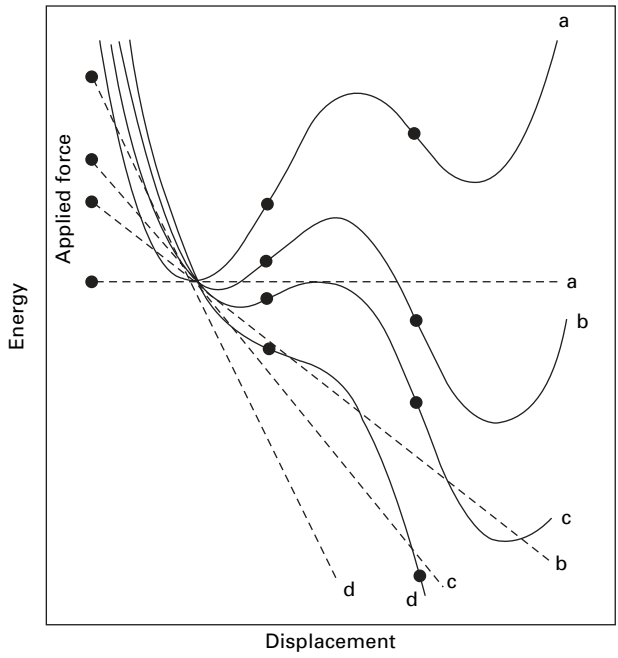

20.54 Generalised effect of stress on an energy barrier. The dotted lines show the work contribution of successively higher applied force (a–d), causing a progressive change in the energy barrier. It should be noted that the points of inflection remain in the same position, but that the maxima and minima change in position as well as height.

$$\frac{f_{c,t}}{f_{c,o}} = 1 - \left[\left(\frac{kT}{\Delta F}\right)\log_e vt\right]^{1/2} \tag{20.55}$$

A similar equation should apply to fracture stress, since fracture is merely a special case whereby the second trough in the curves is at infinity.

It may be noted that, depending on the absolute height of the energy barriers present (which will be determined by the nature of the interaction and the number of units acting cooperatively together), the following different modes of response may occur:

- very low barrier – an immediate achievement of the equilibrium state;
- low barriers – a sluggish approach to equilibrium;
- medium barriers – a rate-dependent yield, but no spontaneous recovery;
- high barriers – yield at a stress independent of rate.

An increase of temperature will increase the magnitude of thermal fluctuations, so that the barriers are easier to cross and seem less high.

20.7.7 The superposition principle in primary creep

Another form of analytical approach is found in Leaderman's study [65] of the primary creep of fibres. He found that this could be represented by the relation:

$$x_t = x_0 + \phi(F)\ \psi(t) \tag{20.56}$$

where x_t = extension after time t, x_0 = instantaneous extension, $\phi(F)$ is a function of force and $\psi(t)$ is a function of time.

As a special case of this relation, we can put $\phi(F) = x(90)$ and $\psi(t) = \Psi(t)$, as defined earlier in Section 16.2.2. The important feature of the relation is that, although creep is not a linear function of force, the effects of force and time can be separated into two functions. This gives a much simpler relation than a single function involving force and time.

In order to test equation (20.56), Leaderman made use of the relative delayed deformation, $x(t)$, defined as the difference between the deformation at the time t and the deformation at 1 min. This removes uncertainty about the value of the instantaneous deformation. Thus we have:

$$x(t) = x_0 + \phi(F)\ \psi(t) - x_0 - \phi(F)\ \phi(1) = \phi(F)\ [\psi(t) - \psi(1)] \tag{20.57}$$

$$\log x(t) = \log[\phi(F)] + \log[\psi(t) - \psi(1)] \tag{20.58}$$

Graphs of log $x(t)$ against t or log t should therefore be parallel to one another and displaced only by the differences in log $\phi(F)$. Leaderman found this to be so. An example is given in Fig. 20.55.

A reduced deformation can also be obtained by making use of $x(90)$, the deformation between 1 and 90 min, for we have:

$$x(t) = x(90)[\Psi(t) - \Psi(1)] \tag{20.59}$$

$$\text{reduced deformation} = x(t)/x(90) = \Psi(t) - \Psi(1) \tag{20.60}$$

The reduced deformation should be independent of load and a function only of time. This was found to be so.

Boltzmann [72] in 1874 put forward his superposition principle, and this has since been found to apply to many materials. Leaderman decided to test it for fibres. The principle states that the deformation of a body is a function of its entire loading history and is given by a summation of the effects of every previous change of load.

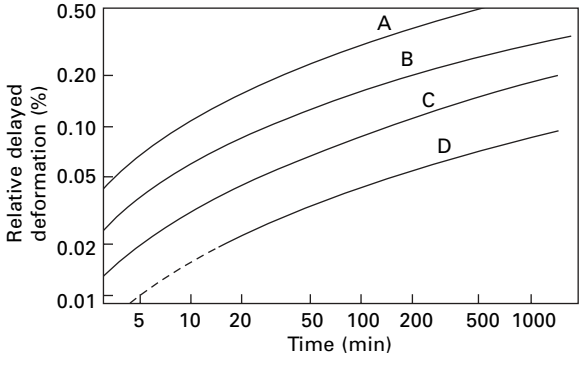

20.55 Plots of relative delayed deformations of viscose rayon for different loads [65]: A 31.0 mN/tex; B 25.2 mN/tex; C, 15.5 nM/tex; D 10.2 mN/tex.

This is illustrated in Fig. 20.56. The extension curve for each increment of load is put down, and the algebraic sum gives the resultant deformation. It is interesting to note that as a result of the superposition principle, the final creep recovery under zero load may, after a complex loading history, go past the zero position and then reverse direction before reaching equilibrium. An example of the reversal is included in Fig. 20.56, and some actual curves obtained for rubber by Kohlrausch [73] are given in Fig. 20.57. This is a remarkable phenomenon, since it means that under no load the

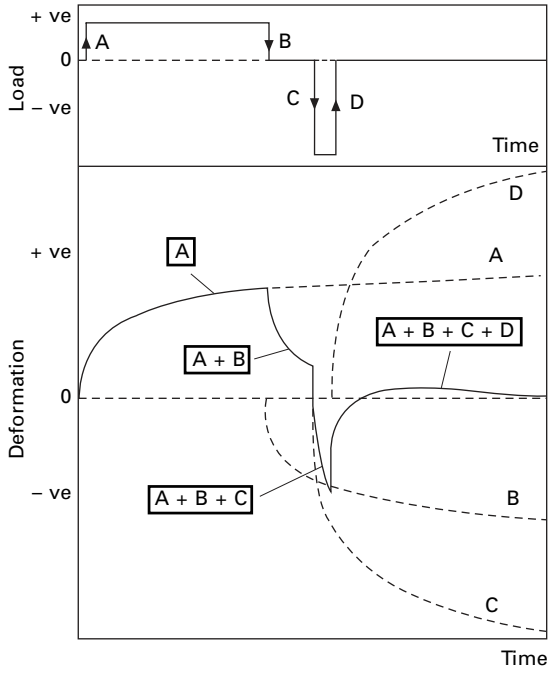

20.56 Applicaton of superposition principle.

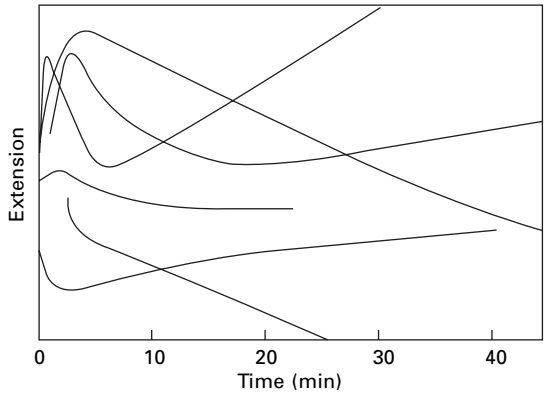

20.57 Creep-recovery of rubber after complex loading histories [73].

material is moving away from its equilibrium position. Inverse stress relaxation can also occur.

One way of testing the superposition principle is by long-duration creep and recovery tests. Suppose a load is left on for a time t_1 and then removed. The creep is given by:

$$x_t = x_0 + \phi(F)\ \psi(t) \tag{20.61}$$

and, by applying the superposition principle, the recovery by:

$$x_t = x_0 + \phi(F)\ \psi(t) - [x_0 + \phi(F)\ \psi(t - t_1)] = \phi(F)[\psi(t) - \psi(t - t_1)] \tag{20.62}$$

Let us call the recovery time $t' = (t - t_1)$ and the change of length during recovery $t'_{t'}$, then:

$$\begin{aligned} t' &= x_0 + \phi(F)\psi(t_1) - \phi(F)[\psi(t) - \psi(t - t_1)] \\ &= x_0 + \phi(F)\psi(t') - \phi(F)[\psi(t + t') - \psi(t_1)] \end{aligned} \tag{20.63}$$

But if $t' << (t_1 + t')$ the last term is very small, since the initial creep has almost ceased and may be neglected in comparison with the second term. This is illustrated in Fig. 20.58. We thus get:

$$x'_{t'} = x_0 + \phi(F)\psi(t') \tag{20.64}$$

This equation is identical in form with Equation (20.61), which means that the changes in length during creep and recovery must follow the same curve. Leaderman showed that this was so, as mentioned earlier (Section 16.2.2).

Another way of testing the superposition principle is by obtaining experimentally the deformation under repeated application and removal of load, as shown in Fig. 20.59. Suppose the first reversal occurs at a time t_1, then at a time t, greater than t_1, we have, writng $\chi(t)$ for x_t:

$$\chi(t) = \phi(F)[\psi(t) - \phi(F)] \tag{20.65}$$

But, if we add this to the creep for a time $(t - t_1)$, we get:

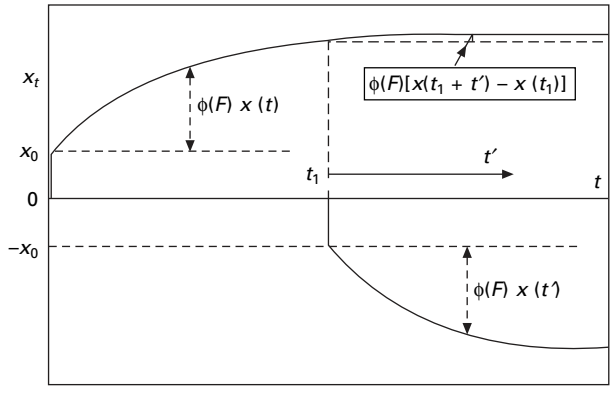

20.58 Long duration creep and recovery.

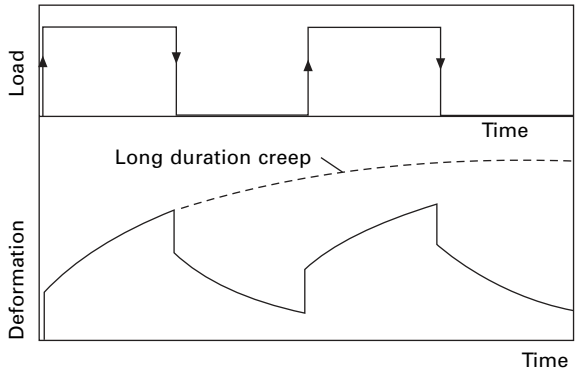

20.59 Creep under repeated applications and removal of load.

$$\chi(t) + \chi(t\ I\ t_1) = \phi(F)[\psi(t) - \psi(t - t_1)] + x_0 + \phi(F)\psi(t - t_1)$$
$$= x_0 + \phi(F)\psi(t) \tag{20.66}$$

This equals the creep at a time t if there had been no reversal of load. Similar relations apply to the other reversals. From these tests, we can therefore calculate a complete creep curve and compare it with the one obtained directly. Leaderman found good agreement.

There is thus evidence that the superposition principle applies to primary creep in fibres, with the exceptions already noted (see Section 16.2.2), namely, the incomplete recovery of the instantaneous extension of silk and the behaviour of nylon at high loads. The value of the superposition principle lies in the fact that the behaviour under complex loading histories can be calculated from simple creep tests. It is another form of representation of linear viscoelasticity.

20.7.8. An integral theory

An example of an integral theory is the equation put forward by Nutting [74]:

$$x = \psi^{-1} f^{\beta} t^{K} \tag{20.67}$$

where x = strain, f = stress, t = time and ψ, β and K are constants. The constants β and K determine the type of deformation and ψ determines its magnitude. An example of its use is in the relaxation of torsional stress. The strain is constant, so that, taking logarithms, we get:

$$\log f = -\frac{K}{\beta} \log t + \text{constant} \tag{20.68}$$

Experimentally, Permanyer [75] found linear relations between log(stress) and log(time), as shown in Fig. 17.23, but at low twists the slope changed abruptly at one point. It may be noted that the equation is a special case of the creep part of Leaderman's expression [65], $\phi(F)\ \psi(t)$. However, Leaderman has pointed out that a power law does not always fit the experimental results well. In general, although it may be

useful in special cases, the equation is too limited to explain the complicated behaviour of fibres.

20.8 Thermodynamic effects

20.8.1 Thermodynamic equation of deformation

When a net amount of work $\sum dW$ is done on a system, it causes a change in the internal energy U and the entropy S of the system. The combined statement of the First and Second Laws of Thermodynamics for a reversibly isothermal change gives the relations between these quantities

$$\sum dW = dU - TdS \tag{20.69}$$

where T = absolute temperature.

If a fibre is extended by an amount dl through the application of a force F, then the work done on the system is $F\,dl$. We may therefore put:

$$F\,dl + \sum' dW = dU - TdS \tag{20.70}$$

In this equation, $\sum' dW$ is the sum of any other work or heat. Among other possible sources are an increase in volume dV against a pressure P, doing work $(-PdV)$, and the absorption of water liberating the heat of absorption. It is usual in experimental investigations to maintain conditions (e.g. constant volume and constant water absorption) so that the other sources of work may be neglected, and we then have:

$$Fdl = dU - TdS \tag{20.71}$$

$$F = \left(\frac{\partial U}{\partial l}\right)_T - T\left(\frac{\partial S}{\partial l}\right)_T \tag{20.72}$$

This means that the stress caused by a given elastic extension may be divided into two parts, one depending on the changes in internal energy and the other on changes in the entropy. Increases in internal energy on extension come from the bonds between atoms being stretched, bent or rotated as described for crystals and glasses in Section 20.1.2. Changes in entropy come from changes in the degree of order of the system. All systems have a general tendency to take up the most random, least ordered condition, that is, the condition of highest entropy. Consequently, if the extension of a system means that it is increasing in its degree of order, a force must be applied to overcome the fall in entropy. This effect is predominant in the extension of rubbers (as it is for the volume changes of gases) as described in 20.1.2. There are thus two distinct mechanisms involved in determining the equilibrium position of a system and the forces needed to deform it. They are the tendencies, which are often opposed to one another, to achieve positions of minimum internal energy and maximum entropy (maximum randomness). On deformation of the system, there are three possibilities: (a) both the internal energy and the entropy effects may give positive contributions to the force; (b) the internal-energy contribution may be positive and numerically greater than a negative entropy contribution; or (c) the entropy contribution may be positive and numerically greater than a negative internal energy contribution.

For further mathematical development, it is convenient to introduce a quantity $A = (U - TS)$, which is known as the *Helmholtz free energy*. For a general change and substituting from equation (20.71):

$$dA = dU - TdS - SdT = Fdl - SdT \tag{20.73}$$

Thus

$$\left(\frac{\partial A}{\partial l}\right)_T = F \tag{20.74}$$

$$\left(\frac{\partial A}{\partial T}\right)_l = -S \tag{20.75}$$

However, it follows from a general property of partial differentials that:

$$\frac{\partial}{\partial l}\left(\frac{\partial A}{\partial T}\right)_l = \frac{\partial}{\partial T}\left(\frac{\partial A}{\partial l}\right)_T \tag{20.76}$$

Consequently, substituting from equations (20.74) and (20.75) we have:

$$\left(\frac{\partial S}{\partial l}\right)_T = -\left(\frac{\partial F}{\partial T}\right)_l \tag{20.77}$$

This means that the entropy contribution may be worked out from the change of force with temperature for a specimen extended by a constant amount. Equation (20.72) then gives internal energy contribution by subtraction from the force.

It has been shown experimentally that, for rubbers, $F \approx T(\delta F/\delta T)_l$, which indicates that the internal-energy contribution is negligible and that the rubber-like extension depends on entropy effects. Rubber-like elasticity is also characterised by a negative coefficient of linear expansion (see Section 6.2.3).

20.8.2 Application to fibres

There have been several investigations aimed at determining the extent of the energy and entropy effects in fibre extension. To do this, it is necessary, as we have seen, to measure the change of stress on a fibre held at constant extension. However, the stress on such a fibre will change owing to relaxation, apart from the change of temperature. This is an important experimental difficulty. It is one aspect of the general proposition that the thermodynamic equations are not applicable to irreversible effects, such as occur in the deformation of fibres. Experiments can therefore be made only on fibres in which the stress has relaxed to a fairly constant value, and even then the results must be viewed with caution.

Experiments have been made on both dry and wet fibres. In the latter case, corrections should be applied for the change of absorption on extension as described by Bryant and Wakeham [76].

The results of experiments on cellulose fibres given in Table 20.4 show that for dry fibres the positive contribution to the force is derived from the internal energy

Table 20.4 Internal energy and entropy contributions in cellulose fibres

Fibre	Elongation (%)	Temp. (°C)	Total stress (mN/tex)	Energy contribution $\left(\frac{\partial U}{\partial l}\right)_T$	Entropy contribution $-T\left(\frac{\partial S}{\partial l}\right)_T$
Dry fibres					
Isotropic rayon	1	25	12.4	41.9	– 29.5
Textile rayon	1	25	29.1	60.3	– 31.2
Tyre-cord rayon	1	25	36.2	66.6	– 30.4
Stretched rayon (fibre G)	1	25	50.4	81.1	– 30.7
Wet fibres					
Cotton yarn	1	25	1.06	2.90	– 1.84
Trye-cord rayon	1	25	1.06	3.16	– 2.10
Stretched rayon (fibre G)	1	25	7.68	23.4	– 15.8
Saponified acetate (highly oriented)	1	25	14.2	36.4	– 22.2
Textile rayon	1	25	1.15	1.84	– 0.70
	10	25	24.8	25.5	– 7.36
	1	75	1.17	0.33	+ 0.83
	10	75	24.8	24.0	+ 0.77
Acetate	1	25	0.31	0.70	– 0.38
	28	25	1.96	3.40	– 1.44
	1	75	0.11	2.05	– 1.94
	28	75	1.97	1.15	– 0.82

Calculations from original data [76, 77] by Wakeham [61].

effect, but this is reduced by a fairly large negative entropy term. The energy term derives from the stretching or angular deformation of the inter-atomic bonds and becomes greater the more highly oriented the fibre. The negative entropy term means that the structure is moving towards a less ordered state on deformation. For wet fibres, both the energy and the entropy terms are numerically less, and the latter becomes positive at higher temperatures.

An application to wool is shown in Figure 20.60. This indicates that the energy term predominates, which was interesting at the time, because it was thought that the large extension shown by wool was due to a rubber-like type of elasticity depending on an alignment of disordered chains. The subsequent observation of the $\alpha \leftrightarrow \beta$ transition confirmed the energy change, though there is an entropic contribution from the matrix.

By contrast, Fig. 20.61 shows that in casein at low extensions the entropy effect predominates and is combined with a negative internal-energy effect. This suggests that, in this almost completely non-crystalline material, the chains are bent at random and the order increases on extension. The decrease in internal energy would derive from a more favourable interaction between the molecules.

It is well known that if stretched rubber is cooled to a low temperature, its oriented structure is 'frozen in', and it exhibits a stress–strain curve similar to that of a textile

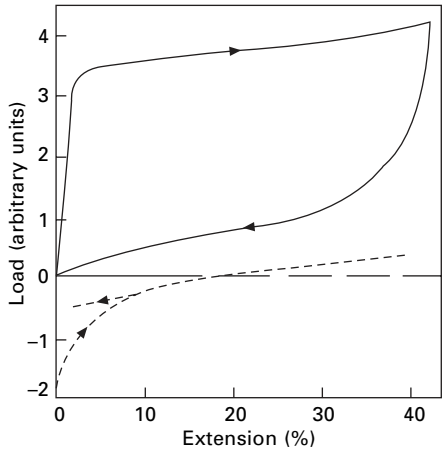

20.60 Extension and recovery curves of wool fibre in water [78]. Full line; total load. Dotted line: entropy contribution.

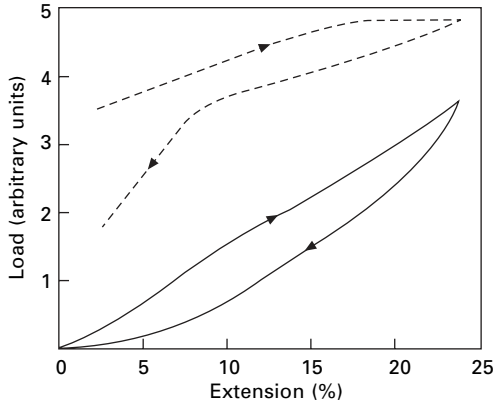

20.61 Extension and recovery curves of casein fibre in water [78]. Full line: total load. Dotted line: entropy contribution.

fibre. Clark and Preston [79] have observed the reverse effect with nylon and *Vinyon*. When heated above a certain temperature, these fibres contract and then show rubber-like properties, namely, a large extension and a large entropy effect as shown in Fig. 20.62. There is, however, a divergence from ideal rubber-like elasticity because the internal-energy effect is not negligible.

Rather different results were obtained by Dart [80], who found that, in nylon and polyester and acrylic fibres, the internal energy term was dominant and the entropy effects were small.

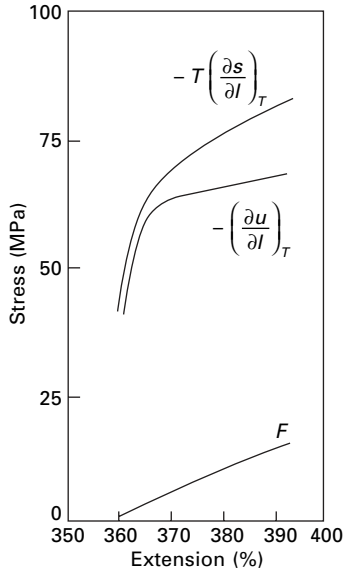

20.62 Stress–strain relations for nylon in the range 150–180 °C.

20.9 References

1. L. R. G. Treloar *The Physics of Rubber Elasticity*, 3rd edition, Clarendon Press, Oxford, 1975.
2. P. J. Flory. *Principles of Polymer Chemistry*, Cornell University Press, Ithaca, NY, 1953, p. 427–428.
3. J. W. S. Hearle. *Polymers and Their Properties*, Ellis Horwood, Chichester, 1982.
4. J. W. S. Hearle. *J. Polymer Sci. C*, 1967, No. 20, 215.
5. R. W. Work. *Text. Res. J.*, 1949, **19**, 381.
6. J. W. S. Hearle. *J. Appl. Polymer Sci.*, 1963, **7**, 1635.
7. R. J. E. Cumberbirch and C. Mack. *J. Text. Inst.*, 1960, **51**, T458.
8. R. J. E. Cumberbirch and C. Mack. *J. Text. Inst.*, 1961, **52**, T382.
9. J. W. S. Hearle. *J. Polymer Sci. C*, 1967, No. 20, 215.
10. D. C Prevorsek, P. J. Harget, R. K. Sharma and A.C. Reimschussel. *J. Macromol. Sci*., 1973, **B-8**, 127.
11. J. W. S. Hearle and R. Greer. *J. Text. Inst*., 1970, **61**, 243.
12. N. S. Murthy, A. C. Reimschussel and V. J, Kramer. *J. Appl. Polymer Sci*., 1990, **40**, 249.
13. J. W. S. Hearle. *J. Appl. Polymer Sci., Appl. Polymer Symp.*, 1978, **31**, 137.
14. J. W. S. Hearle, R. Prakash and M. A. Wilding. *Polymer*, 1987, **28**, 441.
15. J. W. S. Hearle, M. A. Wilding and G. W. Du, unpublished reports to Du Pont, 1985–90.
16. J. W. S. Hearle. *J. Appl. Polymer Sci.: Appl. Polymer Symp*., 1991, **47**, 1.
17. S. D. Long and I. M. Ward. *J. Appl. Polymer Sci.*, 1991, **42**, 1921.
18. I. M. Ward *J. Textile Inst*., 1995, **86**, 289.
19. H. A. Davis. *J. Textile Inst*., 1991, **82**, 86.
20. P. E. Rouse *J. Chem. Phys*., 1953, **21**, 1272.
21. P. J. Barham and A. Keller. *J. Mater. Sci.*, 1985, **20**, 2281.
22. G. S. Fielding-Russell. *Text. Res. J.*, 1971, **41**, 861.
23. R. Meredith. *Text. Prog.*, 1975, **7**, No.4.
24. Y. Termonia and P. Smith. *Polymer*, 1986, **27**, 1845.
25. G. Wobser and S. Blasenbrey. *Kolloid-Z. Z. Polymer*, 1970, **241**, 985.

26. D. J. Johnson, L. Karacan and J. G. Tomka. *J. Textile Inst.*, 1990, **81**, 421
27. M. G. Northolt. *Polymer*, 1980, **21**, 1199.
28. M. G. Northolt and R. van der Hout. *Polymer*, 1985, **26**, 310.
29. M. G. Northolt, A. Roos and J. H. Kampschreur. *J. Polymer Sci., Physics Edition*, 1989, **27**, 1107.
30. M. G. Northolt and D. J. Sikkema. *Adv. Polymer Sci*., 1990, **98**, 115.
31. M. G. Northolt, J. J. M. Baltussen and B. Schaffers-Korff. 1995, **36**, 3485.
32. J. J. M. Baltussen and M. G. Northolt. *Polymer*, 2001, **42**, 3835.
33. J. W. S. Hearle, P. Grosberg and S. Backer. *Structural Mechanics of Fibers, Yarns, and Fabrics*, Volume I, Wiley-Interscience, New York, 1969.
34. R. Meredith. In *Proceedings of Fifth International Congress on Rheology*, University of Tokyo Press, Tokyo, Japan, 1969, Volume 1, p. 43.
35. J. W. S. Hearle and J. T. Sparrow *J. Appl. Polymer Sci*., 1979, **24**, 1857.
36. J. W. S. Hearle. In *Mechanics of Flexible Fibre Assemblies*, J. W. S. Hearle, J. J. Thwaites and J. Amirbayat (Editors), Sijthoff and Noordhoff, Alphen an den Rijn, Netherlands, 1980, p. 51.
37. J. J. Thwaites. In *Mechanics of Flexible Fibre Assemblies*, J. W. S. Hearle, J. J. Thwaites and J. Amirbayat (Editors), Sijthoff and Noordhoff, Alphen an den Rijn, Netherlands, 1980, p. 87.
38. S. Timoshenko. *Strength of materials Part II*, Van Nostrand, New York, 1957, p. 259.
39. D. L. House. MSc thesis, Georgia Institute of Technology, 1966.
40. R. Meredith. *J. Textile Inst*., 1954, **45**, T489.
41. J. T. Sparrow, The fracture of cotton, PhD thesis, University of Manchester, 1973.
42. J. W. S. Hearle. *Wool Tech. Sheep Breeding*, 2003, **35**, 95.
43. J. W. S. Hearle. 11th *Int. Wool Textile Res. Conf*., 2005, Leeds.
44. J. W. S. Hearle. *Textile Horizons*, 1997, August/September, 12.
45. H. Liu and W. G. Bryson. *J. Textile Inst*., 2002, **93**, 121.
46. M. Feughelman. *Textile Res. J*., 1959, **29**, 223.
47. B. M. Chapman. *Text. Res. J.*, 1969, **39**, 1102.
48. J. W. S. Hearle. *Int. J. Biological Macromolecules*, 2000, **27**, 123.
49. B. M. Chapman *J. Textile Inst*., 1970, **61**, 448.
50. J. W. S. Hearle and M. Susitoglu. *Proc. 7th Int. Wool Textile Res. Conf*., Tokyo, Japan, 1985, **1**, 214.
51. J. W. S. Hearle, B. M. Chapman and G. S. Senior. *Appl. Polymer Symp*., 1971, **18**, 775.
52. B. M. Chapman. PhD thesis, University of Manchester, 1968.
53. K. Arai, G. Ma and T. Hirata. *J. Appl. Polymer Sci*., 1991, **42**, 1125.
54. W. A. Munro and G. A. Carnaby. *J. Textile Inst*., 1999, **90**, 123.
55. W. A. Munro. *J. Textile Inst*., 2001, **92**, 213.
56. F. T. Peirce. *J. Text. Inst.*, 1927, **18**, T486.
57. J. D. Ferry, *Viscoelastic Properties of Polymers*, 2nd edition, Wiley, New York, 1970.
58. A. V. Tobolsky and H. Eyring. *J. Chem. Phys.*, 1943, **11**, 125.
59. G. Halsey, H. J. White and H. Eyring. *Text. Res. J.*, 1945, **15**, 295.
60. S. Glasstone, K. J. Laidler and H. Eyring. *The Theory of Rate Processes*, McGraw-Hill, New York, 1941.
61. H. Wakeham. In *Cellulose and Cellulose Derivatives*, E. Ott and H. M. Spurlin (Editors), Interscience, New York, 1955, Chapter 11, p. 1302.
62. R. Meredith. *The Mechanical Properties of Textile Fibres*, North Holland Publishing Co., Amsterdam, Netherlands, 1956, pp. 87 *et seq*.
63. E. G. Burleigh and H. Wakeham. *Text. Res. J.*, 1947, **17**, 245.
64. F. Andersen. *Trans. Danish Acad. Tech. Sci.*, 1950, No. 3.
65. H. Leaderman. *Elastic and Creep Properties of Filamentous Materials and Other High Polymers*, The Textile Foundation, Washington, DC, 1943.
66. C. H. Reichardt, G. Halsey and H. Eyring. *Text. Res. J.*, 1946, **16**, 382.

67. R. L. Steinberger. *Text. Res.*, 1936, **6**, 191.
68. H. D. Holland, G. Halsey and H. Eyring. *Text. Res. J.*, 1946, **16**, 201.
69. H. Eyring and G. Halsey. In *High-polymer Physics*, Chemical Publishing Co., New York, 1948, p. 98.
70. C. J. Geyer, C. H. Reichardt and G. Halsey. *J. Appl. Phys.*, 1948, **19**, 464.
71. C. H. Reichardt and H. Eyring. *Text. Res. J.*, 1946, **16**, 635.
72. L. Boltzmann. *Pogg. Ann. Physik.*, 1876, **7**, 624.
73. F. Kohlrausch. *Pogg. Ann. Physik.*, 1876, **8**, 337.
74. P. G. Nutting. *J. Franklin Inst.*, 1943, **235**, 513.
75. F. Permanyer. PhD Thesis, University of Manchester, 1947.
76. G. M. Bryant and H. Wakeham. *Text. Res. J.*, 1955, **25**, 224.
77. W. E. Roseveare and L. Poore. *J. Polymer Sci*., 1954, **14**, 341.
78. H. J. Woods. *J. Colloid Sci.*, 1946, **1**, 407.
79. J. F. Clark and J. M. Preston. *J. Text. Inst.*, 1953, **44**, T596.
80. S. L. Dart. *Text. Res. J.*, 1960, **30**, 372.